Analysis of Domain Specific Functions of the Ceramide Synthase Schlank in *Drosophila melanogaster*

Dissertation

zur Erlangung des Doktorgrades (Dr. rer. nat.)
der
Mathematisch-Naturwissenschaftlichen Fakultät
der
Rheinischen Friedrich-Wilhelms-Universität Bonn

vorgelegt von

Anna-Lena Wulf

aus Detmold

Bonn, 2015

Angefertigt mit Genehmigung der Mathematisch-Naturwissenschaftlichen Fakultät der Rheinischen Friedrich-Wilhelms-Universität Bonn.

Erstgutachter:	PD Dr. Reinhard Bauer
Zweitgutachter:	Prof. Dr. Klaus Willecke
Tag der Promotion:	04. Dezember 2015
Erscheinungsjahr:	2016

Eidesstattliche Erklärung

Hiermit versichere ich, dass diese Dissertation von mir selbst und ohne unerlaubte Hilfe angefertigt wurde. Es wurden keine anderen als die angegebenen Hilfsmittel benutzt. Ferner erkläre ich, dass die vorliegende Arbeit an keiner anderen Universität als Dissertation eingereicht wurde.

Bonn, Juni 2015

_____

Anna-Lena Wulf

Summary

Ceramide synthases (CerS) are integral membrane proteins at the center of sphingolipid (SL) biosynthesis. Their enzymatic activity is dependent on the conserved lag1 motif, but from cnidarians onwards many CerS proteins also contain a homeodomain with yet unknown function. Homeodomains are commonly known as DNA-binding domains in transcription factors regulating developmental processes. Previous studies of our group show that the only CerS ortholog in *Drosophila melanogaster* -Schlank- is not only involved in the synthesis of SLs but also in the regulation of body fat. This regulation seems to be independent on the CerS activity. Lately, Schlank was shown to localize in the nucleus in an Importin dependent manner. In this thesis, the functional properties of the Schlank protein were studied in more detail. A genomic engineering strategy where specific mutations were introduced into the *schlank* sequence in it's endogenous locus allowed the direct comparison of Schlank variants. This approach could prove that up regulation of *lipase 3* in *schlank* deficient larvae is due to the absence of the Schlank protein, and not due to absent ceramide synthesis. Mutations within the homeodomain targeting a putative nuclear localization signal (NLS) caused phenotypes in locomotion, behavior and body fat level that are also known from *schlank* P-element mutant alleles, further implying a functional relevance of the homeodomain. Mutations in this NLS reduced the relative amount of nuclear Schlank protein showing it's functionality *in vivo*, whereas mutations in the other predicted NLS did not reduce nuclear Schlank. To address a potential nuclear function of the homeodomain Schlank transmembrane topology was investigated experimentally. Those experiments strongly suggest a cytosolic and nucleoplasmic orientation of the homeodomain. Previously, a cleavage of the Schlank protein has been proposed. As Schlank fragment bands were detected to a different extend under different conditions a regulated reasonable cleavage of the Schlank protein could be hypothesized. Unexpectedly, the site of this cleavage was localized to an amino acid stretch within the homeodomain. Altogether, with this work we gained more insight into the various roles of the Schlank protein apart from it's catalytic activity.

Contents

1 Introduction

Biological lipid species are highly versatile. Cell membranes contain more lipid species than needed to form a simple lipid bilayer (Bretscher, 1973) and lipid composition seems to be important for different signaling events (Pepperl et al., 2013). Additionally, bioactive lipids have been found that themselves have signaling properties (Hannun and Obeid, 2008). For the analysis of the influence of different metabolites on physiology, more and more (animal) models of enzyme deficiencies have been generated and analyzed in the last years (Padmanabha and Baker, 2014). However, manipulating biosynthesis pathways can have unclear effects that could e.g. arise from adapted regulation of other metabolizing enzymes or lack of the manipulated enzyme itself.

1.1 Sphingolipids

Sphingolipids are a class of lipids that arose parallel to the appearance of eukaryotic life and are conserved from yeast to mammals. They were first isolated and characterized from brain extracts in the 1870s (Thudichum, 1874). Sphingolipids are highly diverse and play an important role in the determination of membrane properties (Guan et al., 2009; Silva et al., 2012). They are also involved in signaling events, like their influence on cell recognition, on the behavior of growth factor receptors and extracellular matrix proteins (Hakomori, 1990), on lipid microdomain function (van Zanten et al., 2010; Harder and Simons, 1997; Grassmé et al., 2007) or on the generation of micro-channels within mitochondrial membranes (Siskind et al., 2002; Colombini, 2010). Some are considered bioactive lipids involved in survival, stress response and apoptosis (Hannun and Obeid, 2008).

The distribution of sphingolipids within subcellular compartments varies (Hannich et al., 2011) and little is known about the overall regulation of sphingolipid metabolism even though many intermediates show high impact on cell survival. The uptake of sphingolipids with food does not appear to be essential but may be a functional com-

ponent of food (Vesper et al., 1999). In rodents they are taken up by intestinal cells in the form of ceramide or sphingoid bases and degraded to fatty acids or reincorporated into complex sphingolipids that remain associated primarily with the intestine (Nilsson, 1968; Schmelz et al., 1994).

Sphingolipid synthesis is organized along the secretory pathway. Sphingoid bases, the backbones of sphingolipids, are synthesized at the endoplasmic reticulum (ER). They can be acylated by Ceramide Synthases to form (dihydro)ceramide, which can be subsequently modified. Most of those (complex) sphingolipid species are synthesized in the Golgi apparatus. The carbon chain length and saturation of the acyl chain residues, and the different modifications of the sphingoid bases like phosphorylation or addition of choline or sugar residues/branches lead to the high variability of sphingolipids (fig. 1.1).

The *de novo* biosynthesis of sphingolipids starts with the condensation of L-serine and palmitoyl-CoA (in *Drosophila* lauryl-CoA) by the Serine Palmitoyl Transferase (SPT). Resulting 3-keto-sphinganine is reduced to sphinganine. Sphinganine is acylated by a Ceramide Synthase and desaturated by a Ceramide Desaturase to form Ceramide (fig. 1.1). Ceramides can be directly transported to the Golgi in a non-vesicular mechanism by the Ceramide Transporter protein (CERT, Hanada et al., 2003) but also through vesicular transport. The Golgi is the site of synthesis of sphingomyelin and glucosylceramide, which is the precursor for complex glycosphingolipids. Delivery of sphingomyelin and complex glycosphingolipids to the plasma membrane appears to occur by vesicular transport. The endosomal pathway is involved in the degradation and salvage of sphingolipids (Hannun and Obeid, 2008).

In the last years more and more diseases have been linked to aberrations in sphingolipid levels and their metabolizing enzymes. E.g.:

- Sphingolipidoses are lipid storage diseases resulting mainly from defects in the degradation of sphingolipids like Niemann-Pick disease, Fabry disease, Gaucher disease and Tay-Sachs disease (Pentchev and Barranger, 1978; Sandhoff, 2012).
- Sphingolipids have been associated with neuronal apoptosis and therefore neurodegeneration (Arboleda et al., 2009) like Alzheimer's disease (Farooqui et al., 2010; Mielke and Lyketsos, 2010; van Echten-Deckert and Walter, 2012) and Parkinson's disease (Abbott et al., 2014).
- Studies show, that sphingolipids are associated with the development of metabolic syndrome. E.g. inhibiting *de novo* ceramide synthesis reduces insulin resistance

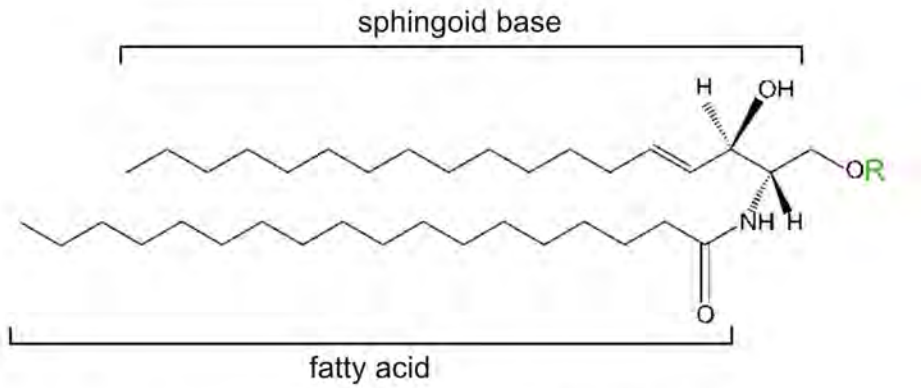

R - group	Sphingolipid
H	Ceramide
Phosphate*	Ceramide-1-phosphate
Phosphocholine	Sphingomyelin
Phosphoethanolamine	PE-ceramide
Sugar	Glycosphingolipid
°single sugar residue	Cerebroside
°oligosaccharide residue + sialic acid	Ganglioside

* Sphingoid bases can be phosphorylated as well to form sphinganine/sphingosine-1-phosphate

Figure 1.1: Sphingolipid species. Sphingoid bases -here Sphingosine- are N-acylated by Ceramide Synthases to form ceramide, a simple sphingolipid. Different groups can be added at C1 by different enzymes to form more complex sphingolipids. Some abundant are listed in the table. PE: phosphoethanolamine, R: residue. Ceramide backbone modified from Neumann and van Meer, 2008.

(Holland and Summers, 2008; Holland et al., 2007b; Ussher et al., 2010), and serum levels of sphingomyelin with distinct saturated acyl chains correlate with the parameters of obesity, insulin resistance, liver function and lipid metabolism in patients (Hanamatsu et al., 2014).

– The ceramide/sphingosine-1-phosphate rheostat is important in cancer development and progression (Ogretmen and Hannun, 2004). Whereas ceramide is a pro-apoptotic signaling molecule, sphingosine-1-phosphate has counteracting function promoting proliferation, differentiation and migration in various cell types (Oskouian and Saba, 2010).

Therefore, sphingolipd metabolism is more and more considered as a therapeutic target and a diagnostic marker. A good understanding of the enzymes involved is fundamental for the development of such new tools.

1.2 Sphingolipids and sphingolipid metabolizing enzymes in *Drosophila*

In *Drosophila melanogaster*, most of the enzymes of the sphingolipid metabolism are described and are encoded by less paralogs than in mammals (Acharya and Acharya, 2005). The lipidome of *Drosophila melanogaster* during development has been analyzed via mass spectrometry (Carvalho et al., 2012; Guan et al., 2013). For several enzymes of the sphingolipid biosynthesis pathways mutants have been described. For example, *ceramide kinase (cerk)* mutants accumulate ceramide and show reduced energy levels. Metabolic adaption occurs via the Akt/FOXO pathway, enhancement of glycolysis and lipolysis in the gut. Ceramide Kinase phosphorylates ceramide to form ceramide-1-phosphate (Nirala et al., 2013). *Alkaline ceramidase* mutants show increased lifespan and anti-oxidative stress capacity. Ceramidases catalyze the hydrolysis of ceramides to generate sphingosine and fatty acids (Yang et al., 2010). Metabolites, like glucosylceramide, sphingosine-1-phosphate and ceramide have been linked to fat storage in *Drosophila* (Kohyama-Koganeya et al., 2011; Walls et al., 2013).

Even though there are Sphingomyelinases encoded in the genome, sphingomyelin is nearly absent. *Drosophila* Sphingomyelinases could be responsible for the generation of the more abundant phosphoethanolamine ceramide (PE-ceramide; Kraut, 2011).

1.3 Ceramide Synthases

Ceramide Synthases (CerS) catalyze the reaction of sphinganine (or sphingosine) and a fatty acylCoA to form (dihydro-) ceramide (+CoA). Therefore, they are right at the center of sphingolipid metabolism (Mullen et al., 2012).

These enzymes belong to a family of transmembrane proteins containing a conserved TLC (Tram, Lag and CLN8) domain (Winter and Ponting, 2002; fig. 1.2). The contained lag1 motif is important for the catalytic activity of CerS (Spassieva et al., 2006). An additional ("new") motif essential for catalytic activity has been reported by Mesika et al. (2007). Since cnidarians onwards many CerS contain a homeodomain (Voelzmann and Bauer, 2010; Holland et al., 2007a) usually associated with sequence specific DNA interaction of transcription factors during development (Gehring and Hiromi, 1986; Gehring et al., 1994a). Studies on the transmembrane topology revealed a cytoplasmic C-terminus for yeast CerS (Lag1p and Lac1p) and mouse CerS6 (Kageyama-Yahara and Riezman, 2006; Mizutani et al., 2005).

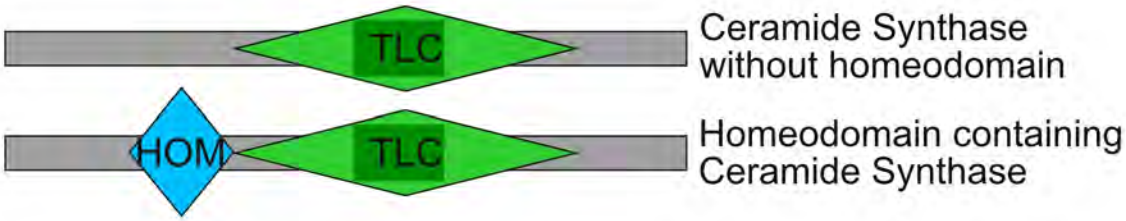

Figure 1.2: Domain structure of Ceramide Synthases. There are CerS proteins without a homeodomain e.g. CerS1 and Lac1p and CerS proteins with a homeodomain N-terminally to the TLC domain e.g. CerS2 and Schlank. HOM (blue): homeodomain, TLC (green): TLC domain, dark green: lag motif.

Mammals encode six CerS (CerS1-CerS6), each with a different tissue distribution and preferred chain length of fatty acylCoA (Levy and Futerman, 2010; Stiban et al., 2010; Kremser et al., 2013). For example, CerS1 - the only mammalian CerS without a homeodomain- is mainly expressed in muscle and brain and has a preference for C18-acylCoA, CerS2 shows the over-all highest abundance in most tissues and has a preference for very long chain acylCoAs (C20-C26). It is hypothesized that sphingolipids with different chain length fulfill different functions (Grösch et al., 2012; Menuz et al., 2009). This is also seen in the different phenotypes of the deficient mice for each *ceramide synthase* that have been generated (CerS1: Zhao et al., 2011; Ginkel et al., 2012, CerS2: Imgrund et al., 2009; Pewzner-Jung et al., 2010a,b; Park et al.,

2013; Zigdon et al., 2013, CerS3: Jennemann et al., 2012; Rabionet et al., 2015, CerS4: Ebel et al., 2014; Peters et al., 2015, CerS6: Ebel et al., 2013; Turpin et al., 2014).

1.4 *Drosophila melanogaster* Ceramide Synthase: Schlank

The *Drosophila melanogaster* genome encodes one *ceramide synthase* gene (*schlank, CG3576, Drosophila longevitiy assurance gene-1 homologue(DLag1)*) that is ubiquitously expressed (Acharya and Acharya, 2005; Bauer et al., 2009; Voelzmann and Bauer, 2011). Schlank has been shown to be a *bona fide* Ceramide Synthase that is involved not only in sphingolipid metabolism but also in the regulation of body fat. *schlank* mutant larvae show (amongst other things) a strong reduction in triacylglycerol (TAG) level that goes along with an up regulation of lipases (*lipase 3, brummer*) and *adipokinetic hormone*, and a down regulation of SREBP and its target genes (e.g. *fatty acid synthase, acetylCoA synthase*) that reverse upon *schlank* over expression. This reversion occurs independent of the capability of the over expressed Schlank protein to form ceramide (Bauer et al., 2009; Voelzmann, 2013; fig. 1.3). As therefore the regulation of body fat should depend on the (N-terminal part of the) Schlank protein itself and as the Schlank protein is a homeodomain containing Ceramide Synthase we hypothesize a gene regulatory function of the CerS homeodomain. Additional findings supporting this hypothesis, are the nuclear localization of endogenous Schlank protein in fat body cells of stage 3 larvae, putative nuclear localization signals (NLSs) and 3D-structure and DNA binding properties of the Schlank homeodomain (fig. 1.4; Voelzmann, 2013; Noyes et al., 2008). The more common opinion however seems to consider the CerS homeodomain as an evolutionary artifact (Venkataraman and Futerman, 2002).

Schlank deficiency also results in many different phenotypes including developmental delay, lethality, modified wingless signaling and defects during eye development and glial ensheathment of axons (Bauer et al., 2009; Pepperl et al., 2013; Voelzmann, 2013; Ghosh et al., 2013). Two *schlank* mutant lines have been analyzed; one stronger allele ($schlank^{P(X)349}$) and one weaker allele ($schlank^{P(X)61}$) that differ in the level of *schlank* expression and therefore in the severity of the phenotype. Larvae of the stronger allele die at the first larval stage whereas there are escapers of the weaker mutant allele that even develop to adulthood.

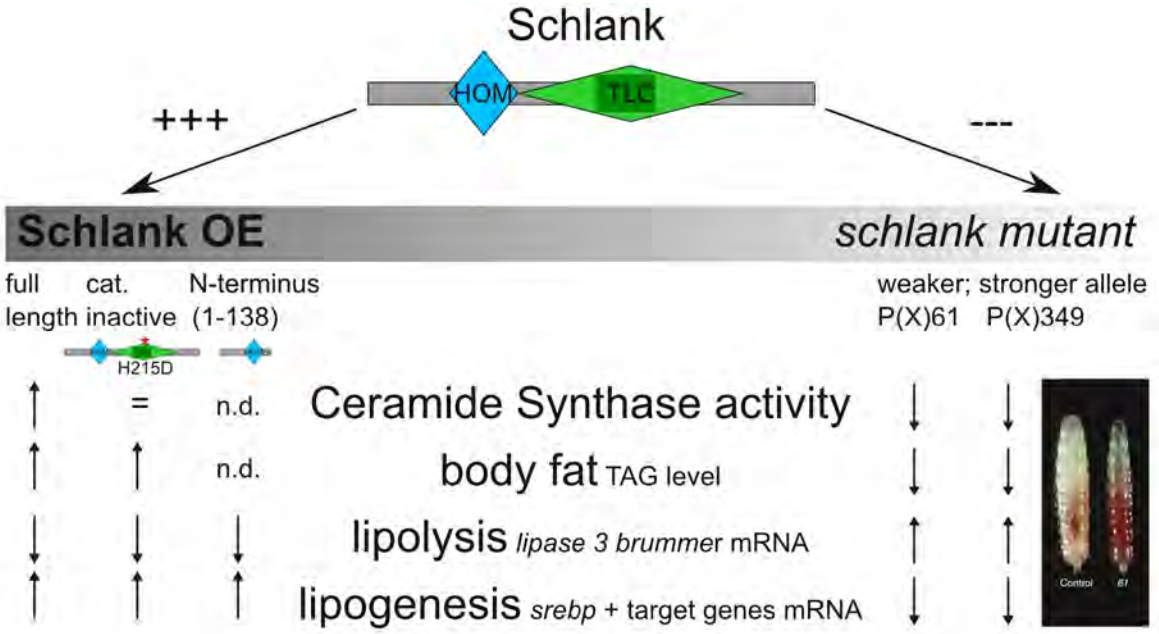

Figure 1.3: Schlank is a player of lipid homeostasis; insulin-and feeding-independent. Modification of Schlank level results in an adaption of triacylglycerol (TAG) level via the regulation of genes involved in lipogenesis (*srebp* and target genes) and lipolysis (*brummer, lipase 3*). This regulation, especially *lipase 3*, seems to be independent of the ability of the Schlank enzyme to synthesize ceramide (catalytically inactive, SchlankH215D) or the presence of the C-terminus (Schlank AA1-138). The picture shows an L3 larva of $schlank^{P(X)61}$: it is thinner and contains less fatbody than control (w^{1118}) larva even though both took up the red stained yeast. n.d.: not determined.

1.5 The CerS homeodomain and nuclear sphingolipid metabolism

Several sphingolipid species have been isolated from nuclear extracts (e.g. sphingomyelin, sphingosine-1-phosphate, sphingosine, ganglioside GM1; Albi et al., 2003; Wu et al., 1995), as well as sphingolipid metabolizing enzyme activity (e.g. Sphingomyelin Synthase, neutral Sphingomyelinase, Ceramidase, Sphingosine-Kinase; Albi and Magni, 1999; Tsugane et al., 1999; Hait et al., 2009). The nuclear sphingolipids have been associated with regulatory and structural functions like chromatin dynamics, histone acetylation and apoptosis, suggesting a nuclear sphingolipid metabolism (Lucki and Sewer, 2012).

The *Drosophila* Ceramide Synthase Schlank shows nuclear localization as well (Voelzmann, 2013; fig. 1.4C). The nuclear import mechanism could be proven to be Ketel dependent, which is a *Drosophila* homologue of Importin-β. This classical nuclear import mechanism is based on the binding of transport receptors (e.g. Importin-β) to nuclear localization signals (NLS) within the sequence of transported cytoplasmic or membrane proteins and their transfer through the nuclear pore complex (NPC; Sorokin et al., 2007). NLSs are highly divers, making predictions complicated (Kosugi et al., 2009). Two putative NLSs have been found in the Schlank homeodomain sequence (fig. 1.4B) which were involved in the nuclear localization of Schlank homeodomain constructs in cell culture experiments (Voelzmann, 2013).

Homeodomains show a classical 3D-structure with three helices in a helix–loop–helix –turn–helix motif (Scott et al., 1989, fig. 1.4A). Consensus residues in helix 3 and in the N-terminal arm contact DNA. All 84 independent homeodomains from *Drosophila melanogaster* have been analyzed concerning their DNA-binding specificity. Also for the Schlank homeodomain a consesus sequence was determined (Noyes et al., 2008).

1.6 Regulation of body fat

Many metabolic pathways are conserved in human and fly. Manipulation of those pathways in *Drosophila* gives rise to e.g. diabetic or obese phenotypes that are also observed in patients (Bharucha, 2009). A metabolically active organ in the fly is the fatbody (a functional analogue of adipose tissue in humans). It stores e.g. triacyglycerols (TAGs), cholesterol ester and glycogen and, like mammalian adipocytes, it is full of lipid droplets. Together with the oenocytes located in the cuticle it also fulfills

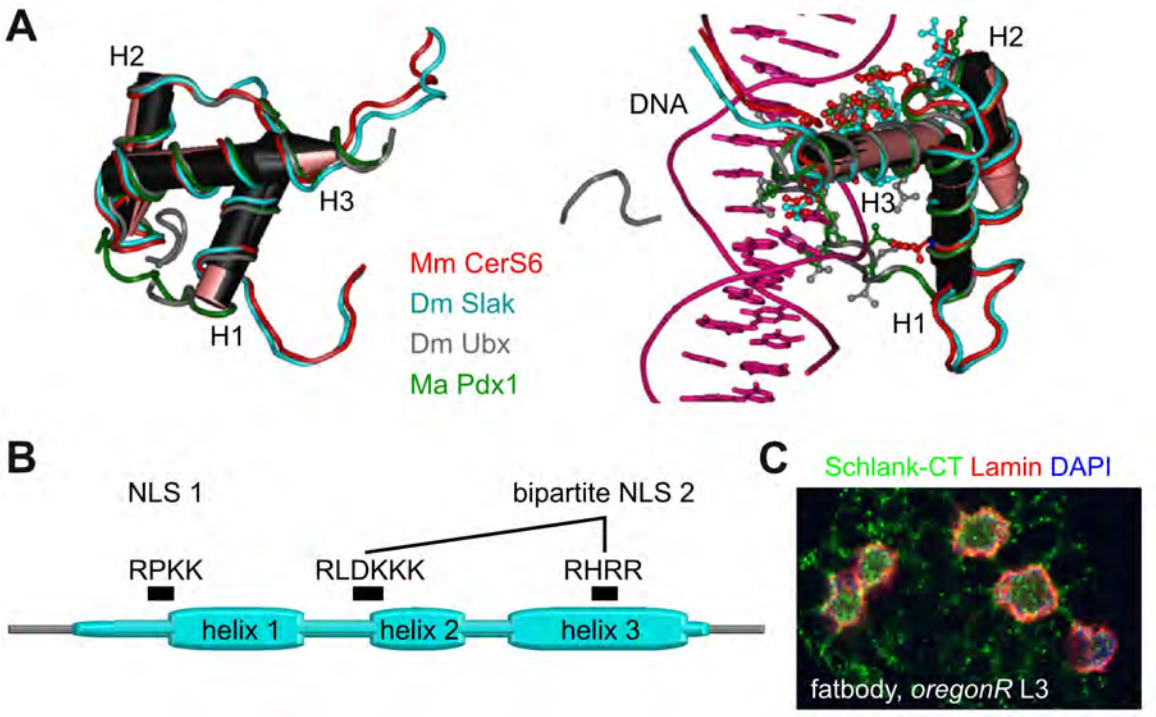

Figure 1.4: Schlank nuclear localization and homeodomain. **A**: 3D structure of CerS homeodomains and classical homeodomains are much alike. X-ray based 3D structure of the classical homeodomains Ultrabithorax from *Drosophila melanogaster* (Dm Ubx) and pancreatic and duodenal homeobox 1 from *Mesocricetus auratus* (Ma Pdx1), NMR based 3D structure of the *Mus musculus* CerS6 homeodomain (Mm CerS6) and the SWISS MODEL prediction of the Schlank homeodomain (Dm Slak). **B**: Sequence analysis showed two nuclear localization signals within the Schlank homeodomain. **C**: Schlank localizes to the nucleus. L3 larval fatbody was stained in immunofluorescence analysis: Schlank: green, Lamin (inner nuclear membrane, INM): red, DAPI (DNA): blue. Modified from Voelzmann, 2013.

the storage function and metabolic regulation of mammalian liver (Gutierrez et al., 2007). Instead of pancreatic cells, specific areas of the brain are responsible for the release of *Drosophila* Insulin-Like-Peptides (DILPs) and the Glucagon-like Adipokinetic hormone (Akh) which systemically controls body fat mobilization. Conserved key regulator genes of lipogenesis are e.g. the Akh receptor (AkhR) target *midway* which encodes the *Drosophila* Diacylglycerol O-Acyltransferase 1 (*Dm*DGAT1) (Buszczak et al., 2002; Baumbach et al., 2014), *srebp* and it's target genes (e.g. *fatty acid synthase (fas), acetylCoA synthase (acs)*) which are involved in the synthesis of fatty acids (Dobrosotskaya et al., 2002). In the cholesterol auxotrophs *Drosophila*, phosphatidylethanolamine regulates the activity of SREBP. SREBP is a membrane bound transcription factor that is cleaved by the proteases S1P and S2P upon cellular demand for fatty acids, freeing the transcription factor domain from the membrane to enter the nucleus and to direct the increased transcription of target genes. Regulator genes of lipolysis are e.g. lipases like *brummer*, the *Drosophila* homologue of human adipocyte triacylglyceride lipase (Grönke et al., 2005) and *lipase 3*, which is highly up regulated upon starvation (Zinke et al., 1999). Lipase 3 is expressed in the larval fatbody and shows high similarity to lysosomal lipases from human and rat (Pistillo et al., 1998).

1.7 Proteases

Proteases (peptidases, proteinases, proteolytic enzymes) are a group of enzymes whose catalytic function it is to hydrolyze peptide bonds. Depending on the active site residue or ion that carries out the catalysis they can be divided into five groups: serine, threonine, cysteine, aspartic and metallo proteases. The activity of proteases is highly regulated. Substrate recognition and specificity depends on a variety of factors such as structural properties of the active site, subcellular compartment and surface accessibility.

In the past, proteases were considered primarily as protein degrading enzymes involved in the digestion and the removal of miss-folded proteins. Now this view has changed as they are known to be important players in signaling events (Ehrmann and Clausen, 2004). Yet, only a minor subset of physiological substrates and protease has been identified (Turk et al., 2012). They play a role in important signaling cascades such as the regulation of apoptosis, unfolded protein response (UPR) and development (Hay and Guo, 2006; Patil and Walter, 2001; Ye and Fortini, 2000). Proteolysis

can influence signaling e.g. by the removal of regulatory proteins/domains (e.g. Caspases, Spaetzle (Toll ligand), Hedgehog) and the influence on a protein's subcellular localization like the release of a formerly membrane tethered domain (e.g. SREBP, Notch, Amyloid Precursor Protein (APP), ATF6). Proteolytic cleavage of a protein can also occur within their transmembrane domains (regulated intramembrane proteolysis; RIP) which has also been shown for the cleavage of SREBP by S2P (Rawson, 2003).

1.8 Aims

Aim of this thesis was the further analysis of the the domain specific function of the *Drosophila melanogaster* Ceramide Synthase Schlank, especially focusing on the homeodomain and the nuclear localization. Additionally, the putative endoproteolytic processing that has been observed was investigated in more detail.

The transmembrane topology of the Schlank protein could solve, whether the homeodomain faces the cytosol -and therefore, the nucleoplasm- enabling DNA-interaction. A *schlank knock out* line should be established based on a method published by Huang et al. (2009). With this method, specific distinct mutations can be introduced into the *schlank* sequence making it possible to study the mutation's impact on fly physiology without dealing with over expression and wildtype background artifacts. First mutations analyzed affect the nuclear localization signals and the catalytic activity of the Schlank protein. Additionally, the observed feeding dependent endoproteolytic processing of the Schlank protein should be analyzed in more detail, including the occurrence in different states (e.g. development, mutants) and the cleavage site.

2 Material

2.1 General materials

Chemicals

Chemicals were purchased from Roche, Promega, Merck, Roth, Invitrogen, Sigma-Aldrich, Bio-Rad, Stratagene, Qiagen, Machery-Nagel and Fermentas.

Consumables

Common laboratory equipment	Faust, Schütt
test/reaction tubes	Roth, Eppendorf
Plastic wares	Greiner
microscope slides	VWR
PVDF membrane	Merck Millipore
Screw cap glasses	Pyrex, Bibby Sterlin Ltd
X-ray films	Fuji Medical X-Ray Film Super RX; BW Plus
$[^{14}C]$ Acetic acid	GE (Amersham)

Equipment

Autoclave	H+P Varioklav Dampfsterilisator EP-2
Agarose gel chambers	Peqlab
Bacteria incubator	Innova 44 New Brunswick scientific
Balances	Sartorius BL 150 S
	Sartorius B211 D
Binocular	S2X 12 and SZ 40, Olympus
	Stemi 2000, Zeiss
Blotting eqipment	BioRad
Centrifuges	J-26 XP, Avanti
	X 15R, Allegra
	AV-720, Beckmann Coulter
	5415 R and 5424 R, Eppendorf
Confocal microscope	Zeiss LSM710
Developer machine	Curix 60 AGFA

Electro pipette	Accu Jet
Gel documentation	Alpha Digi Doc, Biozym
Homogenizer	Precellys Peqlab
Imaging plates (Screens)	GE
PCR machine	C1000 Thermal Cycler BioRad
	MJ Research PTC-200 Peltier Thermal Cycler
Photometer	Nano Drop 2000 PeqLab
pH-Meter	FiveEasy FE20, Mettler Toledo
Pipettes	Eppendorf Research
Plate reader	Fluostar Omega (BMG Labtech)
RealTime PCR machine	iCycler BioRad
Speed-Vac	Speed-Vac SPD 111, Savant
Thermomixer	Thermomixer comfort, Eppendorf
Ultrasonic apparatus	Bandelin SONOPLUS HD2070
Voltage source	Power Pac BioRad
Vortexer	Vortex Genie2
Water bath	Julabo SW22

Software

Adobe Photoshop
Alpha Digi Doc Biozym
CellF Olympus
Clone Manager Sci-Ed
Fiji is just ImageJ
iQ5-Optical System Software Bio-Rad
Microsoft Office 2010
Primer3
Scribus
Zen Light 09 Zeiss

Standards and kits

Nucleic Acid & Protein Purification, NucleoBond, PC 100	Macherey & Nagel
BCA Protein Assay	Pierce
ECL Western Blotting Substrate	Pierce
SuperSignal West Pico, SuperSignal West Femto	
Restore Western Blot Stripping Kit	Pierce
iQTM SYBR Green Supermix	Biorad
QuantiTect, Reverse Transcription Kit	Qiagen
Ready-to-use System for fast Purification of Nucleic Acids, NucleoSpin, Extract II	Macherey & Nagel
Nucleic Acid & Protein Purification, NucleoSpin, RNAII	Macherey & Nagel
NucleoSpin RNA/Protein	Macherey & Nagel
PCR Nucleotide Mix	Roche
Q5 Site-Directed Mutagenesis Kit	NEB
NucleoSpin RNA XS	Macherey & Nagel
DAPI-Fluoromount G	Biozol
NucleoSpin Plasmid QuickPure	Macherey & Nagel
2-Log DNA ladder	NEB
Precision Plus Protein All Blue Standards	Biorad

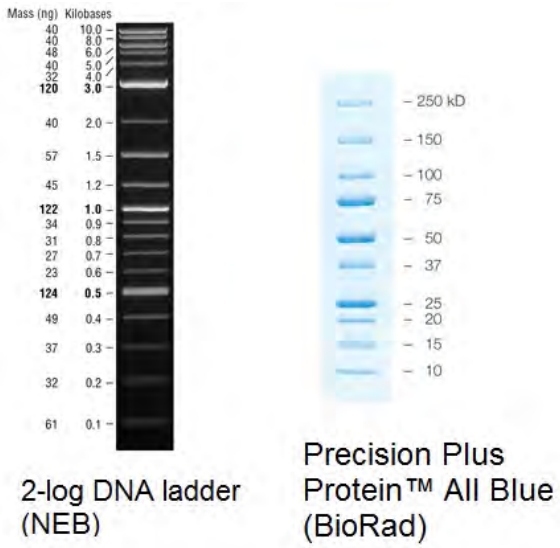

Figure 2.1: Nucleic acid and protein standards.

2.2 Buffers and solutions

Unless otherwise noted, all buffers and solutions were made with double distilled water (A. bidest) and were kept at RT.

General solutions

PBS$^-$ (pH 7,2)	133 mM	NaCl
	2,7 mM	KCl
	8,1 mM	Na_2HPO_4
	1,5 mM	KH_2PO_4
10x TBS (pH 7,5)	100 mM	Tris
	500 mM	NaCl

Work with nucleic acids

Squishing buffer (SB) (pH 8,2)	10 mM	Tris-HCl
	25 mM	NaCl
	1 mM	EDTA
		freshly add
		200 μg/μl Proteinase K
Proteinase K - stock solution	20 mg/ml	Proteinase K
DNA-loading dye (6x)	0,25 % (v/v)	Bromphenolblue
	0,25 % (v/v)	Xylencyanol
	30 % (v/v)	Glycerol
SYBR Safe	10 mg/ml	SYBR Safe (Invitrogen)
		protect from light
TAE-Puffer (pH 8,0) (10 x)	2 M	Tris
	100 mM	EDTA
		adjust pH with acetic acid
Sodium acetate s (pH 4,8)	3 M	Sodium acetate
		autoclave 1 h
RNase	20 mg	RNase A
		ad 10 ml. A. bidest.,
		15 min at 100°C
		store aliquots at -20°C

Alkali 1	50 mM	D(+)-Glukose
	25 mM	Tris
	10 mM	EDTA
		freshly add 1 μl/ml RNase
Alkali 2	0,2 M	NaOH
	1 %	SDS
Alkali 3	3 M	Potassium acetate
	5 M	Acetic acid

Work with protein

RIPA (pH 7,2)	10 mM	Na_2HPO_4
	10 mM	NaH_2PO_4
	0,1 %	SDS
	40 mM	Sodium fluoride
	2 mM	EDTA
	1 %	Triton-X-100
	0,1 %	Deoxycholate
	1x	complete protease inhibitor
5x Laemmli (pH 6,8)	100 mM	Tris-HCl
	3 % (w/v)	SDS
	10 % (v/v)	Glycerol
	0,01% (w/v)	Bromphenol blue
	5 % (v/v)	2-Mercapto-ethanol
SDS-Running buffer 10x	0,25 M	Tris
	1,92 M	Glycine
	1 % (w/v)	SDS
Transfer-buffer (10x)	0,25 M	Tris
	1,5 M	Glycine
Transfer-buffer (1x)	100 ml	Transfer-buffer (10x)
	200 ml	Methanol
	ad 1 l	A. bidest
1x TBS-T	0,2 % (v/v)	Tween 20 in 1x TBS
Blocking solution	7 % (w/v)	Milk powder in TBS-T

Stainings

PBT	0,2 %	Triton X 100 in 1x PBS
Phospate buffer (pH 7,2)	36 ml 14 ml 50 ml 40 mM	Na_2HPO_4 0,2 M NaH_2PO_4 0,3 M A. bidest Natriumfluorid
Methylene blue	1 g 6 g 1 g ad 100 ml	Methylen blue Borax Boric acid A.bidest
Toluidine blue	1 g 6 g 1 g ad 100 ml	Methylen blue Borax Boric acid A.bidest
Toluidine blue stain	1:1	Methylene blue:Toluidine blue

2.3 Media

Ampicillin-Stocks.	5 % (w/v)	Ampicillin ad 50 ml A.bidest store aliquots at -20°C final conc. in selection media 50 μg/ml
LB-Agar (pH 7,4)	1,5 % (w/v) 1 % (w/v) 1 % (w/v) 0,5 %(w/v)	Agar NaCl Trypton Yeast-Extract ad 1 l, autoclave if necessary add antibiotics
LB-Medium (pH 7,4)	1 % (w/v) 1 % (w/v) 0,5 %(w/v)	NaCl Trypton Yeast-Extract ad 1 l, autoclave

Injection buffer, pH 6.8	5 mM	KCl
	0,1 mM	$NaPO_4$
Nipagine-solution	147 ml	Ethanol
	63 ml	A. bidest
	21 g	Nipagine
Apple juice agar	1 l	Apple juice
	100 g	Sugar
	85 g	Agar
	40 ml	Nipagine (15 %)
	3 l	A.bidest
Fly food	80 g	Agar
	165 g	Dry yeast
	815 g	Maise flour
	1 l	Zuckerrübensirup
	10 %	Nipagine
	11 l	Water

2.4 Enzymes

Complete Protease-Inhibitors	Roche
DNase I	Roche
Go-Taq Polymerase	Promega
T4-Ligase	Roche
Phusion Hot Start II Polymerase	Thermo-Scientific
PNGase F	New England Biolabs
Proteinase K	Roth
rAPid Alkaline Phosphatase	Roche
Restriction endonukleases	New England Biolabs
RNase A	Sigma Aldrich

2.5 Antibodies

The following antibodies were used in the concentrations indicated. IF immunofluorescence analysis, IB immunoblotting.

Primary Antibodies

Antibodies	**Host species**	**Dilution**	**Company/ Reference**
αSchlank CT	guinea pig	IB: 1:500	pHD thesis Andre Voelzmann
	sheep	IF: 1:50	
αSchlank HOM	rabbit	IB: 1:250	Bauer et al. (2009)
αLamin	mouse	IF: 1:20	DSHB
αSpectrin	mouse	IF: 1:20	DSHB
αActin	rabbit	IB: 1:500	Sigma
αHA	rat	IF: 1:100, IB: 1:400	Roche
αGFP	rabbit	IB: 1:200	Santa Cruz Biotech
	mouse	IB: 1:200	Santa Cruz Biotech
	goat	IB: 1:200	Santa Cruz Biotech
	chicken	IF: 1:100	Abcam

Secondary Antibodies

Antibodies	**Host species**	**Dilution**	**Company/ Reference**
Alexa 488 anti-mouse	goat	IF: 1:200	Molecular Probes
Alexa 488 anti-chicken	goat	IF: 1:200	Molecular Probes
Alexa 647 anti-rat	goat	IF: 1:200	Molecular Probes
Cy3 anti-rat	goat	IF: 1:200	Molecular Probes
Cy3 anti-sheep	goat	IF: 1:200	Molecular Probes
HRP anti-rabbit	goat	IB: 1:10000	Santa Cruz Biotech
HRP anti-rat	goat	IB: 1:10000	Santa Cruz Biotech
HRP anti-guinea pig	goat	IB: 1:10000	Santa Cruz Biotech

2.6 Vectors

Vector	Reference/Source
pUAST	Brand and Perrimon (1993)
pGX-attP	Huang et al. (2009)
pGE-attB	Huang et al. (2009)
pAc 5.1	Invitrogen

2.7 Oligonucleotides

Following primers were used for qRT-PCR, genotyping and cloning. Mutations introduced via mutagenesis PCR are written boldly. Primer names starting with Q- indicate the use of the Q5 mutagenesis kit (NEB). Restriction sites are noted in the primer name or application column.

qRT-Primer

Gene	Sequence for primer (5'→ 3')	Sequence rev primer (5'→ 3')
rp49	gctaagctgtcgcacaaatg	gttcgatccgtaaccgatgt
actin	gtgcaccgcaagtgcttctaa	tgctgcactccaaacttccac
schlank	gccaactacaaggacctc	atgccaagtgatttgcct
lipase3	tgagtacggcagctacttccct	tcaacttgcggacatcgct
brummer	acgcacagcagcgacatgtat	cttttcgctttgctacgagcc
akh	ggtcctggaacctttttcgag	ttgcacgaagcggaagatc
srebp	cgcagtttgtcgcctgatg	cagactcctgtccaagagctgtt
fas	ccccaggaggtgaactctatca	gacttgaccgatccgatcaac
acs	aaatcccatggaccgatgac	tgtagagcatgaacaatggatcct
midway	aagacaggcctctactattgt	cccatcatgcccataaatgcc
pink	gctttcccctaccctccac	gcactacattgaccaccgatt
parkin	agcctccaagcctctaaatg	cacggactctttcttcatcg
usp30	ttcgctaaactaccggcctg	gctctcggggaagtgtacat
atg1	aggattcagtctcccaatcttgtactg	cagtacaagattgggagactgaatcct
atg8	cgtcattccaccaacatcgg	gccatgccgtaaacattctc
atg18	gccattggaatgtgaaatgct	ggcaactcaaatatcaaagcga

Primer for genotyping

PCR and genotype	Sequence for primer (5'→ 3')	Sequence rev primer (5'→ 3')
PCR 3'HR ($schlank^{KO}$)	ttcgggcccgacgcaaggag	cgaaatggcggcaggtccaattg
PCR 5'HR ($schlank^{KO}$)	agccggcaacgaatttcccacaaaatatta	ggttaccccagttggggcactac
PCR 1 ($schlank^{KO}$)	tccatcatacacactatatatgcctgc	tggtacggctacccgcatcag
PCR 2 ($schlank^{KO}$)	gtaagtgtggagccatgtggcc	ccggcagatcctttatccgatgg
PCR attR ($schlank^{KI}$)	gcgacgacaggtgtgtgtgcg	cagatagataaactgagggccagataatg
PCR attL ($schlank^{KI}$)	gggcgacacggaaatgttgaatactc	gaatgattttccatttattgaaatgaaactaggattc

Primer for cloning		
Primer name	**Primer sequence (5'→ 3')**	**Application**
		SCHLANK KO
5'HRschlankfor	cgagatccgcggcaattagcacctc tcattcatct	cloning of shorter 5'HR
5'HRschlankrev	cgagatggtacctgctatctatctt cgagaccgac	*Sac*II, *Kpn*I
fw5HRelongation	gcatgcaatgcggccgctaccgcgg cccactccatcttcaagttcct	elongation of 5'HR (final)
rev5HRelongation	ggttctttggattttggacgacg	
3'HRSlkBglIfor	cgagatagatctcgaaaaaaagcgg gacggcatcat	cloning of longer 3'HR
3'HRSlkAvrIIrev	cgagatcctaggccttgttctctac atcggataaacattctgagtaaac	
3'HRSlkBglIIfor	s.a.	cloning of 3'HR (final)
1,7kbrev3hrarm	gcttacctagggctgaacgcaacca aggtggg	
		SCHLANK KI
RescueSlkFLfor	tcagtggctagcgttccatagccaa gattacaatag	cloning
RescueSlkFLrev	tcagtgctcgagaaacacgtttgtt ttttggtc	*Xho*I, *Nhe*I
		mutagenesis:
NLS1rpkkrpmm for	agttctaggcct**atgatg**gcggcaaatg	NLS1
NLS1rpkkrpmm rev	catttgccgc**catcat**aggcctagaact	
NLS2rlrralar for	agcgctggtgg**gct**cta**gcc**agggcccagg	NLS2
NLS2rlrralar rev	cctgggcggt**ggc**tag**agc**ccaccagcgct	
lagH215D for neu	cagatgttcatc**gat**cacatggtcacc	H215D
lagH215D rev neu	ggtgaccatgtg**atc**gatgaacatctg	
Q-E118A-for	ccaccagcg**cgc**gatttcgcg	E118A
Q-E118A-rev	cgtctacgc**agagctc**aggataaacc	*Psp*OMI → *Sac*I
		CELL CULTURE
HA-TAGLAG1NTfor	ggaattcaacatggactacccatac gatgttccagattacgctatattga atgagttcagcaatgta	cloning of HA-schlank *Eco*RI
SchlankXhoI-rev	gatctcgagctactcctctctccg ttccgttg	

		mutagenesis of pAcHAschlank:
N21Q-for	tggctgccgccg**caa**acaacctgggcg	N21Q
N21Q-rev	cgcccaggttgtttgcggcggcagcca	
K94N-for	aagacctatgcc**aac**tcgacgcgattg	K94N
K94N-rev	caatcgcgtcgagttggcataggtctt	
P130N-for	gcccaggataaa**aat**tcaacgctggtg	P130N
P130N-rev	caccagcgttgaatttttatcctgggc	
63-NST-64-for	gctacacgctggagcgtttca**actcaacg** tggatatcgcccgtaggcaa	63NST64
63-NST-64-rev	ttgcctacgggcgatatccacgttgagtt gaaacgctccagcgtgtagc	
74-NST-75-for	**gg**caaatcacttggcatatacccatac gatgttccagattacgct**aactcaacg** tctagacgtagttctaggcctaag	74NST75 *Xba*I
74-NST-75-rev	cttaggcctagaactacgtctagacgttg agttagcgtaatctggaacatcgtatggg tatatgccaagtgatttgcc	
84-NST-85-for	ggcctaagaaagcggcaaat**aactcaacg** gttcctattctggagaagac	84NST85
84-NST-85-rev	gtcttctccagaataggaaccgttgagtt atttgccgctttcttaggcc	
105-NST-106-for	acaagaaaaagctggttccg**aactcaacg** ctgtccaagcagacggatat	105NST85
105-NST-106-rev	atatccgtctgcttggacagcgttgagtt cggaaccagctttttcttgt	
119-NST-120-for	gcgagcgcgaaatcgagcgc**aactcaacg** tggtggcgtctacgcagggc	119NST120
119-NST-120-rev	gccctgcgtagacgccaccacgttgagtt gcgctcgatttcgcgctcgc	
178-NST-HA-179-for	ccgcatcagtcgatc**aactcaacgtaccca** **tacgatgttccagattacgcttctaga** agcaatgatatctgg	178NSTHA179 *Xba*I
178-NST-HA-179-rev	ccagatatcattgcttctagaagcgtaat ctggaacatcgtatgggtacgttgagttg atcgactgatgcgg	
Q-301-for	**tacccatacgatgttccagattacgct** ccagcctactacatc	301NSTNSTHA302 *Eco*RI
Q-301-rev	**cgttgagttgaattccgttgagtt** gaacatgggcagaat	
348-NST-EcoRI-for	gatagtgag**aactcaacggaattc** gatctcacagacagt	348NST349 *Eco*RI
348-NST-EcoRI-rev	tgtgagatcgaattccgttgagtt	

	ctcactatcactgga	
98-STOP-XhoI-for	aaatcgacgcgattg**tagctcgag** aagctggttccgctg	98STOP *Xho*I
98-STOP-rev	cagcggaaccagctt**ctcgagcta** caatcgcgtcgattt	
138-STOP-XhoI-for	gtgaagttctgcgagtagctcgag cgttgcatctactat	138STOP *Xho*I
138-STOP-rev	atagtagatgcaacgctcgagcta ctcgcagaacttcac	
HA-TAGLAG1NTfor	ggaattcaacatggactacccatac gatgttccagattacgctatattga atgagttcagcaatgta	HAschlank 1-88
88stop-XhoI-rev	gatctcgagttacagaataggaaca tttgccgctttc	
HA-TAGLAG1NTfor	s.a.	HAschlank 1-108
108stop-XhoI-rev	gatctcgagttacttggacagcggaa ccagctttttc	
		UAS LINES
		cloning of:
HA-TAGLAG1NTfor	s.a.	HAschlank 1-98
1-98-stop-XhoI-rev	gatctcgagttatcgcgtcgatttg gcataggtctt	
99-400-EcoRI-for	gatgaattcatggacaagaaaaagc tggttccgctg	schlank 99-400HA
Schlank-HA-XhoI-rev	gatctcgagctaagcgtaatctgga acatcgtatgggtactcctctctcc gttccgttg	
		DELETION CONSTRUCTS
HA-TAGLAG1NTfor	s.a.	HAschlankMYC
MYC-LAG1-CT-rev	ccgctcgagcggttacagatcctct tcagagatgagtttctgctcctcct ctctccgttccgttgtcgcaa	
HA-TAGLAG1NTfor	s.a.	HAschlankGFP
GFP-rev	tctgggccctcacttgtacagctcg tccatgc	
		mutagenesis of pUAST HAschlankMYC:
del1-for	atgagcgagcgcgaaatcgagaaac	del119-128

	cgtcaacgctggtgaag	
del1-rev	cttcaccagcgttgacggtttctcg	
	atttcgcgctcgctcat	
del2-for	cgtctacgcagggcccaggataaca	del129-138
	cgtggcgttgcatctac	
del2-rev	gtagatgcaacgccacgtgttatcc	
	tgggccctgcgtagacg	
del3-for	acgctggtgaagttctgcgagttca	del139-148
	tctttggcgtgatcgtg	
del3-rev	cacgatcacgccaaagatgaactcg	
	cagaacttcaccagcgt	
del4-for	tgggacaagccctggttttggcatc	del165-174
	agtcgatcagcaatgat	
del4-rev	atcattgctgatcgactgatgccaa	
	aaccagggcttgtccca	
dFur-for	tcgagcgctggtggggtctacgcgg	122
	ggcccaggataaaccg	RLRR → GLRG
dFur-rev	cggtttatcctgggccccgcgtaga	
	ccccaccagcgctcga	
		mutagenesis of pUAST HAslakGFP:
Q-del-minus3-for	gacaagaaaaagct**t**gttccgctgtccaa	del89-98
Q-del-minus3-rev	cagaataggaacatttgccgctttcttagg	*Hind*III
Q-NL-for	aaaaagctggttccgctgtccaagcag	del95-100
Q-NL-rev	tttggcataggtcttctc**g**agaataggaac	*Xho*I
Q-delH2-for	acggatatgagcgagcgc	del101-109
Q-delH2-rev	cttgtccaatcgcgtcgatttggcataggtc	*Xho*I
	ttctc**g**ag	
Q-del-90-110-for	gatatgagcgagcgcgaa	del90-110
Q-del-90-110-rev	ctc**g**agaataggaacatttgc	*Xho*I
HeGFPdel-1F	ggcatacgtagttctcagcctcagc	3xNLS
	aagcggcaaatgttcctattctgga	(mutagenesis on
	gaagacctatgccaaatcgacgcga	pUAST
	ttggacgaggaagagctggttccgc	HAschlank)
HeGFPdel-1R	gacggtttatcctgggcttgctgta	
	gctgccaccagcgctcgatttcgcg	
	ctcgctcatatccgtctgcttggac	
	agcggaaccagctcttcctcgtcca	

2.8 Bacterial strains

Bacterial strain used for plasmid amplification.

***E.coli*-strain**	**Genotype**	**Source**
DH5α	F-*end*A1 *deoR* (φ*80lacZ*ΔM15) *rec*A1 *gyr*A (Nal_r) *thi*-1 *hsd*R17 (r_K-, m_K+) *sup*E44 *rel*A1 Δ(*lac*ZYA-*arg*F)U169	Stratagene

2.9 Fly lines

Name	**Source/Reference**
white$^-$ *(w*$^-$*)*	Bloomington #6326
hsGal 4	Hoch lab stock collection
hs-flp;dicer2;act>CD2>Gal 4,UAS-GFP	Hoch lab stock collection
CG Gal 4	Bloomington #7011
UAS-HAschlank	Bauer et al. (2009)
UAS-schlankHA	Bauer et al. (2009)
UAS-schlank HA1-98	this thesis
UAS-schlank 99-400HA	this thesis
UAS-HAschlankMYC	this thesis
UAS-HAschlankGFP	this thesis
UAS-HAschlankMYC Δ119-128	this thesis
UAS-HAschlankMYC Δ129-138	this thesis
UAS-HAschlankMYC Δ139-148	this thesis
UAS-HAschlankMYC Δ165-174	this thesis
UAS-HAschlankMYC Δ122RLRR $\rightarrow$ GLRG	this thesis
UAS-HAschlankGFP Δ89-98	this thesis
UAS-HAschlankGFP Δ95-100	this thesis
UAS-HAschlankGFP Δ101-109	this thesis
UAS-HAschlankGFP Δ90-110	this thesis
UAS-HAschlank 3xNLS	this thesis
UAS-schlankRNAi	Bauer et al. (2009)
$schlank^{P(X)61} = schlank^{G0061}$	Bauer et al. (2009)
$schlank^{P(X)349} = schlank^{G0349}$	Bauer et al. (2009)
$schlank^{KO}$	this thesis
$schlank^{KI-WT}$	this thesis
$schlank^{KI-NLS1}$	this thesis
$schlank^{KI-NLS2}$	this thesis

$schlank^{KI-H215D}$	this thesis
$schlank^{KI-E118A}$	this thesis
dcerk mutant	Nirala et al. (2013)

3 Methods

3.1 Generation and treatment of transgenic flies

3.1.1 Fly handling

Fly keeping and propagation was carried out after standard procedures. Flies were kept on 25°C for experimental use unless otherwise mentioned and on 18°C - RT for stock keeping. For crosses, 1-30 virgins were crossed to approximately half to the same amount of male flies. For the collection of progeny crosses or fly stocks were transferred into cages where the flies lay their eggs on applejuice-agar plates with some fresh yeast paste put in the middle. Collections were carried out for different time points and afterward kept on 25°C until progeny was in the desired stage for the experiment. If necessary afterwards first instar larvae were sorted under the fluorescent binocular for the absence of the GFP or YFP marker on the balancer chromosome (e.g. FM7, dfdeYFP).

For nomenclature: different chromosomes are sepaprated by semicolon, different alleles of the same chromosome by slash, different constructs on the same chromosome by comma, wildtype chromosomes are +. If not mentioned otherwise fly lines were available in the laboratory.

3.1.2 P-element transgenesis

P-elements are mobile genetic elements that can be used as tools to create transgenes and mutations. Modified P-Elements are used as transformation-vectors in *Drosophila melanogaster* where one vector encodes the transposase (helper plasmid) and a second vector contains the inverted repeats flanking the sequence that should be inserted into the genome (Spradling and Rubin, 1982; Rubin and Spradling, 1982). Injections were carried out using standard procedures (Roberts et al., 1986) in the lab by Sabine Büttner or by the BestGene Inc.

Injections of pUAST vectors into white eyed flies (*white*$^{-}$, w^{1118}) enabled the identification of transgenes by red eye color, as pUAST encodes the *white* gene. Identification of the insertion chromosome was carried out by crossing to balancer fly lines. The fly stocks were kept homozygously or heterozygously over a balancer chromosome.

3.1.3 Gal4-UAS System

The Gal4-UAS system is an ectopic expression system to over express transgenes in a certain temporal and spatial manner in *Drosophila melanogaster* (Brand and Perrimon, 1993). Driver lines or activator strains express the yeast transcription factor Gal4 under the control of a certain enhancer. UAS lines or effector strains carry the upstream activator sequence (UAS) in front of a geneX. After crossing those lines Gal4 binds to UAS and the geneX is expressed.

3.1.4 Ends Out Gene Targeting

For a generation of a *schlank* null mutant/*schlank*^{KO} line with the possibility to re-introduce *schlank*-DNA, *Ends Out Gene Targeting* was performed (Huang et al., 2008, 2009). The target sequence is replaced by a donor sequence via homologous recombination. The donor sequence contains a *white* gene for selection flanked by loxP sites to allow the removal of the selection gene by crossing to a Cre-recombinase expressing fly line. Additionally, the donor sequence contains an attP site that allows the re-introduction of DNA-fragments targeted to the *schlank*^{KO} locus.

Generation of a *schlank knock out* line

5' and 3' homologous regions (HR) were cloned into the donor vector pGX-attP which contains the donor sequence, a *UAS-reaper* sequence, 5' and 3' P-element sequences and FRT and *Sce*I sites to excise and linearize the donor construct (see section **??**). The vector was used to generate the donor fly line via P-element transgenesis. Lines were selected for red eye color and insertion chromosome was found out (as the *schlank* gene is localized on the X-chromosome, donor lines were chosen were the P-element inserted on the 2nd or 3rd chromosome). Then, the donor lines were tested for their ability to mobilize the donor construct (by crossing to *yw/Y,hs-hid;hs-Flp,hs-I-SceI/CyO,hs-hid;+/+* flies, heat shock of the progeny to activate Flp and *Sce*I and screen for mosaic eyes resulting from the loss of the *white* gene where the mobilization occurred) and for the functionality of the apoptosis gene *reaper* (by crossing to

yw/Y;Pin/CyO;Gal4^{221w-}*/Gal4*$^{221w-}$ flies that express Gal4 under the control of a strong neuronal promotor and screening for pupal lethaliy). *UAS-reaper* allows the identification of false-positive lines as the sequence gets lost if homologous recombination was successful.

The generation of the *schlank*^{KO} line was carried out with the following crosses:

Targeting cross:

$$\frac{yw}{Y,hs-hid};\frac{hs-Flp,hs-I-SceI}{CyO,hs-hid};\frac{+}{+}\ \text{x}\ \frac{w}{w};\frac{P\{donor\}^{rpr+}}{P\{donor\}^{rpr+}};\frac{+}{+}$$

Before homologous recombination the donor construct has to be mobilized and linearized. FRT sites are recognized and recombined by the Flippase (Flp). The resulting circular DNA-fragment is linearized by *Sce*I. Both enzymes are expressed under the control of a *hs*-promotor. Crosses (≈30) were kept on 25°C, flipped every day and progeny was heat shocked in the water bath (38°C, 90 min) on day 2 and 3.

Screening cross:

$$\frac{yw}{Y};\frac{Pin}{CyO};\frac{Gal4^{221w-}}{Gal4^{221w-}}\ \text{x}\ \frac{yw}{schlank^{KO}};\frac{hs-Flp,hs-I-SceI}{\Delta donor^{rpr+}};\frac{+}{+}$$

From the targeting cross resulting mosaic eyed virgins were collected (male progeny carries the cell death gene *hid* induced by heat shock) and crossed to males of the "screening"-line. Noted here is the genotype after excision of the donor sequence and the *UAS-reaper* and successful homologous recombination. The majority of potential targeting events may be unspecific and not located on the X-chromosome.

Mapping cross:

$$\frac{FM6}{Y};\frac{+}{+};\frac{+}{+}\ \text{x}\ \frac{yw}{schlank^{KO}};\frac{Pin-or-CyO}{hs-Flp,hs-I-SceI-or-\Delta donor^{rpr+}};\frac{Gal4^{221w-}}{+}$$

Red eyed progeny from the screening cross that did not show any reaper phenotype were crossed to a balancer line. Only red eyed females were crossed as a *schlank*^{KO} would result in homozygous or hemizygous lethality like the stronger *schlank* mutant alleles. The progeny was then screened for male lethality (no males with red eyes should be obtained) and females with red and kidney shaped eyes (resulting from the bar mutation in the balancer) were crossed to males of the balancer line again to obtain a stable stock.

To screen for *schlank* related lethality females of the putative *schlank*^{KO} lines were crossed to males carrying the *schlank* mutant allele (*schlank*$^{P(X)349}$ on the X-chromosome and a duplication of the Y-chromosome:

$$\frac{schlank^{P(X)349}}{Y^{dp}};\frac{+}{+};\frac{+}{+}\ \text{x}\ \frac{schlank^{KO}}{FM6};\frac{+}{+};\frac{+}{+}$$

This should result in progeny with red eyed males (*schlank*^{KO}*/Y*^{dp}) but no red eyed females without "bar" eyes (*schlank*$^{P(X)349}$*schlank*^{KO} lethal).

The *schlank*^{KO} lines were kept as stable stocks over the balancers *FM7dfdeYFP* or *FM7krGal4UASGFP* to allow selection of *schlank*^{KO}/*Y* larvae. By crossing with a Cre expressing line a *white*$^{-}$ *schlank*^{KO} line was established.

Generation of *schlank knock in* lines

The *schlank* target sequence (deleted genomic DNA) was cloned into the integration vector pGE-attB-GMR. Mutations of the target sequence were introduced via mutagenesis PCR. Vectors were injected into the *white*$^{-}$ *schlank*^{KO} line by The BestGene Inc. φC31 integrase dependent re-integration results in the integration of the whole vector into the genome at the locus of the attP-site. Expression of the *white* gene will lead to red eyes as a selection marker. Red eyed flies were sent and balanced over *FM7dfdeYFP*. Lines were kept homozygously if possible.

3.1.5 Assays

Survival assay

For the survival assay, only male larvae were taken. Females of homozygous stocks were crossed to FM7dfdeYFP carrying males. Eggs were collected for 4 h on apple juice agar plates and approx. 15 larvae were sorted for the absence of the dfd-eYFP marker 44 h AEL and transferred to a new plate. Survival and larval stage was monitored every 24 h. Pupae were transferred to a petri dish with a filter soaked in PBS to avoid decomposing of the slow developing *schlank*$^{KI-NLS2}$. Experiment was repeated 5 times.

Measuring of larval size

Larvae were transferred into PBS and heated to 60°C for 10 minutes in a heating block. Images were taken with a Olympus SZX binocular and larval length was measured via CellF software.

Climbing assay

Up to 20 male flies of the analyzed genotypes were transferred into a measuring cylinder (30 cm long) and recovered from CO_2 treatment for 2 h. Flies were knocked down and the climbing was videotaped. This was done again 5 times and experiment was

repeated with different flies 3 times. For analysis, the video was stopped every 10 s and walking distance of each fly was monitored.

3.2 Cell culture

3.2.1 Cell handling and transfection

Schneider cells (S2) were grown in T75 flasks in PAN Schneider's medium supplemented with 10 % FCS and Pen/Strep at 25°C and were split 1:3-1:6 when too dense. Transfections were carried out using the reagent FectoFly (Promega) as per the manufacturers instructions.

3.3 Molecular biological techniques

3.3.1 Isolation of nucleic acids

Isolation of gDNA from flies

Genomic DNA (gDNA) was isolated from single flies (Gloor et al., 1993). The fly was anesthetized and mashed with a yellow pipet tip containing 50 μl sqishing buffer (SB) in a microzentrifuge tube. The rest of SB was ejected and tubes were kept on 25-37°C for 20-30 min. Then the Proteinase K was inactivated 2 min at 95°C. gDNA was kept at 4°C.

Isolation of plasmid DNA from bacteria

Analytical preparation (Mini Prep). 2 ml of LB medium containing the appropriate antibiotic and a master plate are inoculated with a single colony of transformed bacteria and are incubated in over night at 37°C with vigorous shaking. The culture is filled into a microcentrifuge tube and centrifuged at maximum speed for 1 min. The bacterial pellet is re-suspended in 100 μl alkaline lysis solution I, followed by the addition of 200 μl alkaline lysis solution II and inverting 6-8 times. Then, 150 μl of alkaline solution III are added and the mixture is inverted 6-8 times, followed by centrifugation at 12000 g for 6 min (at 4°C). The supernatant is transferred to a fresh tube containing 500 μl ethanol absolute, vortexed and centrifuged at 12000 g for 6 min (at 4°C). The pelleteted DNA is now washed with 70 % ethanol, the pellet is dried in the speed vac and then re-suspended in 100 μl water.

Preparative scale (Midi Prep). For the preparative scale DNA isolation the Nucleo Bond PC AX100 Kit from Macherey Nagel was used. 50 ml of LB medium containing antibiotics were inoculated and culture grew o.n. at 37°C and shaking. Plasmid was isolated as per the manufacturers instructions and dissolved in 100-150 μl autoclaved A.bidest and stored at -20°C.

Isolation of RNA from tissue

For the isolation of RNA larvae or flies were collected into buffer RA1. To isolate RNA from L1 larvae the Nucleospin RNA XS kit and to isolate RNA from L3 larvae and adult flies the Nucleospin RNA II kit was used as per the manufacturers instructions. Homogenization was obtained using Precellys 3x 15s 5000Upm. Beta-mercaptoethanol was added afterwards.

Photometric estimation of DNA/RNA concentration

Concentration of DNA or RNA was measured using the nanodrop2000.

3.3.2 Polymerase chain reactions (PCR)

Genotyping and colony PCRs

Genotyping and colony PCRs were carried out using GoTaq Polymerase (Promega) as per the manufacturers instructions. For colony PCR 25 μl master mix was provided in the wells of a 96-well plate. With a pipet tip bacterial colonies were touched, then a master plate was inoculated and then bacteria were transferred to the master mix by pipetting up and down. PCRs were analyzed in agarose gel electrophoresis.

PCR for molecular cloning

PhusionTaq (Hot Start II, Thermo-Scientific) was used for the amplification of genes that should be cloned into a vector. 4x50 μl reactions containing DMSO were pipetted and treated as per the manufacturers instructions.

Vector mutagenesis PCR

For direct mutagenesis of plasmids (point mutations, insertions and deletions) vector mutagenesis PCR was performed. For this, complementary missmatch primers were used to integrate the mutations into the template during the PCR reaction. If needed,

silent mutations resulting in a endonuclease restriction site were introduced as well. The PCR product contains the complete plasmid sequence with the included mutation(s), also in a circular nicked manner. After PCR reaction with standard reaction conditions (Phusion Taq), the template DNA (bacterial plasmid) was digested by the restriction enzyme *Dpn*I, which is specific for methylated DNA for 1 h, 37°C. Chemically competent bacteria were transformed with the PCR product and incubated on agar plates. The bacteria ligate the mutated PCR product to a circular plasmid.

For some mutations the Q5 Site-Directed Mutagenesis Kit (NEB) was used as per the manufacturers instructions or with halved reaction volumes. With this protocol, primers are not complementary or overlapping. The performed PCR reaction results in a linear product that is phosphorylated and blunt-ligated in the following KLD reaction.

Reverse transcription and real time qRT-PCR

Reverse transcription of RNA into copy DNA (cDNA) for qRT-PCR analysis was carried out using the QuantiTect Reverse Transcription Kit (Qiagen) as per the manufacturers instructions. 500 ng RNA (or as much as possible) were incubated with 1 μl gDNA wipeout buffer in a 7 μl reaction volume 3-5 min at 37°C. For the -RT control 1 μl of different RNA samples were pooled. Then, 2,5 μl RT-buffer/primer and 0,5 μl RT were added (except to the -RT control) and incubated for 30 min at 42°C followed by 3 min at 95°C. Then, 40 μl of water was added.

qRT-PCR was performed to analyze gene expression on mRNA level. Primer were designed with optimums for amplicon length (120 bp), primer length (20 bp), annealing temperature (59°C) and GC-content (50 %). Primer pairs were diluted to a concentration of 5 pmol/μl in A.bidest. Primer efficacy was tested in a dilution series with additional test for the formation of primer dimers in a melting curve analysis. Only primers that had an efficacy of more than 80 % were used.

Reactions were performed in duplicates or triplicates in 96-well plates in a 15 μl reaction volume as follows:

qRT-PCR reaction	
0,75 μl	cDNA
6 μl	A.bidest
0,75 μl	Primer pair
7,5 μl	SYBR-Green supermix

The BioRad I-cycler with an IQ5 optical system was used, using fluorescence of SYBR-Green supermix (BioRad)/DNA complexes to detect amplification of DNA after each PCR cycle. The following program was used:

PCR-program

step 1	denaturation and initiation of polymerase	95°C	3 min
step 2	denaturation	95°C	10 s
step 3	annealing	50°C	20 s
step 4	elongation	72 °C	15 s

45 PCR-cycles of step 2-4

Control conditions included -RT samples, where no Reverse Transcriptase was added, and water controls. Data was calculated according to the ΔΔ-CT method by the Bio-Rad software. Expression was normalized to housekeeping genes (rp49 and actin5c) and compared to a control condition which was set to 1. Analysis was carried out with at least three, usually 5-7 independent biological replicates.

3.3.3 Molecular cloning

For classical cloning cDNA or gDNA was amplified via PCR using 4 reactions of PhusionTaq. Endonuclease resitriction sites and/or small tags were inserted into the primer sequences. Reactions were loaded on agarose gels containing SYBR Safe (Invitrogen) and after electrophoresis bands were excised under UV light and DNA was extracted using Nucleospin Extract II kit. Insert was eluted in 17-43 μl A.bidest.

Vector and insert were digested using type II restriction endonucleases (NEB) in a 50 μl reaction volume (1-2 h, 37°C) and vector backbone was dephosphorylated with alkaline phosphatase (Roche, 20 μl reaction volume, 20 min 37°C, then 2 min, 72°C).

DNA fragments were ligated with T4-DNA-ligase (NEB) 1-2 h at RT. Usually, 1 μl vector and 7 μl insert were incubated with 1 μl fresh T4-DNA-ligase buffer and 1 μl T4-DNA-ligase.

After ligation plasmids were transformed into bacteria: 50 μl chemically competent *E.coli* were thawed on ice, the ligation mixture was added and incubated on ice for 20 min. Then, a heat shock was applied (1 min, 42°C) and after a short incubation on ice, LB0 was added and the mixture was placed in a gently shaking heat block (37°C, 1 h). Bacteria were grown over night on agar plates with appropriate selection media at 37°C.

Selection of positive clones was performed with Mini prep and enzymatic digestion of

10 μl in a 20 μl reaction volume or colony PCR followed by agarose gel electrophoresis. Additionally, positive clones were analyzed by sequencing by Seqlab (Göttingen).

3.4 Biochemical techniques

3.4.1 Protein biochemistry

Preparation of protein extracts

Protein extracts were prepared on ice in RIPA buffer or directly in 2xLaemmli. Homogenization was carried out either using a pistil fitting the microcentrifuge tube or Precellys (3x 15s 5000Upm). Samples were sonicated and centrifuged. Supernatant was transferred to a new tube and protein concentration was determined with the BCA assay or absorbance at 280 nm.

Determination of protein concentration using BCA-reagent

Protein concentration was determined with the BCA kit from Thermo Scientific. For few samples assay was carried out in microcentrifuge tubes (sample ad 50 μl, BCA reagent 950 μl), for many in a 96-well plate (sample ad 10 μl, BCA reagent 200 μl). Absorbance was measured in the Nanodrop or a plate reader, respectively. Standard curve was always prepared in parallel with BSA in the respective buffer.

SDS-PAGE and transfer of proteins on PVDF membrane

Discontinuous sodium-dodecyl-sulfate-polyacrylamide-gel-electrophoresis (SDS-PAGE) was used for the separation of proteins according to their molecular weight (Laemmli, 1970). Different polyacrylamide concentrations lead to different pore sizes which can be used to efficiently separate different proteins.

Laemmli buffer was added to the samples, cooked and loaded on the gels which were run at 20 mA/stacking gel, 25 mA/separating gel.

For antibody detection separated proteins were transferred to a PVDF membrane via tank blotting. The PVDF membrane was activated in methanol and placed together with the gel between 3 layers of whatman paper and foam pads in transfer buffer. The membrane was oriented to the anode, whereas the gel was oriented to the cathode. The blotting apparatus was filled with the holder, an ice block and transfer

component	separating gel (2 gels, 10 %)	(2 gels, 15 %)	stacking gel (5 %)
A.bidest	2,5 ml	3,55 ml	3,6 ml
Acrylamide (40 %)	4,8 ml	3,75 ml	630 μl
1,5 M Tris-HCl pH8,8	2,5 ml	2,5 ml	-
1,0 M Tris-HCL pH6,8	-	-	630 μl
10 % SDS	100 μl	100 μl	50 μl
10 % APS	100 μl	100 μl	50 μl
TEMED	10 μl	10 μl	5 μl

buffer and transfer was carried out 1 h, 100 V. Transfer was checked with PonceauS staining.

Antibody binding and ECL detection

After the transfer of separated proteins on a membrane, the membrane was blocked in 7 % milk powder in TBS-T for 1 h followed by incubation with primary antibodies over night at 4°C in TBS-T. After 3 washing steps with TBS-T the membrane was incubated with secondary HRP conjugated antibodies 1 h at RT. After 3 more washing steps (10 min, TBS-T, RT) detection was carried out with ECL reagent (Pierce). Chemiluminescence was visualized on X-ray films and a curix60 developer machine.

Deglycosylation of proteins

Deglycosylation of protein in whole extracts was carried out using PNGaseF (NEB) as per the manufacturers instructions.

3.4.2 Scanning-N-glycosylation mutagenesis

Analysis of transmembrane topology was carried out with Scanning-N-glycosylation mutagenesis (Cheung and Reithmeier, 2007). Glycosylation sites (NST) were introduced at different positions into the *schlank* sequence using mutagenesis PCR and the cell culture expression vector pAc-HA-schlank. Vectors were transfected into S2 cells in a 12-well plate and when green fuorescence was visilble in the control well (transfected with pAc-GFP) after 24-72 h cells were harvested, washed and lysed in RIPA buffer. Analysis was then performed with western blotting using the α-HA antibody.

3.4.3 Analysis of Triacylglycerols (TAG)

Lipids were extracted from larvae with chloroform/methanol extraction. Larvae were collected and washed in water (3-5 L3 larvae, 30-50mutant L1). They were homogenized in 150 μl A.bidest using Precellys (3x 15s 5000Upm) and protein concentration was determined with the BCA assay. 100 μl of the lowest concentrated sample were taken and the other samples protein content was adjusted to that (in a 100 μl volume in microcentrifuge tubes). 3.75 Vol (375 μl) of chloroform/methanol 1:2 were added, vortexed properly, then 1.25 Vol (125 μl) of chloroform was added, vortexed and 1.25 Vol (125 μl) of A.bidest was added, vortexed and centrifuged for 1 min at full speed. The lower phase was transferred completely to a new tube and dryed in the SpeedVac for approx. 20 min at 45°C. Dried lipids were dissolved in 15-20 μl chloroform/methanol 1:1.

Thin layer chromatography (TLC) was performed using the running solvent 70:30:1 n-hexane/di-ethyl-ether/acetic acid and a HPTLC silica gel plate (Millipore). 1,5 cm were left to sides and bottom, spacers between lanes were marked with a pencil. Samples were added. Standards were prepared from butter or oil or commercially available TAG etc in chloroform/methanol 1:1. After migration the plate was dried and incubated for 10-30 s in a bath of 10 % copper sulfate and 8 % phosphoric acid (in water). The plate was dried leaning against something and then baked in a preheated oven (180°C, top and bottom heating) until bands appeared well. Plates were scanned and band intensity was analyzed using ImageJ/Fiji.

3.4.4 *in vivo* CerS assay/metabolic labeling of lipids

Ceramide synthase activity was determined by measuring *de novo* ceramide generation after 12 h labeling of larvae with $[^{1-14}C]$- acetic acid. For metabolic labeling, larvae were fed with inactivated yeast paste containing $[^{14}C]$- acetic acid (61 Ci/mol) as a C1-precursor for lipids. Larvae were homogenized, lyophilized and weighed. Lipids were extracted in chloroform/methanol/water (2:5:1 v/v/v). Same amounts of radioactivity of the desalted lipid extract were applied to each line on the TLC plates. Unpolar lipids (fatty acid, triacylglycerol) were separated with n-hexane/di-ethyl-ether/glacial acetic acid (70:30:1, v/v/v) and ceramides with chloroform/methanol/glacial acetic acid (190:9:1, v/v/v). Radioactive bands were visualized with a Typhoon FLA 7000 (GE, Germany) and quantification was performed with the image analysis software ImageQuantTL (GE, Germany). Lipids were identified using commercially available

reference standards (ceramide (C18:1/C18:0) (Sigma, Germany), phytoceramide (Cosmoferm, Delft, Netherlands), trioleoylglycerol (Sigma, Germany), and stearic acid (Fluka)). Assay was performed in collaboration with Dr. Bernadette Breiden, AG Sandhoff.

3.5 Stainings

3.5.1 Immunofluorescent stainings of larval fatbody

Wandering L3 larvae were ripped open in ice cold PBS either like a sardine can or prepped inside out and directly transferred to ice cold methanol free formaldehyde (4 % in PBS). The following fixation step was for 50-60 min at RT on a rotating wheel. Afterwards larvae were washed several times with PBT, blocked 1 h 5 % goat serum in PBT and incubated with first antibodies over night at 4°C. After several washing steps and a second blocking step for half an hour incubation with fluorescent coupled secondary antibodies followed for 2 h at RT. Samples were washed 6x 10 min with PBT, then fatbody was prepped and mounted in Fluoromount Dapi.

3.5.2 Toluidin blue staining of brain sections

Flies were decapitated and fixed for 20 min in 25 % glutaraldehyde in phosphate buffer (0,1 M). After short washing steps with phosphate buffer heads were fixed in 1 % osmium/2 % glutaraldehyde for 30 min on ice in the dark and after additional short washing steps heads were fixed in 2 % osmium 60 min on ice in the dark, followed by short washing steps in A.bidest. After sequential dehydration to 100 % ethanol (50,70,90,96 %, 5 min on ice each, 100 % 2x 10 min), samples were washed twice for 10 min in 100 % acetone. The eyes were equilibrated in acetone araldite solution (1:1) at 4°C overnight. The solution was exchanged for araldite, eyes were incubated for more than 4 h at RT and then placed in molds and incubated at 60°C o.n. Brains were sectioned (1 μm), placed on slides and stained with toluidine blue stain. Samples were rinsed in water and mounted in DePeX for imaging.

3.5.3 Imaging

Antibody stainings were imaged with the Zeiss LSM710 system. Mean staining intensities were calculated for defined regions of interest in Fiji.

3.5.4 Statistical analysis

Significance was tested using an unpaired 2-tailed Student's t-test (Microsoft Excel) with at least 3 independent biological replicates (n). *p<0,05, **p<0,01, ***p<0,001.

4 Results

The aim of this study was the investigation of Schlank's dual function in sphingolipid biosynthesis and lipid homeostasis, and putative other roles in physiology. For this, it's membrane topology and glycosylation status was analyzed (section 4.1) . Also, a *schlank* knock out line was generated via homologous recombination replacing large parts of the open reading frame with an attP site. This attP site serves as a platform for the re-integration of different *schlank* versions into the endogenous locus enabling us to study the impact of specific Schlank modifications on organism function (sections 4.2-4.3). In addition, cleavage of the Schlank protein has been observed and further described in section 4.4.

4.1 Transmembrane topology of the Schlank protein

The Schlank homeodomain could only act as such if it faced the nuclear luminal space and thereby is in proximity to DNA. *In silico* analysis using different available transmembrane (TM) topology prediction programs that use different algorithms revealed several results, some of which are presented in figure 4.1A (Punta et al., 2007). Therefore, experimental analysis of the Schlank TM topology was carried out using scanning-N-glycosylation mutagenesis. This method is based on the fact that only parts of proteins that face the lumen of the ER (and if transported to the cell membrane the outside of the cell) are N-glycosylated. During the co-translational process the membrane associated oligosaccharyl transferase complex transfers a preformed oligosaccheride to an asparagine side chain located within the sequon (Asn-X-(Ser/Thr)). Glycosylation sites can be introduced into the protein sequence via cloning. The glycosylation status of the translated protein can be analyzed using immunoblotting as glycosylation influences the moving behavior of a protein in SDS-PAGE. Treatment of lysates with PNGaseF results in the removal of the attached sugar residues from all N-glycosylated proteins (Cheung and Reithmeier, 2007).

For Schlank, an endogenous glycosylation site was predicted at amino acids (AA) 21,

361 and 368 (GlycoEP). To study whether these sites are used N-terminally HA taged Schlank protein (HA-Schlank) was over expressed in larvae using the *hs-Gal4* driver line and in S2 cells using the expression vector pAc. The Schlank full length protein has a predicted molecular weight of approx. 47 kDa. Treatment with PNGaseF lead to a faster moving behavior of HA-Schlank in SDS-PAGE and therefore to a band shift. When *HA-schlank* was expressed that was mutated to render its glycosylation site inactive (*HA-schlankN21Q*) the over expressed protein showed a similar moving behavior as the non-mutated, deglycosylated protein and no band shift was observed upon treatment with PNGaseF (fig. 4.1B). This data suggests a single endogenous glycosylation site in the Schlank protein at AA 21. The prominent band at approx. 15 kDa that also showed a band shift after PNGaseF treatment of larval extracts is a putative Schlank N-terminal cleavage product that is further analyzed in section 4.4.

For scanning-N-glycosylation mutagenesis glycosylation sites were introduced into the Schlank protein sequence at different positions, an overview can be seen in table 4.1. The different, HA-tagged *schlank*-versions were expressed in S2-cells and analyzed via immunoblotting (fig. 4.1C). None of the glycosylation sites introduced into the homeodomain resulted in a shift in band size (fig. 4.1C, lane3-4,6-12), neither the glycosylation site introduced after the last putative TM (fig. 4.1C, lane20). However, when the glycosylation site was introduced after the second putative TM (178NST) or before the last putative TM (301NST) a band shift was observed (fig. 4.1C, lane13 and 18). When the endogenous glycosylation site was mutated, treatment with PNGaseF still resulted in a band shift (fig. 4.1C, lane14,15 and 21,22). This shows, that the artificially introduced glycosylation site was recognized by the oligosaccharyl transferase complex and that therefore, those parts of the protein face the luminal site of the ER.

Figure 4.1D shows the TM topology model based on the prediction programs but also on the experimental data just mentioned. As those parts of the Schlank protein around AA 21, AA 178 and AA 301 face the lumen of the ER, but most likely not the homeodomain and probably not the very last C-terminus (around AA 348) the Schlank protein most likely contains an uneven number of TM domains. Five TM domains as predicted e.g. by TMHMM (I) or seven TM domains as predicted e.g. by Phobius (II).

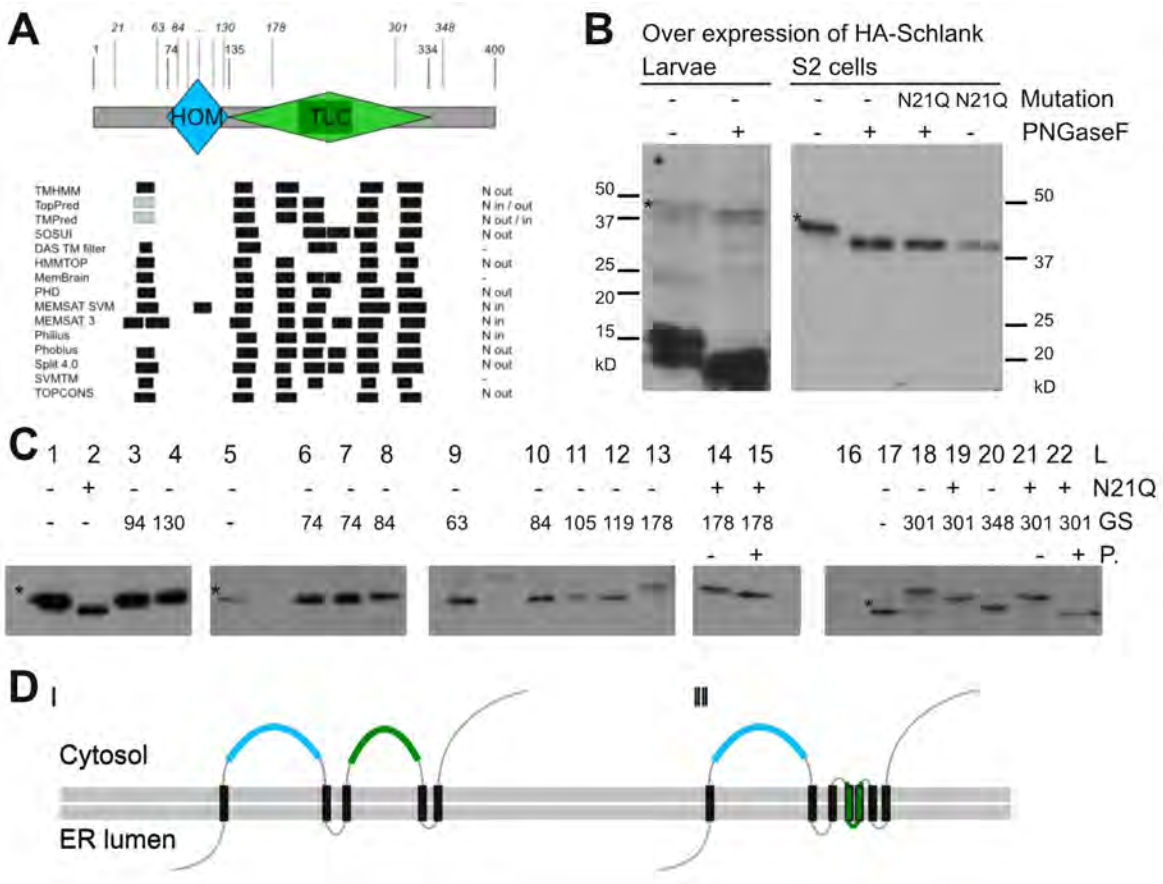

Figure 4.1: Schlank topology studies. **A**: Predictions for Schlank TM topology using different programs. Numbers represent AA positions, black or gray boxes represent predicted or putative TM domains, respectively. N in/out indicates the prediction of the localization of the Schlank N-terminus towards the in- or outside of the cell. Results from 15 different algorithms are shown. **B**: Glycosylation status of Schlank over expressed in larvae and S2 cells. Left blot shows the expression of HA-Schlank in L 3 larvae using the *hs-Gal4* driver line with and without treatment of PNGaseF, right blot shows the over expression of full length Schlank -with and without a mutation of the predicted N-glycosylation site at AA 21- in cell culture (pAcGal4 expression vector), Schlank full length is marked with a (*). **C**: Scanning-N-glycosylation mutagenesis. Glycosylation sites have been introduced into the Schlank sequence and moving behavior in SDS-PAGE has been analyzed. Non mutated HA-Schlank is marked with a * (lanes 1, 5, 17). Mutation of the endogenous glycosylation site (+-N21Q), the position of the introduced glycosylation site (GS) and PNGaseF treatment (+-P.) are indicated. For the closer description of glycosylation sites introduced see table 4.1. Lane 2: HA-SchlankN21Q; lanes 3, 4, 6-12 glycosylation sites introduced within the homeodomain; lane 20: glycosylation site introduced after the last putative TM; lane 13: glycosylation site introduced after the second putative TM; lane 18: glycosylation site introduced before the last putative TM; lanes 14 and 15, lane 21 and 22: additional mutation of the endogenous glycosylation site. Lane 16 shows a negative control. L:lane, GS: glycosylation site introduced, P:PNGaseF. **D**: TM models derived from experimental data. Homeodomain blue, lag motif green, TM black.

No.	Mutation	Position
21	N21Q, point mutation of endogenous glycosylation site	before 1st putative TM
94	K94N, point mutation resulting in a glycosylation site at AA 94	in homeodomain
130	P130N, point mutation resulting in a glycosylation site at AA 130	in homeodomain
63	63NST64, introduction of a glycosylation site after AA 63	before homeodomain
74	74NST75, introduction of a glycosylation site after AA 74	in homeodomain
84	84NST85, introduction of a glycosylation site after AA 85	in homeodomain
105	105NST106, introduction of a glycosylation site after AA 105	in homeodomain
119	119NST120, introduction of a glycosylation site after AA 119	in homeodomain
178	178NST-HA179, introduction of a glycosylation site and a HA-tag after AA 178	after putative 2nd TM
301	301NST-NST-HA302, introduction of 2 glycosylation sites and a HA-tag after AA 301	before putative last TM
348	348NST349, introduction of a glycosylation site after AA 348	after putative last TM

Table 4.1: Introduced mutations for scanning-N-glycosylation analysis.

4.2 Genomic engineering of the *schlank* locus

The observed dual function of Schlank in sphingolipid biosynthesis and lipid homeostasis, it's domain structure and it's nuclear localization - all lead to the question of the homeodomain function. To address domain specific functions of proteins *in vivo* Huang et al. developed a method called genomic engineering /ends out gene targeting. This method is a two step procedure where first, a *knock out (KO)* line is produced via homologous recombination replacing the gene of interest with an attP site, and second, this attP site is used for site directed re-integration of (modified) DNA (Huang et al., 2008, 2009).

Generation of such a $schlank^{KO}$ line replacing large parts of the *schlank* gene with an attP site followed by the generation of *schlank knock in (*$schlank^{KI}$*)* lines carrying distinct mutations within the homeodomain or the catalytic domain enables us to study the impact of such mutations on fly physiology. Many specific mutations can be analyzed without the artificial effects of over expression and background of wildtype Schlank protein.

The generation of the $schlank^{KO}$ line was performed in cooperation with PD Dr. Reinhard Bauer (Diploma thesis' Luo, 2011; Peters, 2012; Bachelor thesis Hannes Maib).

4.2.1 Genomic engineering strategy

The *schlank* gene is located on the X-chromosome. The endogenous locus and the genomic engineering strategy are visualized schematically in figure 4.2. The targeted sequence is spanning from exon 2 until the end of the 3'untranslated region (UTR). This sequence includes all predicted functional domains of the Schlank protein; the homeodomain is encoded by exon 2 and 3, the TLC domain is encoded by exon 3-6. However, exon 1 including the start codon has been excluded as the first intron is very long and contains the gene *CG3781*. The homologous regions (HR) flanking the target sequence were cloned into the donor vector pGE-attP. The 5'HR is a region of 6 kb upstream of the splice acceptor site of exon2. It contains the whole open reading frame (ORF) of the gene *CG3781*. The 5'HR was chosen to be comparatively long because the 3'HR had to be shortened. A first attempt with a longer 3'HR failed due to homozygous lethality of the flies of the produced donor line. When a 3'HR of 1,7 kb was used that does not include the start codon of the adjacent gene *spx* this lethality could be avoided. After the donor line was generated homologous recombination was

carried out. This included three crosses as described by Huang et al. (2008) and in section 3.1.4 leading to the exchange of the target sequence by the donor sequence (attp site, *white* gene). Verification of successful homologous recombination was carried out thoroughly and is described in section 4.2.2.

After the identified *schlank*^{KO} line was crossed to a Cre-recombinase expressing line leading to the excision of the *white* gene this line could be used for φC31 integrase dependent re-integration of target DNA. This system is based on the bacteriophage derived φC31 integrase that mediates sequence-directed recombination between a bacterial attachment site (attB) and a phage attachment site (attP). The target sequence was cloned into the integration vector -where it could be easily modified- and used for re-integration.

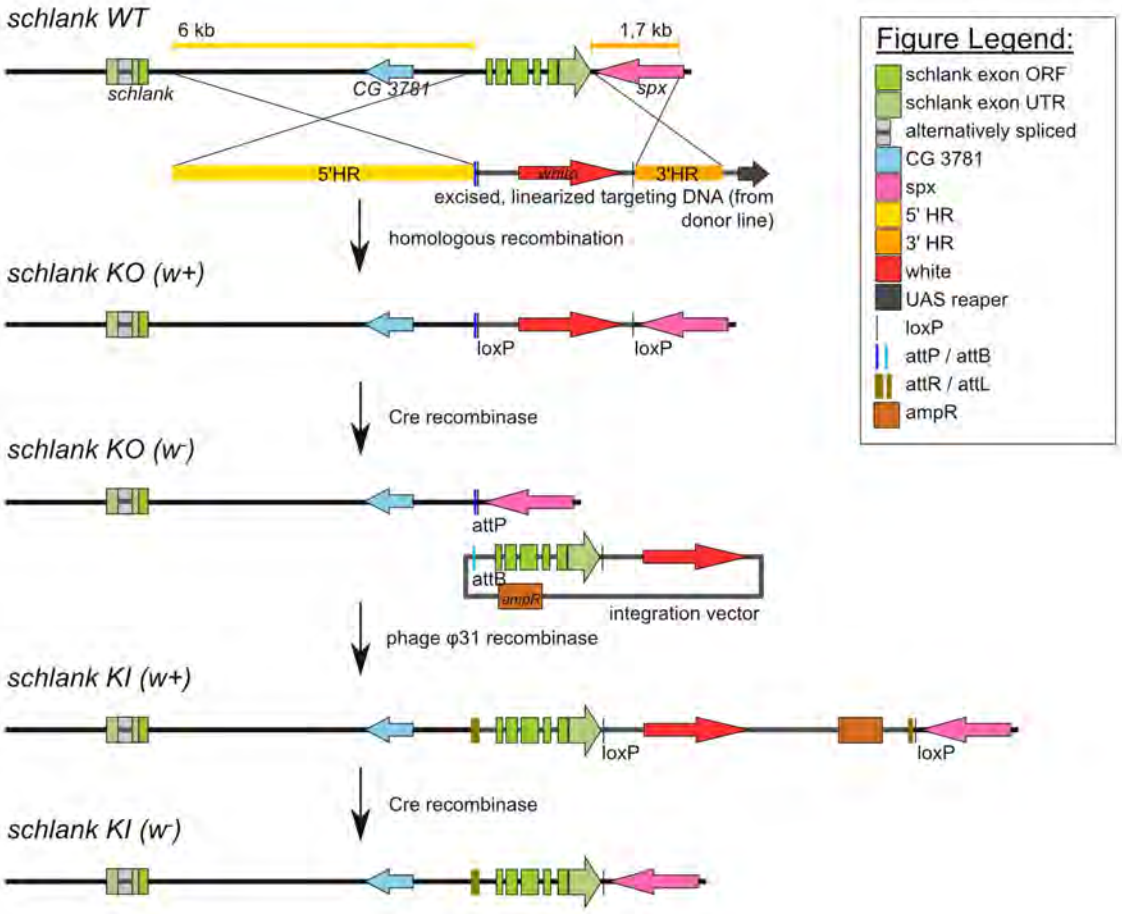

Figure 4.2: Genomic engineering of the *schlank* locus. The *schlank* gene is located on the X-chromosome (exons: green boxes) with the gene *CG3781* (blue arrow) located within intron 1. 5' and 3' homologous regions (HR) were chosen as represented by yellow and orange bars, respectively. The *UAS reaper* (black arrow) is a negative selection marker. After homologous recombination *schlank* exons 2- 6 are replaced by the *white* gene (red arrow) and the attP site (dark blue bar)- resulting in the $schlank^{KO}$ line. Crossing this line to a Cre-recombinase expressing fly line, Cre-recombinase mediates the excision of DNA between the two loxP sites (black bars) $\rightarrow$ *schlank KO* (w^-). φC31 integrase mediates the recombination between an attP and an attB site and can now be used for the re-integration of wildtype or mutated *schlank* DNA $\rightarrow$ $schlank^{KI}$, *schlank KI* (w^+). Afterwards the donor vector backbone can be removed by Cre-recombinase $\rightarrow$ *schlank KI* (w^-).

4.2.2 Verification and characterization of the *schlank knock out* line

To verify the correct homologous recombination the putative *schlank*^{KO} lines underwent some verification crosses and PCR reactions. Additionally, the *schlank* expression was analyzed.

First, the putative *schlank*^{KO} lines were screened for lethality which results in the absence of adult male flies with red eyes as the *schlank* gene is located on the X-chromosome and lack of *schlank* expression leads to lethality. Additionally, if females of a *schlank*^{KO} line (*schlank*^{KO}*/FM7*) were crossed to males of the P-element allele over a duplication on the Y (*schlank*$^{P(X)349}$*/Y*^{dp}) no female flies without the balancer but male flies with red eyes could be observed.

To further verify the *schlank*^{KO} lines PCRs were carried out on isolated gDNA (fig. 4.3A). Primer pairs were designed spanning the 3'HR or the 5'HR, always one primer binding in the donor sequence and one primer binding outside the respective HR. The 5'HR was too large to lead to an amplicon, but the PCR spanning the 3'HR worked fine. To furthermore proof the lack of *schlank* PCRs were carried out to amplify regions within the *schlank* gene. Those PCRs should only lead to an amplicon if there is no deletion of the target sequence (fig. 4.3B). To check if the gDNA preparation was successful a primer pair amplifying a part of the actin gene was used as a control.

To check if *schlank* expression was diminished qRT-PCR was carried out on RNA isolated from homozygous *schlank*^{KO} larvae. Analysis showed that there was no *schlank* transcript left (fig. 4.3C).

De novo Ceramide synthase activity was measured *in vivo* by feeding radioactively labeled acetic acid and measuring it's incorporation into ceramide. *schlank*^{KO} larvae showed similar results as the stronger *schlank* mutant and *de novo* CerS activity was strongly reduced as compared to *white*$^{-}$ controls. Also, incorporation into triacylglycerols (TAGs) and free fatty acids (FAs) was measured and was similar in *schlank*^{KO} and *schlank* mutant larvae (fig. 4.3D, Bauer et al., 2009).

Taken together, those results indicate that the *schlank*^{KO} line was successfully generated.

Like flies of the stronger *schlank* mutant allele the flies of the *schlank*^{KO} line showed severe growth defects, developmental delay and lethality in early development (fig: 4.4). Larval length was measured 24, 48 and 72 h after egg laying (AEL). The size of control larvae increased rapidly after hatching from the egg whereas *schlank*^{KO} larvae showed

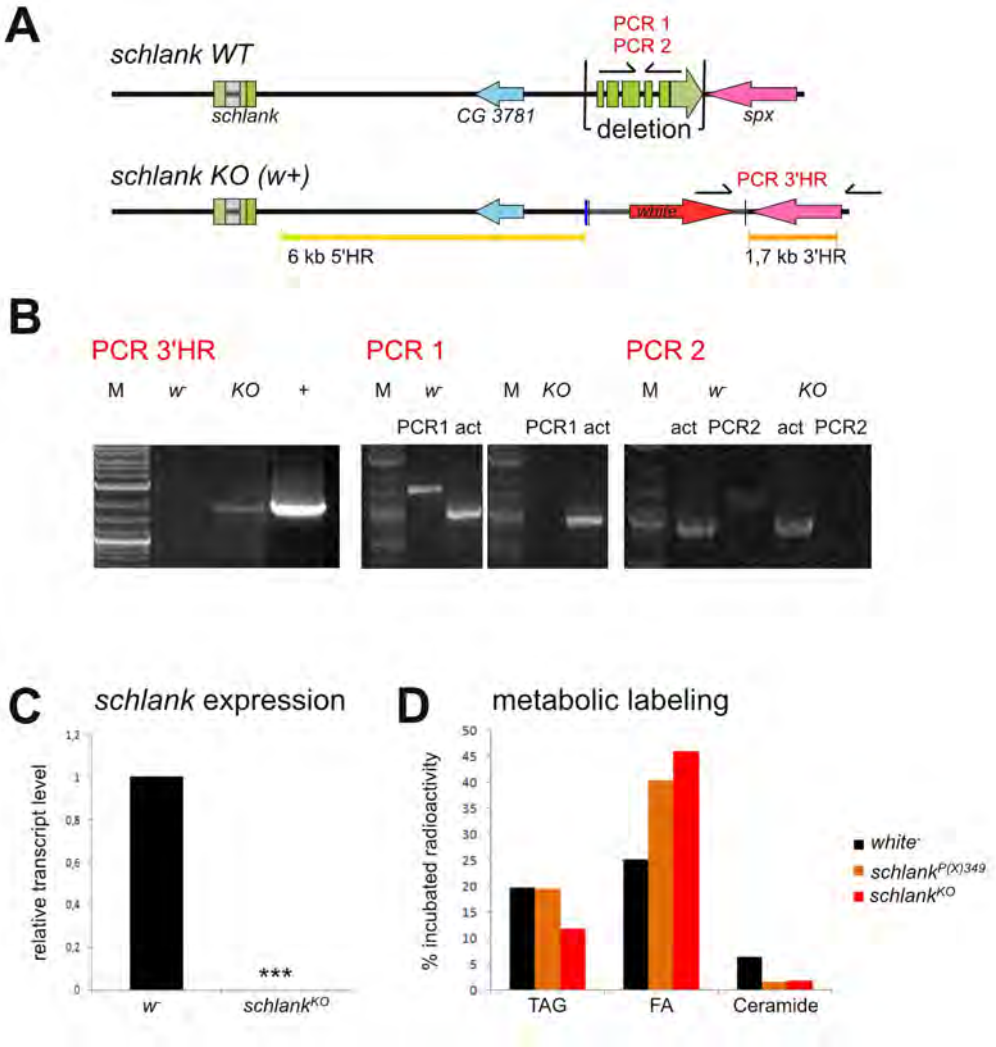

Figure 4.3: Verification of the *schlank*^{KO} line. **A**: Scheme of wt *schlank* and the *schlank* locus after correct homologous recombination, primer pairs used for the verification via PCR are shown by ⇌. **B**: PCR reactions carried out for the *schlank*^{KO} line. **C**: qRT-PCR analysis of *schlank* mRNA expression (n=6) in the *schlank*^{KO} line, 43-47 hAEL. mRNA level in *white*$^{-}$ larvae was set to 1. Significance was tested using an unpaired 2-tailed Student's t-test. ***p<0,001. **D**: Metabolic labeling of L1 larvae. Larvae were fed with radioactively labeled acetic acid and incorporation into triacylglycerols (TAG), fatty acids (FA) and Ceramide was measured. n=1.

no growth (fig: 4.4A). After 72 h all *schlank*^{KO} larvae were dead. Survival shows a high similarity between the *schlank*^{KO} line and the *schlank* mutants (fig: 4.4B).

In the qRT-PCR analysis of genes known to be regulated in *schlank* mutants (Bauer et al., 2009) the same genes were up or down regulated, respectively. The transcript level of the *lipase 3* gene was significantly increased. Less significantly increased were the transcript levels of the other tested triacylglycerol lipase *brummer* and the glucagon homologue *adipokinetic hormone, akh*. The regulation of *srebp* and its target genes *fas* and *acs* was similar to their regulation in the stronger *schlank* mutant allele (*schlank*$^{P(X)349}$; Bauer et al., 2009; fig: 4.4D). Strong down regulation could be observed in the weaker *schlank*$^{P(X)61}$ mutant allele (Bauer et al., 2009). Overall, the *schlank*^{KO} line resembles the phenotype of the stronger *schlank*$^{P(X)349}$ mutant allele.

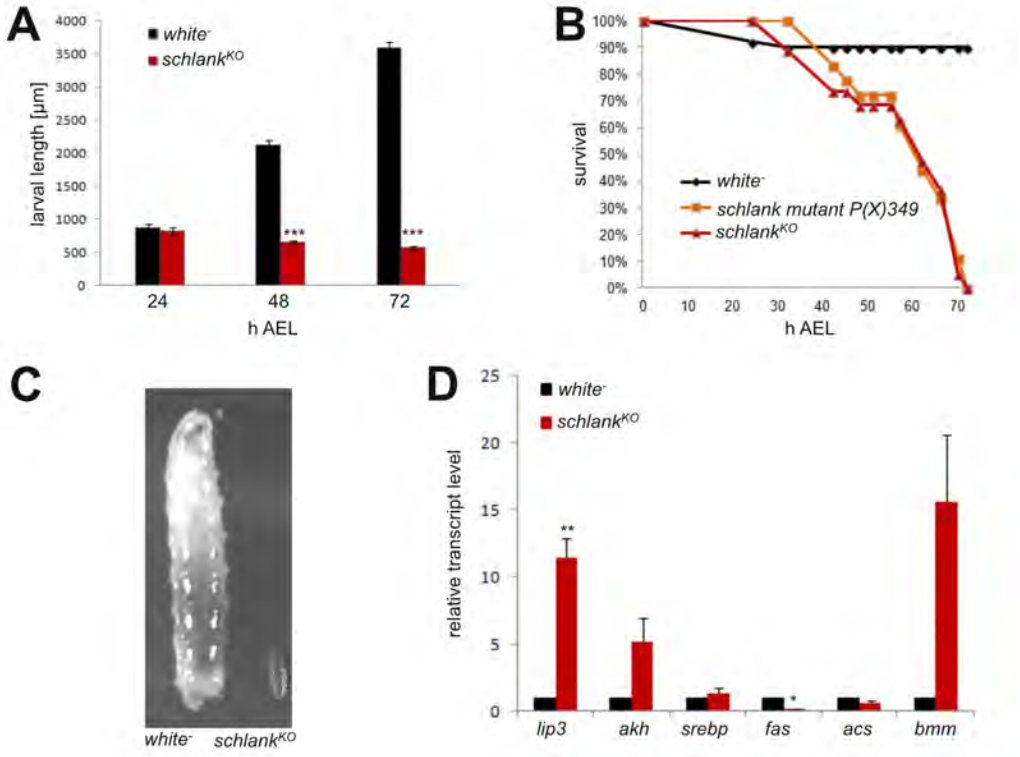

Figure 4.4: Chracterization of the *schlank*^{KO} line. **A**: Larval size of *white*$^{-}$ and *schlank*^{KO} larvae were measured 24, 48 and 72 hours after egg laying (hAEL). **B**: Survival of *white*$^{-}$, *schlank*$^{P(X)349}$ and *schlank*^{KO} larvae. **C**: Larvae 72 h AEL. Dyed yeast was taken up and could be visualized in the gut. **D**: qRT-PCR analysis of genes known to be regulated in *schlank* mutants, 43-47 hAEL (n=3-5). mRNA level in *white*$^{-}$ larvae was set to 1. Significance was tested using an unpaired 2-tailed Student's t-test (Microsoft Excel). *p<0,05, **p<0,01, ***p<0,001. Error bars: SEM.

4.3 Targeted mutations to address domain specific functions of Schlank

The established $schlank^{KO}$ line was used for the site specific re-integration of the target sequence. The first step was to re-integrate the *schlank* wildtype sequence ($schlank^{KI-WT}$). For the investigation of the nuclear function of Schlank two *knock in* lines were generated each carrying point mutations within one of the predicted nuclear localization signals (NLS) ($schlank^{KI-NLS1}$, $schlank^{KI-NLS2}$). The fly line $schlank^{KI-H215D}$ was generated to analyze the phenotypes resulting from the absence of Ceramide Synthase activity - with the Schlank protein still being there (fig. 4.5).

The fly line $schlank^{KI-WT}$ was generated as a proof-of-principle and can later on serve as a control. The mutation carried by the fly line $schlank^{KI-NLS1}$ is K80M/K81M which is localized within the first nuclear localization signal resulting in the sequence being modified from RPKK to RPMM. The second NLS is mutated from RLRR to ALAR (R122A/R124A) in the fly line $schlank^{KI-NLS2}$. The positively charged amino acids within the NLSs (like lysine (K) and arginine (R)) are important for their recognition and function and were exchanged to amino acids with neutral residues. Therefore, if the predicted NLSs had a functional role *in vivo* less Schlank protein should localize to the nucleus and resulting phenotypes could be linked to those point mutations and a role of nuclear Schlank. The mutation of histidine (H) at position 215 to aspartate (D) has been reported to abolish the ceramide synthase activity of the Schlank protein (Bauer et al., 2009). A fly line carrying this point mutation has been generated to study the difference between a complete *knock out* versus a situation where the Schlank protein is there but not the product of its enzymatic activity (ceramide). This enables us to study the functions that result from ceramides apart from the functions of the Schlank protein. Those functions could include a role in lipid homeostasis as observed before in over expression studies.

4.3.1 Verification of the *schlank knock in* lines

To check for the correct re-integration of target DNA, gDNA was isolated from the fly lines that showed red eye color after the procedure of φC31 integrase dependent recombination. PCRs were performed as shown in figure 4.6. The PCR using primers flanking the attR site results in a larger amplicon if the attR site is there as compared to the wildtype sequence. The forward primer in the attL PCR is binding in the ampicillin

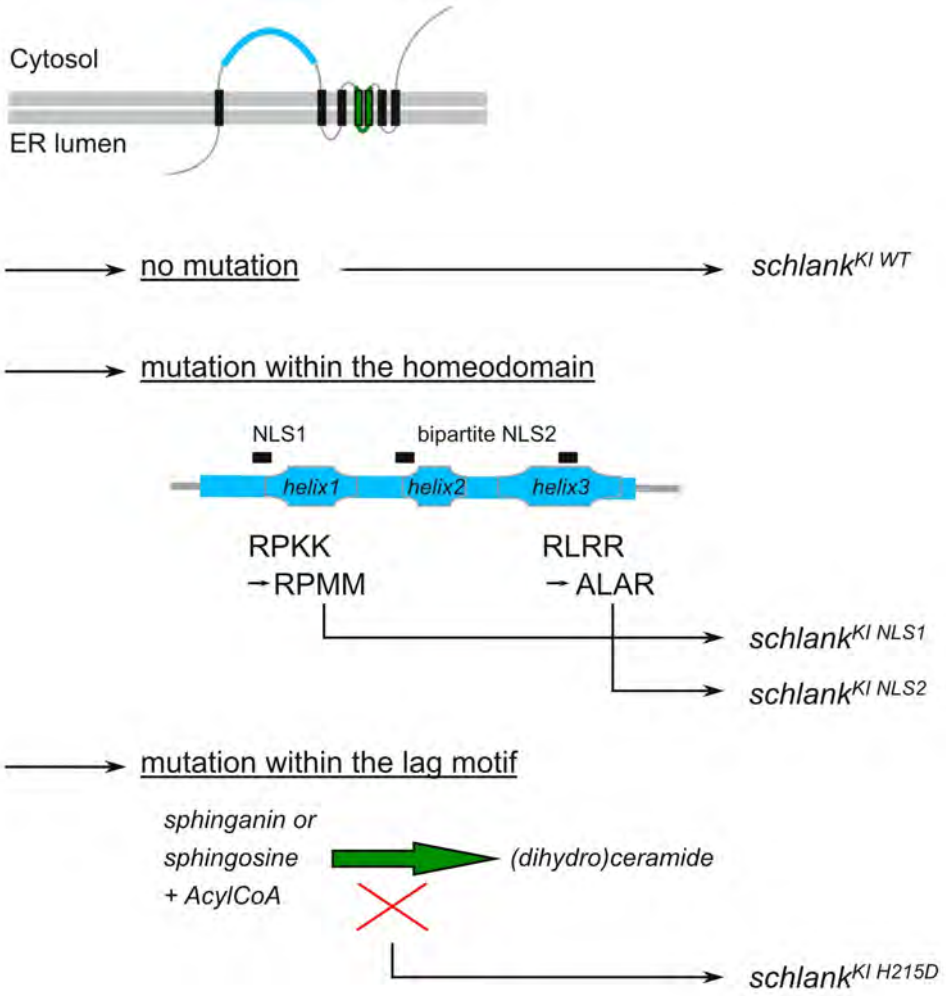

Figure 4.5: Established *schlank knock in* lines. The re-integration of *schlank* DNA into the $schlank^{KO}$ line was carried out with the following constructs: Wildtype *schlank* DNA was used to generate the fly line $schlank^{KI-WT}$. In the fly lines $schlank^{KI-NLS1}$ and $schlank^{KI-NLS2}$ the *schlank* DNA was mutated in the predicted NLSs as indicated. A catalytically inactive Schlank version is encoded in the $schlank^{KI-H215D}$ fly line.

resistance cassette and therefore no band will be observed if the recombination didn't occur. All lines tested so far had a positive test outcome. Additionally, the *schlank* expression was analyzed in those lines and showed wildtype mRNA and protein level. First larval stage was chosen to avoid differences due to developmental delay. For a quantification of the protein level the experiment has to be repeated as the number of biological repeats were not enough.

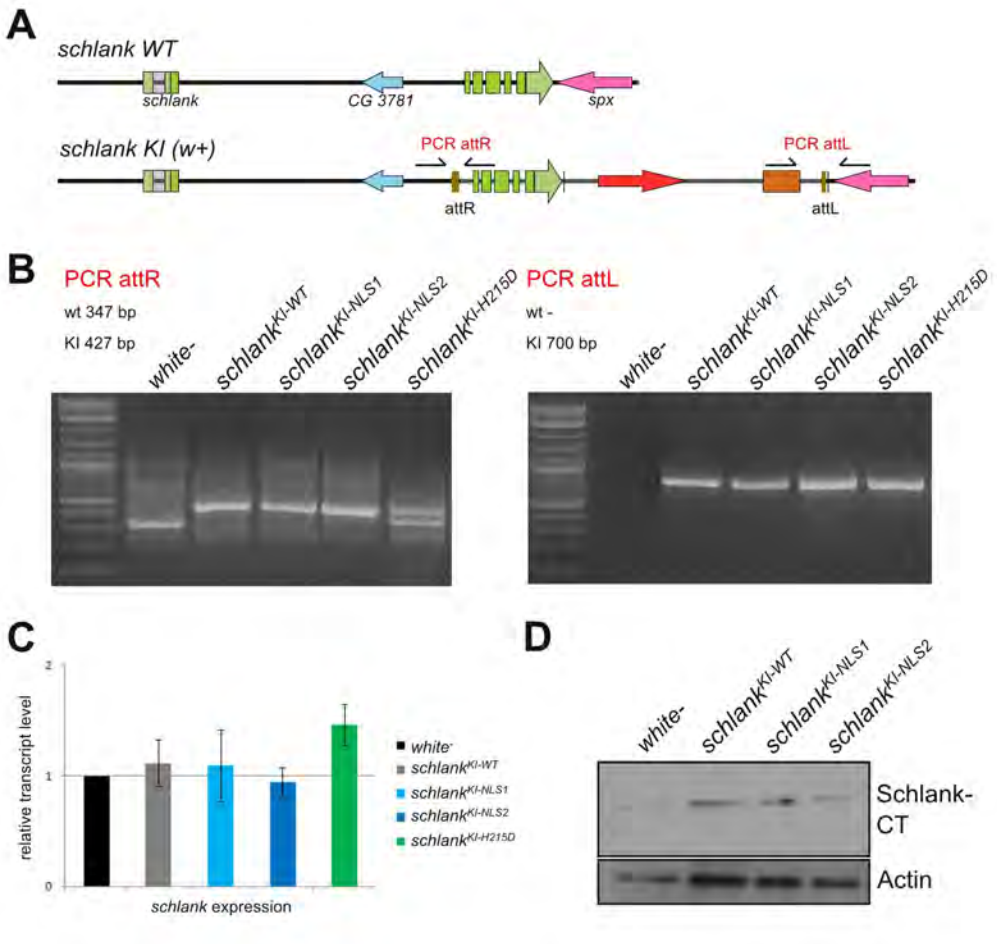

Figure 4.6: Verification of the *schlank knock in* lines. **A**: Scheme of wt *schlank* and the *schlank* locus after correct integration of the donor vector, primer pairs used for the verification via PCR are shown by ⇌. **B**: PCR reactions carried out for four *schlank KI* lines. $schlank^{KI-H215D}$ heterozygous over a balancer. **C**: qRT-PCR analysis of *schlank* mRNA expression 43-47 hAEL (n=4-5). mRNA level in $white^{-}$ larvae was set to 1. Significance was tested using an unpaired 2-tailed Student's t-test. Error bars: SEM. **D**: Immunoblot analysis of Schlank protein expression in the $schlank^{KI}$ lines 43-47 hAEL using the αSchlankCT antibodies. Actin was used as a loading control.

4.3.2 Basic characterization of the *schlank knock in* lines

Four *schlank knock in* lines have been generated, three of which carry distinct mutations in different functional domains. To analyze those lines, first, a basic characterization was performed. The influence of the mutations on ceramide synthase activity, survival rates, nuclear localization of the Schlank protein and on the expression of genes known to be regulated in *schlank* mutants was checked.

Ceramide Synthase activity

To be able to differentiate between protein and metabolite function Ceramide Synthase activity in the different *schlank knock in* lines had to be determined. *De novo* CerS activity was measured *in vivo* by feeding radioactively labeled acetic acid and measuring it's incorporation into ceramide. CerS activity in $schlank^{KI-WT}$ and $schlank^{KI-NLS2}$ was equivalent to CerS activity in $white^{-}$ stage 1 and stage 3 larvae, whereas the CerS activity in $schlank^{KI-NLS1}$ larvae was reduced by about 20 % in both stages (fig. 4.7).

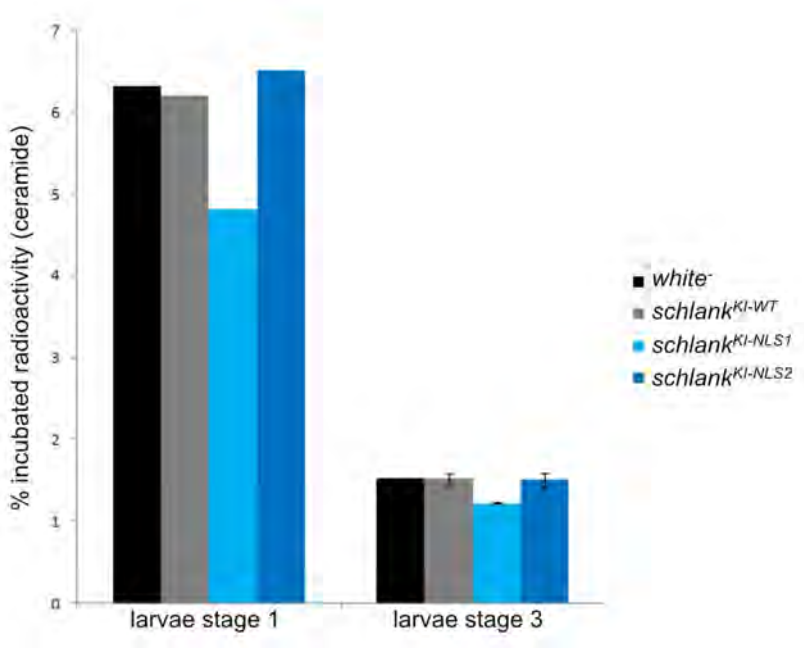

Figure 4.7: *De novo* ceramide synthase activity in the *schlank knock in* lines. Metabolic labeling with $[^{14}C]$- acetic acid was performed with stage 1 (n=1) and 3 (n=3) larvae. Error bars: SEM.

Survival and development

The survival and development of the established *schlank knock in* lines were analyzed and compared to *white*$^{-}$, which is the background of the lines, and to the *schlank*^{KO} line. Like the *schlank*^{KO} line the *schlank*$^{KI-H215D}$ and the *schlank*$^{KI-NLS2}$ lines were not homozygous viable if kept as a stock on normal fly food. For analysis, the homozygously viable fly lines (*white*$^{-}$, *schlank*$^{KI-WT}$ and *schlank*$^{KI-NLS1}$) were crossed to males carrying the FM7 balancer (FM7/Y) to be able to separate male progeny for better comparability.

white^{-}, *schlank*$^{KI-WT}$ and *schlank*$^{KI-NLS1}$ flies showed comparable development and survival rates (fig, 4.8A). *schlank*^{KO} and *schlank*$^{KI-H215D}$ larvae both died a few days after hatching from the egg as stage 1 larvae. *schlank*$^{KI-NLS2}$ flies showed developmental delay: larvae stayed approx. double the amount of time in each larval stage, pupal stage was slightly elongated and first flies hatched after 17 days (as compared to 9-10 days for wildtype flies). Only about 8 % of collected *schlank*$^{KI-NLS2}$ larvae reached adulthood whereas there was no difference between *white*$^{-}$, *schlank*$^{KI-WT}$ and *schlank*$^{KI-NLS1}$ (fig. 4.8B).

Comparing the size at late first larval stage (fig. 4.8C) showed that *schlank*$^{KI-WT}$ and *schlank*$^{KI-NLS1}$ grow as fast as *white*$^{-}$ controls, whereas *schlank*$^{KI-NLS2}$ larvae were reduced in size. *schlank*$^{KI-H215D}$ larvae showed a similar size as of *schlank*^{KO} larvae, that is not much different from the size of a newly hatched larva.

Nuclear localization

The mutations of the NLSs could not be tested in flies so far as over expressed Schlank protein doesn't localize to the nucleus. To test the amount of nuclear Schlank^{NLS1} and Schlank^{NLS2} as compared to Schlank^{WT} immunofluorescent stainings were performed using the antibodies directed against the Schlank C-terminus. Co-staining with an anti-Lamin and an anti-Spectrin antibody helped in visualizing the outline of the nuclei and the cells as cytoskeleton components were stained that underlie the inner nuclear membrane (INM) or the plasma membrane (PM), respectively. Those markers were used in the quantification to outline the areas defined as nucleus and cytosol. The mean fluorescence intensity (MFI) of the nucleus was divided by the mean fluorescence intensity of the cytosol and the ratios were compared between the genotypes. Antibody specificity was tested using *schlank*RNAi clones (data not shown).

The MFI nucleus/MFI cytosol ratios of immunofluorescent stainings of *schlank*$^{KI-WT}$,

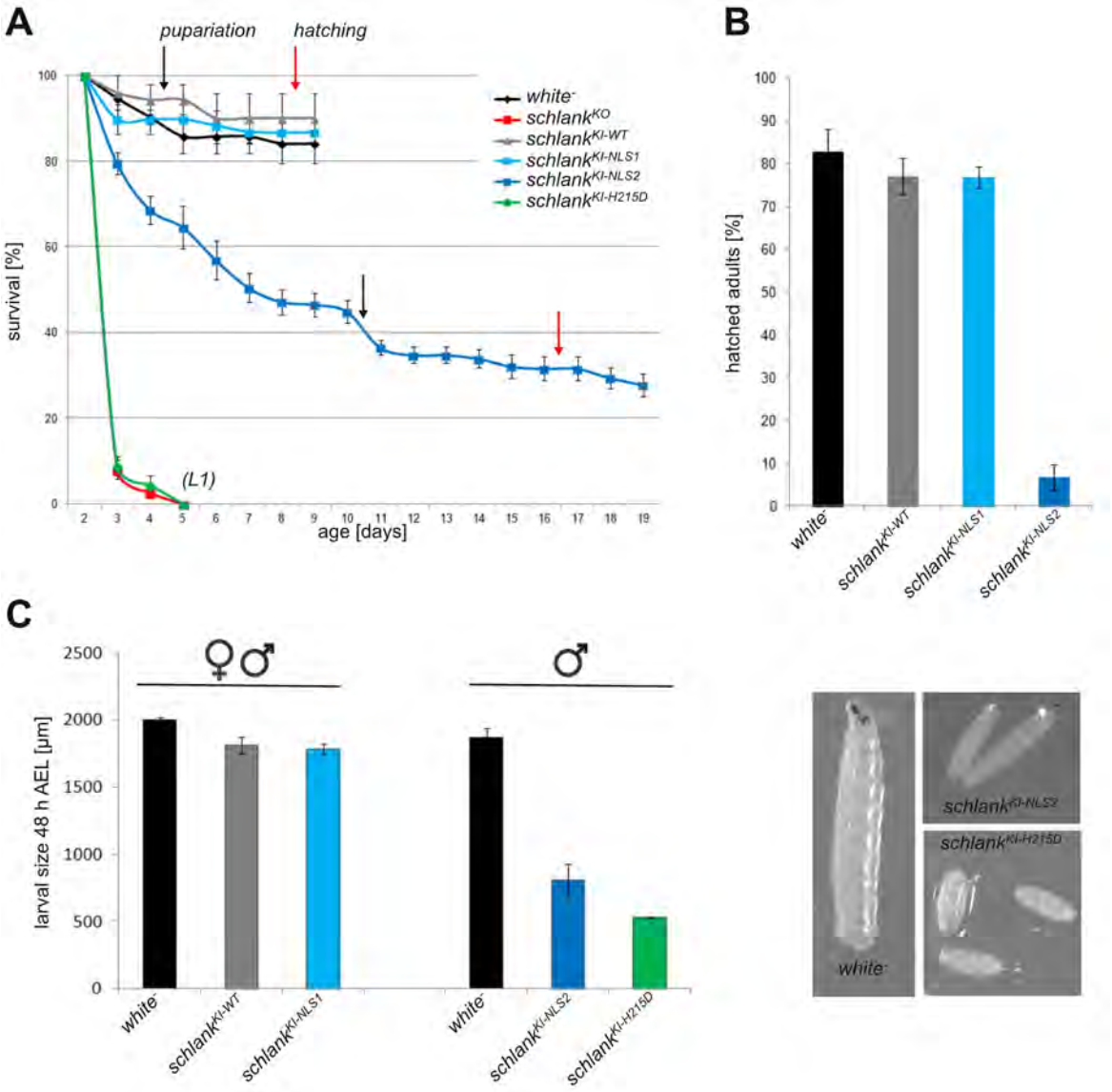

Figure 4.8: Survival and size of the $schlank^{KI}$ lines. **A**: Hemizygous larvae of the indicated phenotypes were collected approx. 44 h AEL. Survival was examined daily. Black arrows show the beginning of pupariation, red arrows beginning of hatching of adult flies from pupal cages. $white^{-}$, $schlank^{KI-WT}$, $schlank^{KI-NLS1}$ pupariated at day 5 and nearly all hatched at day 9. $schlank^{KI-NLS2}$ larvae started pupariating at day 11 and first flies hatched at day 17. $schlank^{KO}$ and $schlank^{KI-H215D}$ larvae died after a few days in first larval stage. **B**: Amount of hatched adult flies four days after first flies hatched. $schlank^{KI-NLS2}$ has a significantly elevated lethality as compared to $schlank^{KI-WT}$ (p=0,0002) and to $white^{-}$ (p=0,0007), Student's t-test. Assay performed by Schwarzkopf (2015). **C**: Analysis of larval size in the $schlank^{KI}$ lines 48 h AEL. Larvae of $white^{-}$, $schlank^{KI-NLS2}$ and $schlank^{KI-H215D}$ are shown. Error bars: SEM.

schlank$^{KI-NLS1}$ and *schlank*$^{KI-NLS2}$ early L3 larval fatbody are shown in figure 4.9B. One representative picture of each genotype is shown in figure 4.9A. In *schlank*$^{KI-NLS2}$ fatbody cells nuclear Schlank protein was reduced significantly, but not completely. Unexpectedly, in fatbody cells of *schlank*$^{KI-NLS1}$ larvae nuclear Schlank was enriched.

As in all pictures the same magnification was used the mean size of the cells was measured as well (fig. 4.9C). The result clearly showed that fatbody cells of *schlank*$^{KI-NLS2}$ larvae were highly reduced in size.

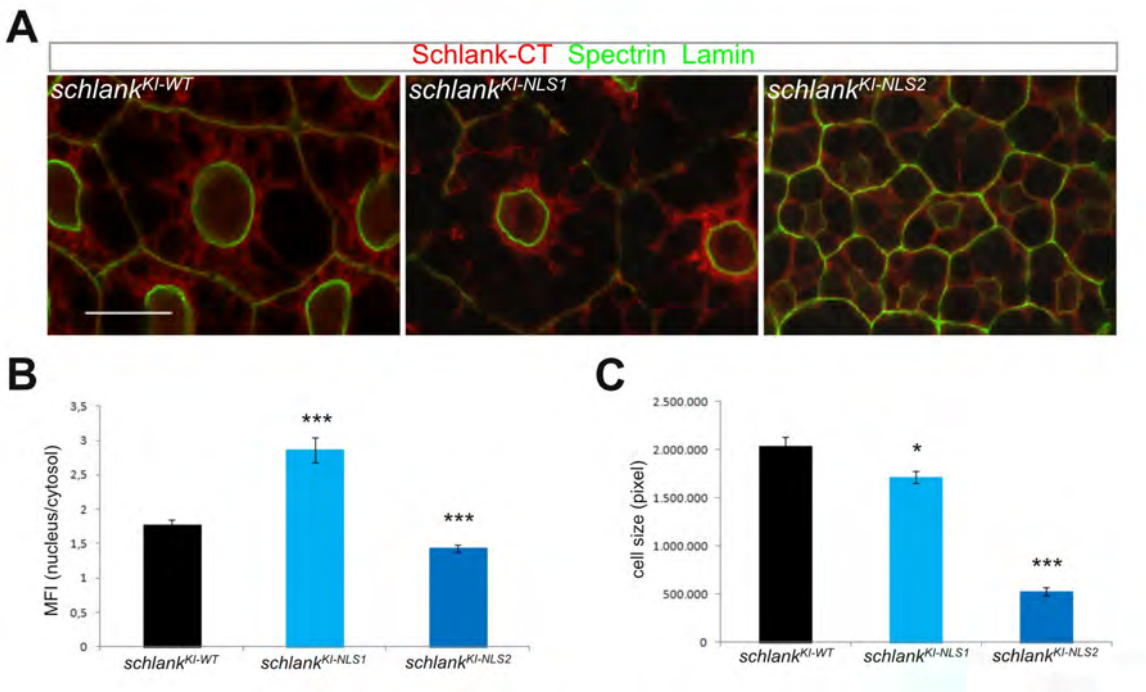

Figure 4.9: Nuclear localization of Schlank in *schlank*$^{KI-NLS1}$ and *schlank*$^{KI-NLS2}$. **A**: Immunofluorescent stainings of L3 fatbody cells using αLamin and αSpectrin antibodies as markers for nuclear and cell membrane (green), respectively. Schlank was stained with the αSchlankCT antibodies (red). Scale bar: 20 μm. **B**: Quantification of nuclear Schlank protein. Mean fluorescent intensities (MFI) of the nucleus and the cytosol were measured (6 independent stainings, at least 10 cells each) and relative nuclear Schlank was determined. **C**: Cell size was determined as well. Significance was tested using an unpaired 2-tailed Student's t-test. *p<0,05, **p<0,01, ***p<0,001. Error bars: SEM.

Gene expression

In *schlank* mutants not only sphingolipid levels are reduced but also triacylglycerol (TAG) levels. This may be due to the up regulation of TAG lipases such as *lipase 3* and *brummer* and the down regulation of lipogenesis factors like *srebp* and its target

genes (e.g. *fas*). As the increase of TAG and *lipase 3* expression upon over expression of *schlank* is independent of the ceramide synthase activity it is interesting to know how those genes are regulated in the *schlank knock in* lines.

RNA was isolated from L1 larvae of the different *schlank knock in* lines and the expression of *lipase 3*, *akh*, *brummer*, *srebp* and *fas* was analyzed using qRT-PCR (fig. 4.10). In $schlank^{KI-WT}$ larvae non of the genes were regulated as compared to $white^{-}$ control. Expression of *lipase 3* was strongly down regulated in $schlank^{KI-NLS1}$ larvae but not regulated in the other *schlank knock in* lines. In $schlank^{KI-H215D}$ larvae *brummer* expression was up regulated and *fas* expression was down regulated in $schlank^{KI-NLS2}$ larvae. Expression of *srebp* was not altered in any of the lines tested.

The lack of up regulation of *lipase 3* in $schlank^{KI-H215D}$ larvae supported the result obtained from classical rescue experiments (sec. 6.1). There was no up regulation of *lipase 3* in $schlank^{KI-NLS2}$ larvae as would be expected if the nuclear Schlank protein was responsible for this regulation, and if the reduction of this nuclear Schlank pool was sufficient in $schlank^{KI-NLS2}$ first instar larvae. However, preliminary data on $schlank^{KI-NLS2}$ stage 3 larvae showed a strong up regulation of *lipase 3* (data not shown).

In section 4.3.3 the expression of these genes in $schlank^{KI-H215D}$ larvae is directly compared to their expression in $schlank^{KO}$ larvae, in section 4.3.4 expression is analyzed in adult flies of the other genotypes.

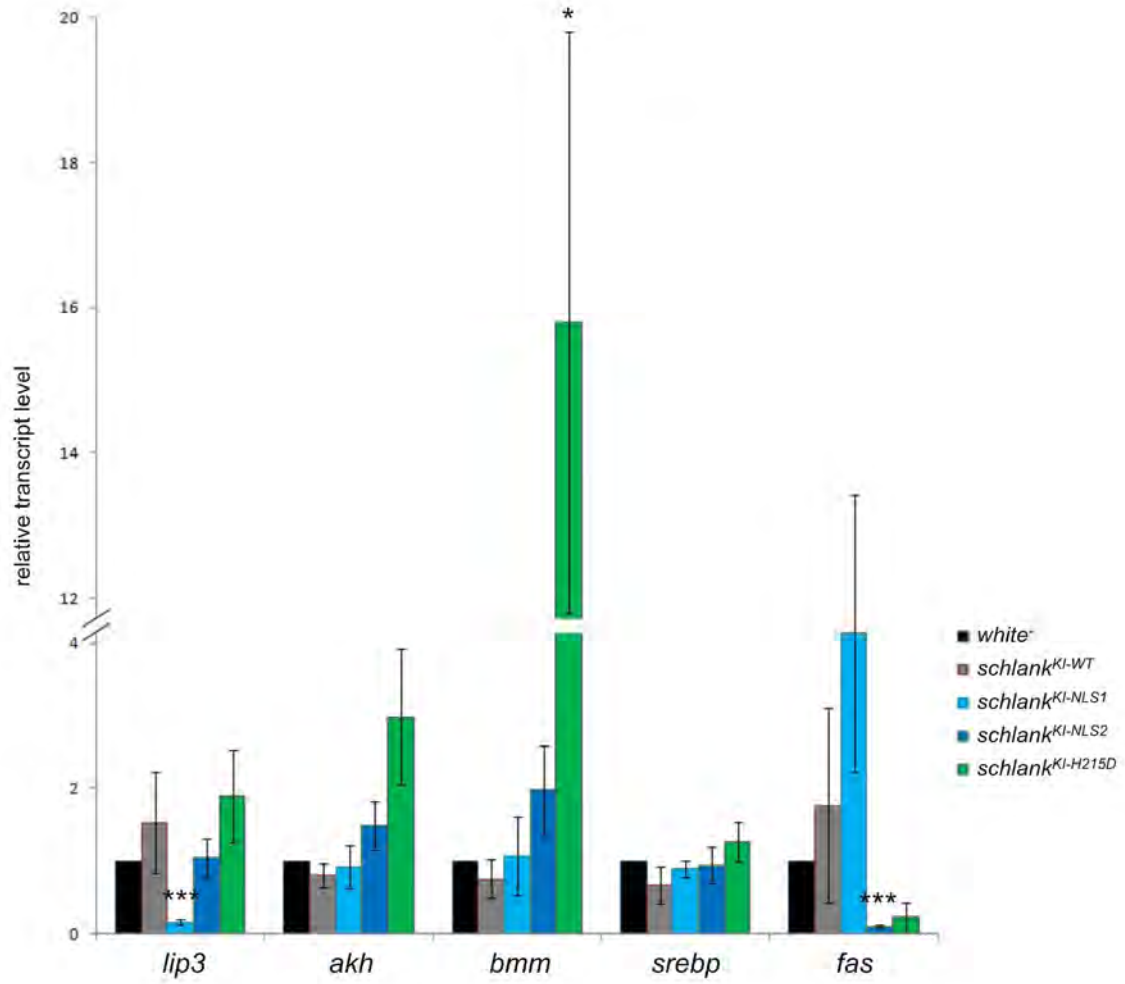

Figure 4.10: Analysis of gene expression in the *schlank knock in* lines. L1 larvae were collected 43-47 h AEL and genes known to be regulated in *schlank* mutants were analyzed via qRT-PCR (n=3-9). mRNA level in *white*$^{-}$ larvae was set to 1. Significance was tested using an unpaired 2-tailed Student's t-test. *p<0,05, **p<0,01, ***p<0,001. Error bars: SEM.

4.3.3 Loss of enzyme activity vs loss of complete protein

Larvae of the $schlank^{KI-H215D}$ line showed a similar behavior as compared to the larvae of the $schlank^{KO}$ line. After hatching from the egg they did not grow, moved very slowly and were most likely to be found on the periphery of the apple juice agar plates whereas wildtype larvae all crawled into the yeast at the center of the plate. In both lines the ceramide synthase activity of Schlank should be completely absent, the only difference is the presence of the Schlank protein itself. As the additional functions of the protein is the main topic in this thesis the two lines were compared directly in qRT-PCR analysis and TAG-level determination.

If larval size was compared directly, there was no significant difference between $schlank^{KO}$ and $schlank^{KI-H215D}$ larvae (fig. 4.11A).

The analysis of TAG-level was performed using thin-layer-chromatography (TLC). Homozygous $schlank^{KO}$ and $schlank^{KI-H215D}$ larvae were collected and lipids were extracted. Using this method no difference between the TAG content in $schlank^{KO}$ and $schlank^{KI-H215D}$ could be observed (fig. 4.11B).

The expression of *lipase 3*, *akh*, *brummer*, *srebp* and *fas* was analyzed in $schlank^{KO}$ and $schlank^{KI-H215D}$ L1 larvae. qRT-PCR analysis showed a significant lower expression of *lipase 3* and *brummer* in $schlank^{KI-H215D}$ larvae (fig. 4.11C). Expression of the other genes tested was not altered.

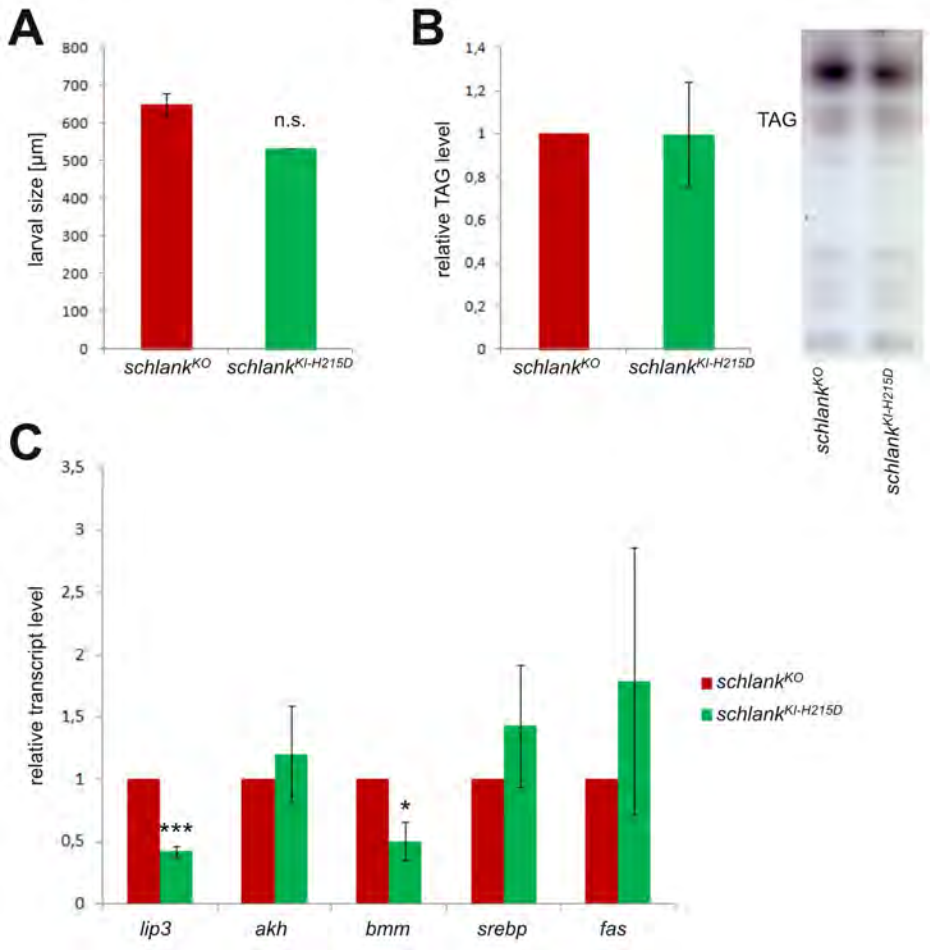

Figure 4.11: Analysis of $schlank^{KO}$ and $schlank^{KI-H215D}$. **A**: Larval size of $schlank^{KO}$ and $schlank^{KI-H215D}$ larvae 43-47 h AEL, **B**: TAG level of $schlank^{KO}$ and $schlank^{KI-H215D}$ larvae 43-47 h AEL was determined via lipid extraction and TLC. One representative section of a TLC plate is shown. **C**: qRT-PCR analysis of the genes known to be regulated in *schlank* mutants (n=4). mRNA level in $white^{-}$ larvae was set to 1. Significance was tested using an unpaired 2-tailed Student's t-test. n.s. not significant, *p<0,05, **p<0,01, ***p<0,001. Error bars: SEM.

4.3.4 Mutations in nuclear localization signals

Mutations of the NLSs were introduced into the *schlank* sequence to study their impact on the fly organism. The fly lines $schlank^{KI-NLS1}$ and $schlank^{KI-NLS2}$ were generated and their basic characterization is described above in this section (4.3). It has been shown that in the fly line $schlank^{KI-NLS2}$ indeed less nuclear Schlank was found in fatbody cells of L3 larvae whereas in the fly line $schlank^{KI-NLS1}$ the opposite is the case. In vials $schlank^{KI-NLS1}$ flies were homozygous viable and vital, $schlank^{KI-NLS2}$ flies only survived to adulthood if they were separated -and then development was retarded, many died, larvae appeared slim and larvae and flies moved less. Additionally flies showed wing abnormalities of different kinds.

To investigate the phenotypes that arise from mutations in the Schlank NLSs in more detail several additional experiments have been performed.

Alterations in lipid homeostasis

From previous experiments it was concluded that the homeodomain might have a nuclear function in the transcriptional regulation of lipid homeostasis, e.g. by the regulation of *lipase 3* gene expression. As in larval stage 1 the lipid homeostasis is just being established analysis of gene expression was also carried out in adults (fig. 4.10, fig. 4.12A). RNA was isolated from one or five day old adult $schlank^{KI-WT}$, $schlank^{KI-NLS1}$ and $schlank^{KI-NLS2}$ flies, transcribed into cDNA and analyzed via qRT-PCR. Overall regulation of the analyzed genes (*schlank, lipase 3, fas, brummer, midway*) was not much. *midway* was down regulated in 1 day but not 5 days old $schlank^{KI-NLS2}$ flies.

Triacylglycerol levels of $schlank^{KI-NLS2}$ were analyzed in early larval stage 3 to see the impact of the point mutation on body fat. $White^{-}$ larvae were taken as a control. Due to a large developmental delay staging was carried out looking at the mouth hooks -and collecting really early $white^{-}$ larvae as the content of body fat is steadily increasing in larval stages (Carvalho et al., 2012; Guan et al., 2013). Results of the TLC analysis are shown in figure 4.12B. As expected, TAG level were decreased in $schlank^{KI-NLS2}$ larvae. Additionally, the intensity of the band that most likely represents free fatty acids (FA) was elevated in $schlank^{KI-NLS2}$ larvae (no standard for free FA was used).

Feeding of $schlank^{KI-NLS2}$ larvae was monitored by the administration of Carmin-red stained yeast. It was indeed taken up by the larvae and could be seen throughout

the guts (data not shown).

The *de novo* rate of the formation of TAGs and FAs was addressed via metabolic labeling with $[^{14}C]$- acetic acid. Within the 12 h labeling period, $schlank^{KI-NLS2}$ stage 3 larvae built up 10-15 % less TAGs than $white^{-}$ and $schlank^{KI-WT}$ controls. In $schlank^{KI-NLS1}$, stage 1 larvae and free fatty acids no change has been observed (fig. 4.12C)

Analysis of additional phenotypes

The impression of a slower movement of $schlank^{KI-NLS2}$ flies was quantified using the negative geotaxis or climbing assay. The climbing assay is commonly used to determine behavioral and neuronal dysfunction in *Drosophila*. 1 day old adult $white^{-}$, $schlank^{KI-WT}$ and $schlank^{KI-NLS1}$ flies showed similar climbing ability. $schlank^{KI-NLS2}$ flies however failed to climb higher than the 10 cm mark in one minute with a mean climbing distance of 2 cm, as compared to about 15 cm (in 1 min) for flies of the other genotypes (fig. 4.13A).

Another phenotype of the $schlank^{KI-NLS2}$ line were wing abnormalities observed in several flies hatched. Those wing abnormalities included wrinkled wings and wings that do not abut upon the abdomen like in wildtype flies but hang down or spread from the fly body. Examples are shown in figure 4.13B.

As such wing phenotypes are also observed in *Drosophila* models of Parkinson's disease (Greene et al., 2003), genes miss regulated there were analyzed via qRT-PCR. Those genes are related to mitophagy. Additionally, genes involved in autophagy were analyzed. There was no strong up or down regulation observed of any gene tested (fig. 4.13C).

The brain morphology and apoptosis of brain cells were analyzed via toluidine blue staining of semi-thin section of adult heads. This methodology depends on the nuclear and cytoplasmic condensation that occurs during apoptosis (Elmore, 2007). Preliminary data is visualized in figure 4.14. Vacuolization (holes) or apoptosis (dark fragmented nuclei) were not visualized in $schlank^{KI-NLS2}$ flies, but elongated cells within the ganglion cell layers could be observed. Overall, the $schlank^{KI-NLS2}$ brains seemed smaller/narrower and there may be a reduction of brain fatbody. This however has to be studied in more detail.

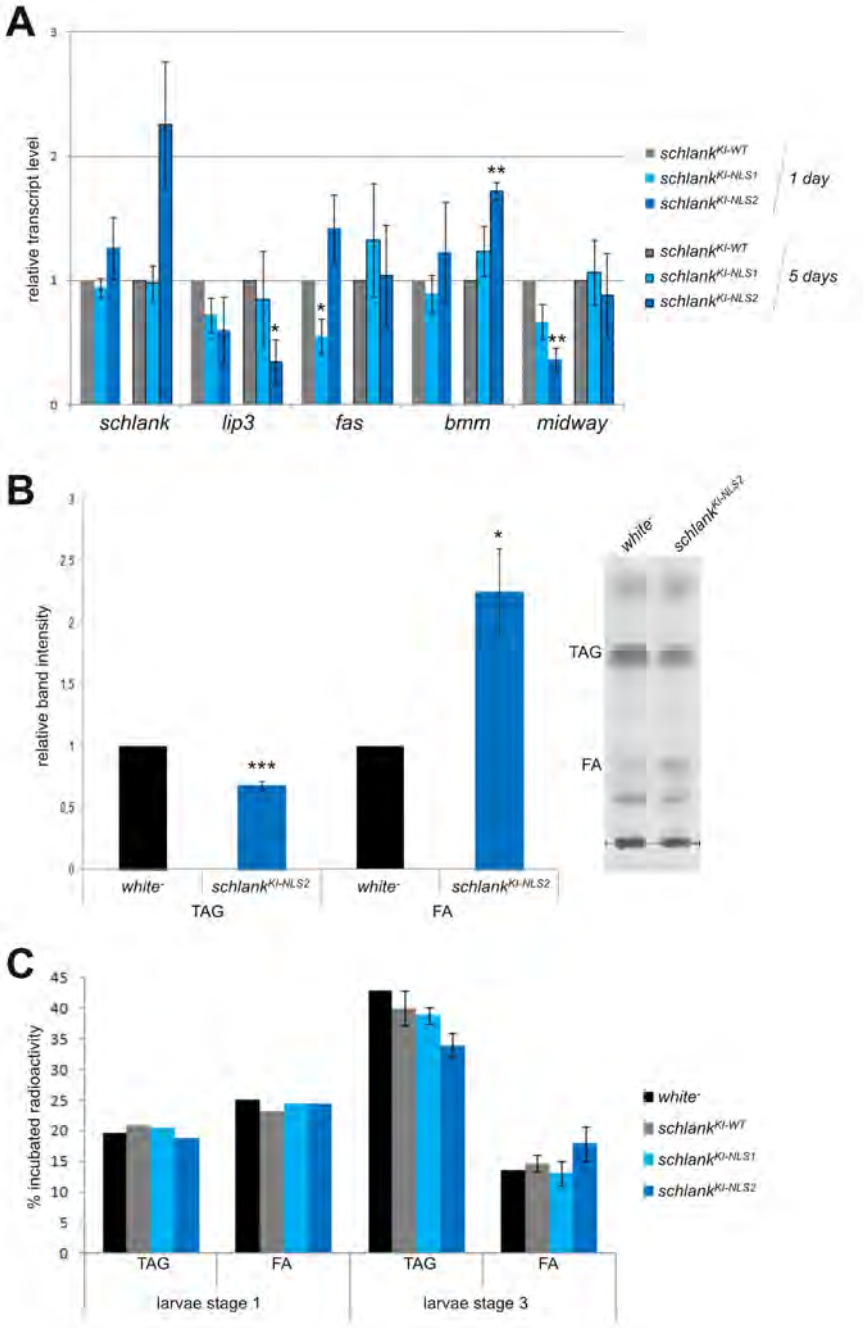

Figure 4.12: Mutations within the NLSs: analysis of body fat. **A**: qRT-PCR analysis of 1 (n=4-10) and 5 (n=4-5) day old adult flies on genes involved in lipid homeostasis. Adults of $schlank^{KI-WT}$, $schlank^{KI-NLS1}$ and $schlank^{KI-NLS2}$ were analyzed. **B**: Triacylglycerol (TAG) level of $schlank^{KI-NLS2}$ (early) stage 3 larvae were compared to TAG level of $white^{-}$ early stage 3 larvae via TLC. One representative lane of each genotype is shown. **C**: Metabolic labeling with $[^{14}C]$- acetic acid of stage 1 and 3 larvae; analysis of *de novo* TAG and FA. Error bars: SEM. Significance was tested using an unpaired 2-tailed Student's t-test. *p<0,05, **p<0,01, ***p<0,001. Level in $white^{-}$ or $schlank^{KI-WT}$ was set to 1.

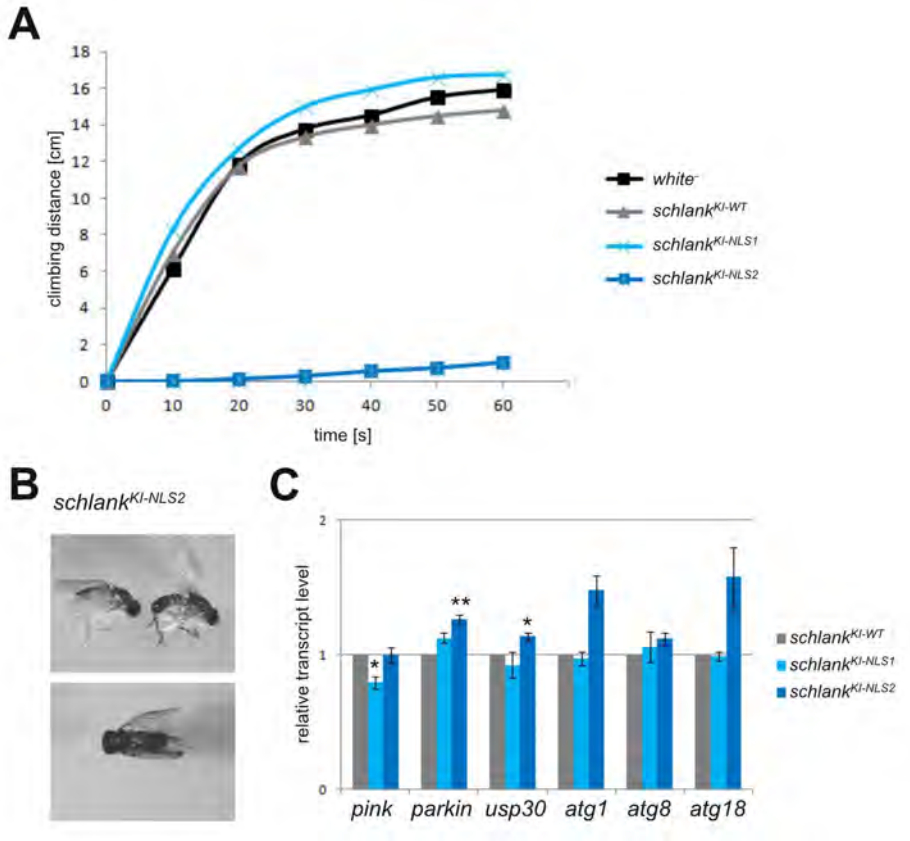

Figure 4.13: Mutations within the NLSs: analysis of additional phenotypes. **A**: Climbing assay performed with *white*$^{-}$, *schlank*$^{KI-WT}$, *schlank*$^{KI-NLS1}$ and *schlank*$^{KI-NLS2}$ flies (1 day old). Mean distance is plotted over the time. Assay performed by Schwarzkopf (2015). **B**: *schlank*$^{KI-NLS2}$ flies show wing abnormalities. Some wings are curved/wrinkled and/or rise up or hang down from the fly thorax. Picture taken by PD. Dr. Reinhard Bauer. **C**: qRT-PCR analysis of 1 day old adult flies on genes involved in mitophagy (*pink1, parkin, usp30*, n=3-4) and autophagy (*atg1, atg8, atg18*, n=3). Error bars: SEM. Significance was tested using an unpaired 2-tailed Student's t-test. *p<0,05, **p<0,01, ***p<0,001. Level in *schlank*$^{KI-WT}$ was set to 1.

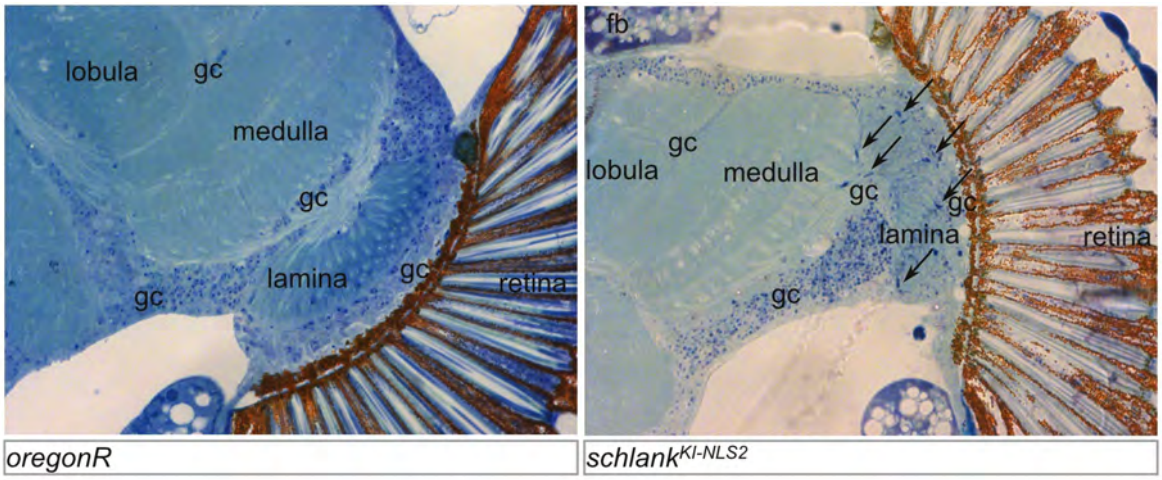

Figure 4.14: Sections of $schlank^{KI-NLS2}$ adult brain. 6 day old $schlank^{KI-NLS2}$ adult heads were fixed, embedded, sliced into semi-thin sections and methylene/toluidine-blue stained. *oregonR* (WT) males were taken as a control. gc: gangliar cells, fb: fatbody. Arrows point to elongated cells that are not seen in WT brain. Preliminary data, in collaboration with Dr. Mélisande Richard and Melanie Thielisch.

4.4 Cleavage of the Schlank protein

A cleavage of the Schlank protein was observed before the start of this thesis (PD Dr. Reinhard Bauer, personal communication; Bachelor thesis Simon Healy). In immunoblot analysis of larval extract with over expressed N- or C-terminally tagged Schlank protein two specific bands were detectable: full length Schlank with a size of approximately 47 kDa and a N-terminal fragment of about 16 kDa or a C-terminal fragment of about 31 kDa, respectively. This cleavage could also be observed using antibodies directed against an epitope derived from a N-terminal part of the Schlank homeodomain (α Schlank-HOM) on wildtype larvae, and to a smaller extend when the larvae were starved before lysis.

Back then, the following hypothesis was formulated: The homeodomain is cleaved off from the full length Schlank protein in a feeding dependent manner, is then able to enter the nucleus and directly or indirectly regulates genes, like e.g. *lipase 3*. Another hypothesis is based on a nuclear full length Schlank protein with the homeodomain facing the nucleoplasm, also allowing transcriptional regulation of target genes.

4.4.1 Cleavage of the Schlank protein is observed under different conditions

Confirmation of feeding dependent cleavage of taged and endogenous Schlank protein

The confirmation of feeding dependent cleavage of taged and endogenous Schlank protein is shown in figure 4.15. Representative blots are shown. The α Schlank-HOM antibodies seemed to have a higher affinity to the smaller N-terminal fragment in immuoblot analysis than to the full length Schlank protein as this full length band was detected rarely. Additionally, antibodies were used directed against the Schlank C-terminus (α Schlank-CT). α Schlank-CT antibodies detect the full length Schlank protein and a weaker signal at about 31 kDa.

To over express N- or C-terminally HA-taged Schlank virgins of the driver line *hs Gal4* were crossed to males of the UAS-lines *UAS-HA-schlank* or *UAS-schlank-HA*, respectively. Progeny was collected in L3 larval stage 8 hours (h) after a heat shock of 1 h at 37°C. Larvae were lysed and immunoblot analysis was performed using the α HA antibody. Full length Schlank and N- and C-terminal Schlank cleavage products could be detected (fig. 4.15A).

To analyze the feeding dependence of the Schlank cleavage *white*$^-$ L2 larvae were collected and one half was starved, the other half continued feeding for 6 h. The immunoblot analysis can be seen in figure 4.15B. In the fed condition αSchlankCT antibodies detected a weaker signal of the size of the full length Schlank protein (47 kDa) than in the starved condition whereas the signal at 31 kDa was stronger. The αSchlankHOM antibodies detected a double band at about 15 kDa with both bands being weaker in the starved condition.

Cleavage ot the Schlank protein during development

To analyze whether the cleavage of the Schlank protein is dependent on the developmental stage of *Drosophila melanogaster* individuals of each stage were collected and analyzed (fig. 4.16). In embryonic and pupal stage nearly no cleavage products were detected. In larval stages the intensity of the signal representing the smaller N-terminal fragment decreased with age, whereas the full length signal increased. In adults, the N-terminal fragment was detected weakly with the amount appearing more in females.

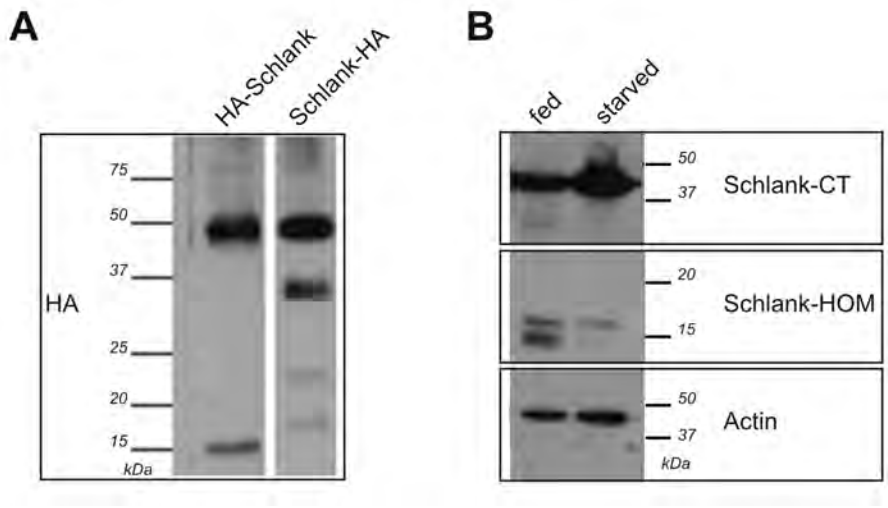

Figure 4.15: Confirmation of feeding dependent cleavage of taged and endogenous Schlank protein. **A**: Larvae stage 3 over expressing *schlank* N- or C-terminally HA-taged (HA-Schlank, Schlank-HA, respectively) under the control of the *hsGal4* driver line were lysed and expression and proteolytic processing was analyzed via immunoblotting using αHA antibody. **B**: Larvae stage 2 were fed or starved for 6 h (*white*$^-$). Schlank protein was detected using αSchlankCT antibodies directed against the Schlank C-terminus and αSchlankHOM antibodies directed against a peptide of the N-terminal part of the Schlank homeodomain. Actin was used as a loading control. Full length Schlank 47 kDa, N-terminal fragment 16 kDa, C-terminal fragment 31 kDa.

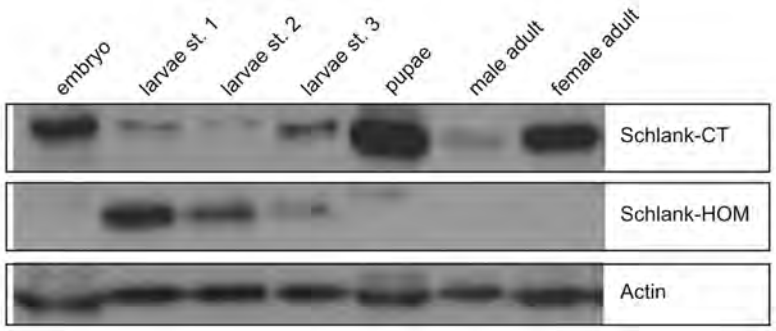

Figure 4.16: Cleavage of the Schlank protein during development. *Drosophila melanogaster* was collected in several developmental stages and immunoblot analysis was performed using the two different α Schlank antibodies: αSchlankCT antibodies directed against the Schlank C-terminus and αSchlankHOM antibodies directed against a peptide of the N-terminal part of the Schlank homeodomain. Actin was used as a loading control (full length Schlank 47 kDa, N-terminal fragment 16 kDa). IB performed by Picciotto (2014).

Organ dependent Schlank cleavage

To also analyze whether the cleavage of the Schlank protein is tissue dependent, organs of L3 *white*$^{-}$ larvae were dissected and fatbodies, guts and brains collected in 2x Laemmli buffer, homogenized and cooked directly (fig. 4.17). Immunoblot analysis showed, that the smaller band recognized by the α-HOM antibodies was detected in extracts of whole larvae and fatbody, this band slightly smaller was detected in gut extracts as well, where also the α-CT antibodies showed the smaller band of approx. 32 kDa. In brain extract only full length Schlank was detected.

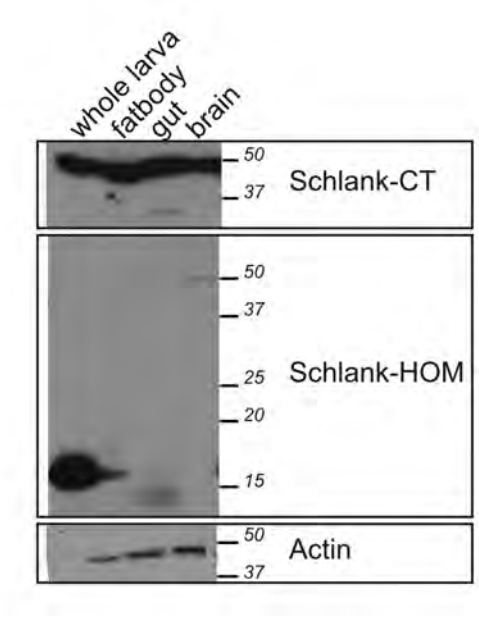

Figure 4.17: Organ dependent Schlank cleavage. Organs were dissected from larvae wandering stage 3 and immunoblot analysis was performed using the two different α Schlank antibodies. αSchlankCT antibodies were directed against the Schlank C-terminus and αSchlankHOM antibodies were directed against a peptide of the N-terminal part of the Schlank homeodomain. Actin was used as a loading control.

Schlank cleavage in *dcerk* mutants

Some mutant lines were tested in respect to Schlank cleavage as well. In *Drosophila ceramide kinase (dcerk)* mutants (Nirala et al., 2013) cleavage appeared reduced (fig. 4.18). Other mutants (*dronc*$^{-}$, *drice*$^{-}$, *dcp*$^{-}$, *srebp*$^{-}$, *ampk*$^{-}$) and RNAi lines (*furinRNAi, laceRNAi*) tested showed no change or unreproducible results.

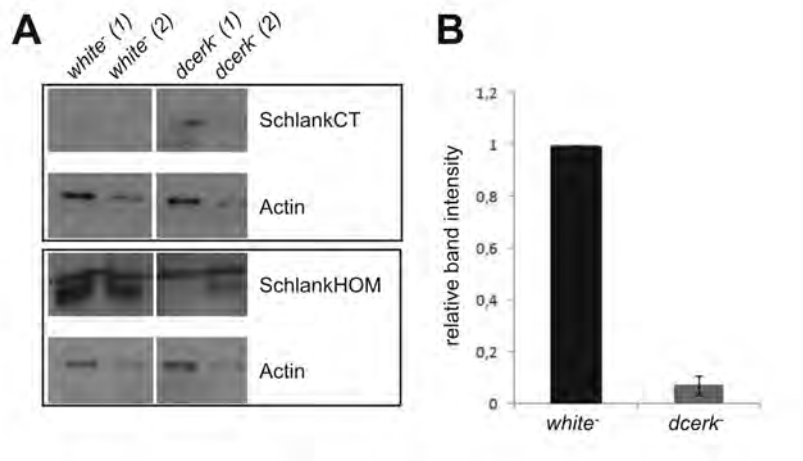

Figure 4.18: Schlank cleavage in *dcerk* mutants. **A**: Immunoblot analysis of Schlank in *white*$^-$ and *dcerk*$^-$ larvae (44-48 h AEL; larval stage 1). One blot of two independent biological replica is shown; (1) and (2). **B**: Quantification of Schlank bands relative to actin. Full length (αSchlankCT) relative to smaller N-terminal fragment (αSchlankHOM) level in *white*$^-$ larvae was set to 1, n=3. Error bars: SEM.

4.4.2 Analysis of the Schlank cleavage site

For a better understanding of the endoproteolytic processing of the Schlank protein the cleavage site was studied.

One approach was the purification of Schlank via immuno-precipitation followed by SDS-PAGE, Coomassie staining and mass spectrometric analysis. As the smaller fragments are only highly abundant in larval tissue purification could not be archived in a sufficient manner. Also establishment and addition of 2D gel electrophoresis did not lead to a satisfying result. One Schlank peptide however could be detected from a Coomassie stained band of the N-terminal fragment size after immuno-precipitation of over expressed HA-Schlank using αHA-coupled columns: AANVPILEK (AA 82-90, see fig 4.20) in collaboration with Dr. Marcus Krueger (MPI, Bad Nauheim; Bachelor thesis Simon Healy). Additionally, *in silico* analysis of Schlank was carried out in collaboration with Dagmar Stumpfe (AG Bajorath, LIMES, Bonn) but no protease restriction site was found/conserved near the estimated site. A TPPII site was found at AA 57, which would result in a smaller N-terminal fragment. TPPII is a tripeptidyl peptidase that was co-purified with 26S proteasomes and may participate in non lysosomal polypeptide degradation (Geier et al., 1999).

Here, two approaches are shown that were carried out to narrow down the Schlank cleavage site and to establish a Schlank version that is not cleaved any more: 1st, truncated Schlank was expressed and the size in SDS-PAGE was compared to the

smaller fragment's size and 2nd, *schlank* deletion constructs were cloned and UAS-lines were generated as there is no cleavage observable in cell culture.

Truncated Schlank versions

Deglycosylation experiments showed, that without the attached sugar residues the N-terminal smaller fragment behaves differently in immunoblot analysis (fig. 4.1B, fig. 4.19). Comparing the moving behavior with the protein standard the size of the non-glycosylated smaller fragment was about 12 kDa. This suggests a cleavage site within the homeodomain. To get closer insight into the smaller fragment's size truncated *schlank* versions of different length have been cloned in a cell culture expression vector (pAc). Cloned Schlank versions included the N-terminus until AA 98 which is located within the first loop of the homeodomain and until AA 138 which is located behind the homeodomain. They were HA-taged and lacking the endogenous glycosylation site to avoid size differences (i.e. if the truncated versions were not transferred into the ER and subsequently glycosylated correctly). After expression in cell culture moving behavior was analyzed in SDS-PAGE followed by immunoblotting and compared to PNGase treated extract from larvae over expressing *HA-schlank* (mimicking WT).

HA-SchlankN21Q-98* showed a comparable moving behavior to the smaller N-terminal fragment cleaved off in larvae (fig. 4.19 B). HA-SchlankN21Q-138* represents a N-terminal fragment until the end of the homeodomain. This construct moved much slower. To see whether a size difference of 10 AA was visible in these SDS-Page conditions HA-SchlankN21Q-88* and HA-SchlankN21Q-108* were expressed and analyzed, and indeed, the size difference to HA-SchlankN21Q-98* was clearly visible implying that the cleavage site is close to AA 98 (fig. 4.19B).

HA-schlank1-98 and *schlank99-400HA* were cloned into pUAST and transgenic flies were generated via P-element transgenesis (fig. 6.3). Those UAS-lines can be used to over express Schlank versions that are closely related to the Schlank cleavage products.

Schlank deletion constructs

To narrow down the cleavage site and to later on establish a fly line where no cleavage takes place different *schlank* deletion constructs were cloned into pUAST and UAS-lines were generated. First six fly-lines generated contained the *schlank* ORF N-terminally HA-tagged and C-terminally Myc-tagged (*HA-schlank-Myc*). Deletions introduced cover 10 AA each focussing on the hypothesis that the homeodomain might

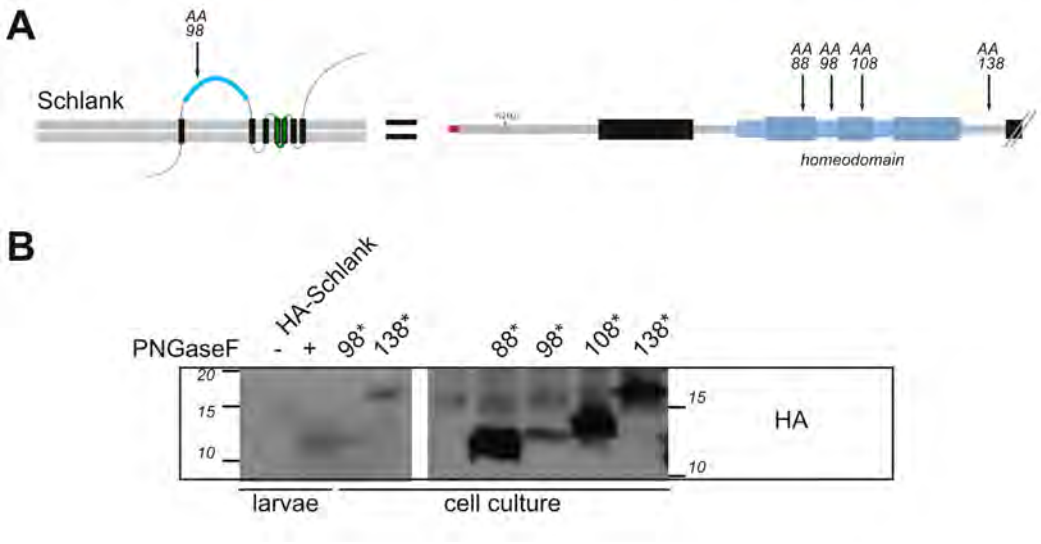

Figure 4.19: Truncated Schlank versions to analyze the Schlank cleavage site. **A**: Scheme of Schlank and the Schlank versions expressed. AA after which a STOP(*) codon was introduced are indicated. Constructs are HA-tagged and the endogenous glycosylation site is mutated (N21Q). Blue: homeodomain, black: TM domain, green: lag motif, red: HA-tag. **B**: PNGaseF treated HA-Schlank over expressing larval extract was analyzed via immunoblotting and the smaller N-terminal Schlank fragment was compared to truncated Schlank versions over expressed in cell culture (88*, 98*,108*,138*; first lane on the right blot shows a negative control: cells transfected with pAcGFP).

be cleaved off: ΔAA119-AA128 and ΔAA129-138 at the end of the homeodomain, ΔAA139-148 and ΔAA165-174 on both sites of the second TM domain, and a putative Furine cleavage site that is the same site as NLS2 has been mutated (122RLRR to GLRG). Furin is a proprotein convertase involved in the maturation of bone morphogenetic proteins like decapentalplegic (DPP; Künnapuu et al., 2009). Mutating the putative Furine site -RXK/RR- originated in an experiment where different mutant and RNAi lines were tested on Schlank cleavage via immunoblotting using αSchlank antibodies. In the *furineRNAi* line the amount of the N-terminal Schlank fragment seemed less abundant. None of the ten lines each generated for *UAS-HAschlankMycΔAA119-AA128* and *UAS-HAschlankMycΔAA165-AA174* showed expression of the transgene (data not shown). The control (*UAS-HAschlankMyc*) and the three other UAS-lines showed expression of the transgene when analyzed via immunoblotting and also the smaller N-terminal band when the αHA antibody was used (data not shown). The αMyc antibody for the detection of the C-terminus never gave a reliable signal.

When the size of the smaller fragment was clearer (see previous section: truncated Schlank versions) new deletion constructs were cloned and five new UAS-lines generated. N-terminal HA-tag and C-terminal GFP-tag were chosen. The following constructs were analyzed: *UAS-HAschlankGFP*, *UAS-HAschlankGFPΔAA89-AA98*, *UAS-HAschlankGFPΔAA95-AA100* missing the loop between helix1 and helix2 of the homedomain, *UAS-HAschlankGFPΔAA101-AA109* missing the second helix and *UAS-HAschlankGFPΔAA90-AA110* missing a larger stretch of AA surrounding AA98. Additionally a fly line was established where all the putative NLSs were mutated, including the first stretch of the bipartite NLS2 (AA100-102, KKK) that was taken into consideration here as well (fig. 4.20A).

All lines generated expressed the transgene and the smaller N-terminal fragment was detected when using the αHA antibody, except for *UAS-HAschlankGFPΔAA90-AA110*. There, in independent lines, the smaller N-terminal fragment was highly reduced or even absent (fig. 4.20B). Expression however was verified as the full length band (HA-Schlank-GFP) was detectable.

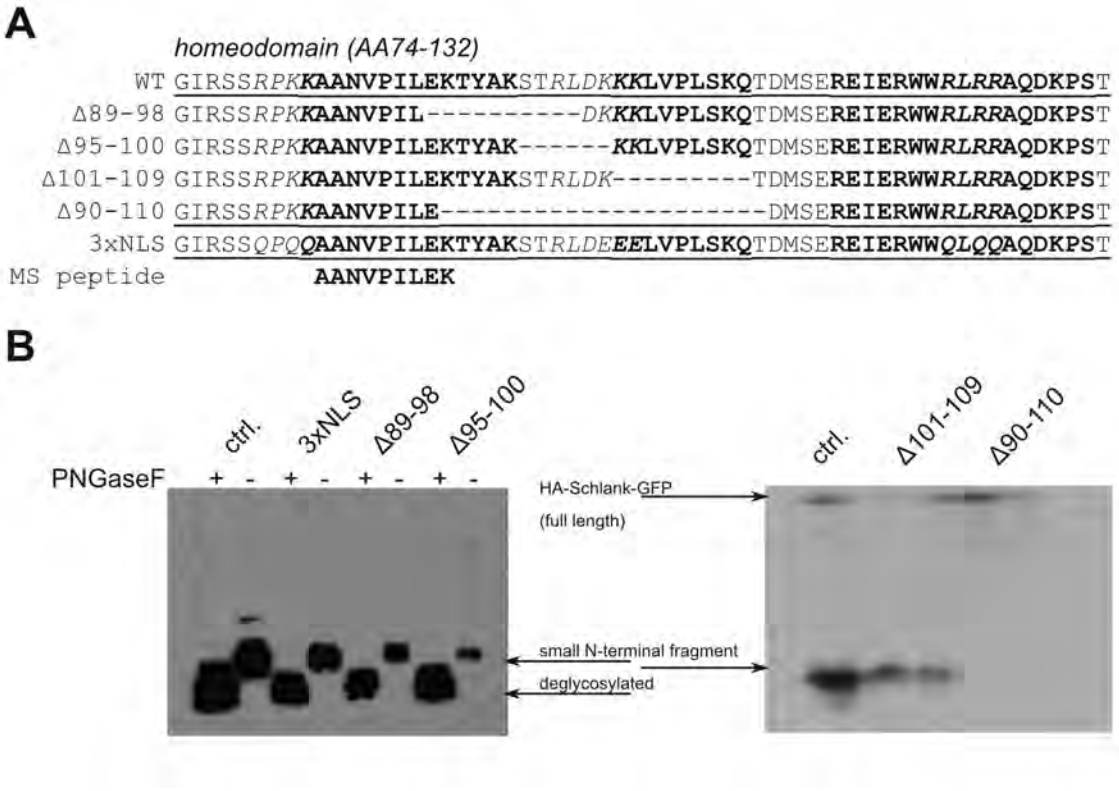

Figure 4.20: Schlank deletion constructs. **A**: Scheme of Schlank deletion constructs; helices are indicated by bold letters, NLSs are written in italic. In the Schlank full length sequence tagged N-terminally with a HA- and C-terminally with a GFP-tag different deletions or mutations were introduced. **B**: Immunoblot analysis of deletion constructs expressed in larvae using the *cg-Gal4* driver line and the αHA antibody.

5 Discussion

The *Drosophila melanogaster* Ceramide Synthase (CerS) Schlank is not only involved in the biosynthesis of sphingolipids but also in the regulation of triacylglycerol (TAG) levels. Second seems to be independent on the catalytic activity of the enzyme (Bauer et al., 2009; Voelzmann, 2013).

This thesis deals with the elucidation of the Schlank non-catalytic function that might arise from the homeodomain encoded in the Schlank sequence. It could be shown that the homeodomain faces the cytosol which in turn means that the nuclear Schlank protein could interact with DNA via this classical DNA-binding domain. A *schlank* deficient fly line has been generated ($schlank^{KO}$) that allows the re-integration of (mutated) *schlank*-DNA into its endogenous locus, enabling the specific analysis of distinct mutations. Analysis of these lines showed, that different *schlank* mutations lead to different phenotypes and might even point to a Schlank function in more than lipid homeostasis, e.g. muscle and brain function.

Additionally, the putative endoproteolytic processing of the Schlank protein has been studied. This cleavage of a N-terminal part of the Schlank protein was observed under different conditions, like feeding status, developmental stage, organ and mutant backgrounds. The former hypothesis of the hoemeodomain being cleaved off and translocating into the nucleus could be disproved as the cleavage site could be narrowed down to a 20 amino acid stretch within the Schlank homeodomain (also in the meanwhile, the full length Schlank protein was shown to be nuclear in immunofluorescent stainings; Voelzmann, 2013).

5.1 Elucidation of the non-catalytic Schlank function

A function of the Schlank protein apart from the synthesis of ceramides is mainly observed in the regulation of *lipase 3* gene expression, and also in the adjustment of body fat. This function could arise from a direct or indirect interaction with enhancer elements influencing expression of genes involved in lipolysis and lipogenesis as the

homeodomain encoded in the Schlank sequence shows several features of a classical homeodomain (sec. 1.5).

5.1.1 Schlank transmembrane topology studies prove the nucleoplasmic orientation of the homeodomain

Until now, only few experimental evidence on CerS transmembrane (TM) topology exists. The yeast CerS orthologs lag1p and lac1p do not contain a homeodomain and the configuration of the lag motif remained suggestive. It most likely contains two TM domains resulting in a total number of eight TM domains, with N- and C-terminus facing the cytosol (Kageyama-Yahara and Riezman, 2006). Also, studies on the homeodomain containing mouse CerS6 protein point to a cytosolic orientation of the C-terminus, but an ER-lumenal orientation of the N-terminus (Mizutani et al., 2005). The resultant cytosolic orientation of the homeodomain in their model is based on predictions of a TM domain between the N-terminal glycosylation site and the homeodomain. Some algorithms however do not predict any TM domain at this position in the Schlank protein (fig. 4.1A).

To investigate the orientation of the Schlank homeodomain to verify it's possible interaction with DNA *in vivo*, topology studies were carried out. Scanning-N-glycosylation mutagenesis can identify protein regions facing the luminal site of the ER. Disuse of introduced glycosylation sites can be due to cytosolic orientation of the analyzed protein region, but also the inability of the oligosaccharyl transferase complex to recognize the glycosylation site. Additionally, acceptor sites have to be located a minimum distance of 12/14 amino acids (AA) away from the luminal membrane surface of the ER in order to be efficiently N-glycosylated. This fact can be used to define ends of TM domains.

The glycosylation site at the N-terminus is conserved in Schlank (AA21) and scanning-N-glycosylation mutagenesis showed ER-luminal orientation of glycosylation sites introduced after AA 178 and 301, but not at the very C-terminus or at six different positions within the homeodomain (fig. 4.1). Additionally, two predicted glycosylation sites at the C-terminus (at AA 361 and 368) were not used *in vivo*. These results strengthen the assumption of the Schlank homeodomain facing the cytosol/nucleoplasm and the existence of the first two (at about AA 43-60, AA 141-158) and the last (at about AA 303-328) TM domains. The N-terminus faces the lumen of the ER and the C-terminus may face the cytosol, resulting in an uneven number of TM domains.

Taking the algorithms into account five or seven TM domains are most likely differentiating in the number of TM domains within the lag motif (0 vs. 2). Due to the fact that the lag motif is involved in the catalytic activity, namely the synthesis of membrane lipids, and comparison with the experimental data from the yeast Ceramide Synthases, Schlank presumably contains seven TM domains (fig. 4.1D II). In this model, the lag motif's orientation within the membrane is equivalent to yeast CerS.

As the orientation of the homeodomain would allow DNA interaction *in vivo*, further studies were carried out to investigate a nuclear Schlank function.

5.1.2 Generation and establishment of *schlank knock out* and *schlank knock in* lines resulted in a *schlank* null allele and *schlank* alleles with restored (mutated) *schlank* expression

To analyze Schlank function without over expression artifacts or off-target effects a $schlank^{KO}$ line was successfully established based on Huang et al. (2008, 2009). The re-integration of *schlank*-DNA lead to fly lines which are expressing wildtype *schlank* or *schlank* mutated in the homeodomain or in the catalytically important lag1 domain under the endogenous promoter control ($schlank^{KI-WT}$, $schlank^{KI-NLS1}$, $schlank^{KI-NLS2}$, $schlank^{KI-H215D}$, $schlank^{KI-E118A}$). The fly lines were analyzed concerning survival, development, gene expression, TAG level *et cetera*.

The basic verification showed that indeed a functional *schlank* null allele was generated (fig. 4.3). Minimal residual *schlank* mRNA and CerS activity could reside from the maternal component(Bauer et al., 2009). The strong analogy to the stronger $schlank^{P(X)349}$ mutant allele further proves the specific deletion of *schlank* (fig. 4.4).

The re-integration of *schlank*-DNA could be proven via PCR, and the *schlank* mRNA and protein expression was shown to be at wildtype level which is important for the further characterization of those *schlank knock in* lines (fig. 4.6).

Analysis of Schlank protein expression in the *schlank knock out* and *schlank knock in* lines has to be repeated with more biological replica to perform a proper quantification. Also, protein expression has to be analyzed in respect to Schlank cleavage. The data generated so far does not allow a reliable evaluation. The Schlank protein expressed in $schlank^{KI-WT}$ larvae is processed like in $white^{-}$ larvae, Schlank^{NLS1} and Schlank^{NLS2} protein however have mainly been observed as full length protein (data not shown). The peptide that was used as the epitope to generate the αSchlankHOM antibodies

-the main tool to analyze Schlank cleavage- includes the NLS1 sequence and thus the antibodies may not be able to bind Schlank^{NLS1}. Over expression of Schlank with the same point mutations within the first NLS using an UAS-line generated (*UAS-HAschlankNLS1*) shows cleavage of the protein when analyzed with the αHA antibody. The mutations in the NLS2 in the UAS-lines differ from those introduced into the *schlank* sequence in the *schlank*$^{KI-NLS2}$ line (RLRR→ALAR vs. RLRR→QLQQ (HASchlank3xNLS) and RLRR→GLRG (HASchlankMycNLS2)). Those mutations did not change Schlank processing.

Also important for the differentiation between Schlank protein and metabolite function is the Ceramide Synthase activity of the mutated expressed Schlank proteins. This was analyzed with an *in vivo* assay via metabolic labeling of larvae. The genomic modifications performed on *schlank*$^{KI-WT}$ did not change CerS activity as compared to *white*$^{-}$, as well as the *schlank*^{NLS2} mutation. In *schlank*$^{KI-NLS1}$ larvae, however, CerS activity is reduced indicating that this mutation has an influence on the catalytical activity of Schlank even though it is located within the first helix of the homeodomain. This part of a CerS protein does not influence CerS activity in mouse CerS5 when deleted (Mesika et al., 2007). However, considering the phenotype of the *schlank*$^{KI-NLS1}$ line, it indicates that a lack of 20 % CerS activity did not affect survival and growth (fig. 4.8) as it does in *schlank*^{KO} and *schlank*$^{KI-H215D}$.

Changes in the amount of the different sphingolipids have also to be considered in the *schlank knock out* and *schlank knock in* lines. Analysis of the sphingolipidome via mass spectrometry is being performed in collaboration with Prof. Dr. Roger Sandhoff (DKFZ, Heidelberg).

The *schlank*$^{KI-E118A}$ line was generated at the end of this thesis and could not be analyzed on grounds of time. The mutation is based on a missense coding single-nucleotide polymorphism (E115A) located in the homeodomain of the *CerS2* gene that was found in a genetic association study of rhegmatogenous retinal detachment (Kirin et al., 2013; Park et al., 2014).

5.1.3 Schlank protein function in lipid homeostasis: comparison of the *schlank*^{KO} with the *schlank*$^{KI-H215D}$ line showed Schlank protein dependent *lipase 3* regulation

The genomic modifications carried out at the *schlank* locus allow the direct comparison of a *schlank* null allele (*schlank*^{KO}) with an allele where the Schlank protein

is still expressed but unable to synthesize ceramide ($schlank^{KI-H215D}$, CerS activity has to be yet determined). Therefore, the Schlank protein function can be analyzed very specifically. Unfortunately, both lines died at first larval stage without showing any growth, similar to $schlank^{P(X)349}$ mutants (fig. 4.4A-C, 4.8A,C, 4.11A). Even though this underlines the importance for ceramide biosynthesis on survival, it also complicates experimental analysis. Measuring TAG level using TLC did not show any differences between the two lines (fig. 4.11B). Stage 1 larvae however do not have much TAG in general and a more sensitive method (like mass spectrometry) could be suited better (Carvalho et al., 2012). Differences in TAG level between $schlank^{KI-H215D}$ and $schlank^{KO}$ larvae are supposed as qRT-PCR analysis showed no up regulation of *lipase 3* in $schlank^{KI-H215D}$ larvae as it is seen in $schlank^{KO}$ and *schlank* mutant larvae (fig. 4.4D, 4.10, 4.11C). Also, *brummer* may not be as highly up regulated in $schlank^{KI-H215D}$ larvae as in $schlank^{KO}$ larvae, whereas *akh, srebp* and *fas* show a similar regulation (fig. 4.11C). The differences in the expression of those lipases may result in modified TAG level and point to the regulation of those genes, especially *lipase 3*, by the Schlank protein and not the ceramide level. On the other hand, the similar regulation of *akh* and *fas* may point to their regulation via ceramide level.

5.1.4 Schlank function in the nucleus: mutations in the NLSs result in a variety of phenotypes affecting lipid homeostasis and behavior

Schlank full length protein was detected in the nucleus and it's import could be linked to Ketel (fly homologue of Importin-β) and two putative NLSs. Schlank Homeodomain - DNA interaction was shown *in vitro* and gene regulation was studied using over expression of deletion constructs (Voelzmann, 2013). Here, *in vivo* function of nuclear Schlank protein pools was addressed using the *schlank knock in* lines carrying mutations within those two NLSs: $schlank^{KI-NLS1}$ and $schlank^{KI-NLS2}$.

The point mutations within the NLSs where chosen to get an insight what the nuclear function of the Schlank protein may be. Nuclear localization of mutated Schlank was changed, indeed, but as the NLSs are localized within the homeodomain also a putative unknown function may be affected. For example, some homeodomains are required for dimer formation (Papadopoulos et al., 2012) and the third helix which contains the second NLS is important for the sequence specific interaction with DNA (Gehring et al., 1994b). In this case, additional effects of the mutations are not known

and therefore need to be studied in more detail. It was shown that mammalian CerS dimerize which affects their CerS activity (Laviad et al., 2012).

As over expressed full length Schlank protein is not found in the nucleus in immunoflourescent stainings, first, the nuclear localization of Schlank^{NLS1} and Schlank^{NLS2} was analyzed to see whether those mutations lead to a disrupted translocation of Schlank into the nucleus, as would be consistent with cell culture experiments with homeodomain constructs obtained by Voelzmann (2013). Indeed, Schlank^{NLS2} showed a weaker, but not absent, nuclear localization as compared to Schlank^{WT}. Unexpectedly, Schlank^{NLS1} showed a stronger nuclear accumulation (fig. 4.9A+B). The reason of an only partial reduction of nuclear Schlank^{NLS2} could be grounded in the two NLSs working together. Therefore, the functional NLS1 could be responsible for the smaller amount of nuclear Schlank^{NLS2}. The accumulation of Schlank^{NLS1} in the nucleus could be based e.g. on the specific mutation used or disrupted nuclear export signals (NES). Predicted NES do not overlap with the NLS1 (Kosugi et al., 2008; Munsie et al., 2012) and the deletion of the first NLS (RPKK) in homeodomain constructs resulted in it's weaker nuclear accumulation in cell culture experiments. In those experiments, mutations in both NLSs (R78A R124A) also reduced nuclear accumulation (Voelzmann, 2013). Here, the NLS1 was mutated to RPMM, because it is followed by two alanine residues and a deletion was considered too invasive.

Schlank homeodomain function in lipid metabolism

Nuclear Schlank accumulation in stage 3 *schlank*$^{KI-NLS1}$ larvae could explain the down regulation of *lipase 3* mRNA in *schlank*$^{KI-NLS1}$ L1 larvae (fig. 4.10). Analysis of TAG level could help figure out if this regulation results in a physiological change. *De novo* TAG and FA synthesis in *schlank*$^{KI-NLS1}$ larvae showed no change (fig. 4.12C). Development of *schlank*$^{KI-NLS1}$ flies was unchanged as compared to the controls (fig. 4.8). Unfortunately, *de novo* CerS activity was reduced by 20 % in this line in first and third instar larvae.

On the other hand, flies carrying the mutation within the second NLS showed unchanged CerS activity, but severe phenotypes. Analysis revealed a delayed development, lethality of about 90 % until adulthood and growth defects (fig. 4.8). In stage 1 larvae *fas* mRNA was down regulated (fig. 4.10), and preliminary data on stage 3 larvae showed a strong up regulation of *lipase 3* transcript level (data not shown). *fas* down and *lipase 3* up regulation is consistent with gene expression in *schlank*^{KO} larvae (fig. 4.4D) and would fit the hypothesis of this gene regulation via the Schlank

homeodomain.

The transfer of this qRT-PCR data on physiological level is observed in a reduced size of fatbody cells, decreased TAG level in stage 3 $schlank^{KI-NLS2}$ larvae and reduced *de novo* TAG synthesis (fig. 4.9C, fig. 4.12B+C). This data strengthens the hypothesis of the (nuclear) Schlank protein being involved in lipid homeostasis.

The qRT-PCR experiments on third instar larvae has to be repeated to confirm the *lipase 3* up regulation in the stage where the body fat phenotype is most obvious. *lipase 3* expression was not up regulated in first instar larvae and adult flies of the genotype $schlank^{KI-NLS2}$. The reason may be that the described expression of this gene is restricted to larval fatbody and that feeding behavior is changed from continuous feeding in larval stages to on-off feeding in adult stage (Pistillo et al., 1998). A gene regulated in adult flies is the AkhR target *midway* (Baumbach et al., 2014), which is down regulated in one day old $schlank^{KI-NLS2}$ flies. It encodes the *Drosophila* Diacylglycerol O-Acyltransferase 1 and mutants have a lean phenotype (Beller et al., 2010).

Reduced TAG level, up regulated lipases and down regulated lipogenesis factors can also be due to starvation or the inability to take up food. $schlank^{KI-NLS2}$ larvae took up red dyed yeast that was visible throughout the gut which shows, that they feed and the food gets along through the intestinal tract. Also, the metabolic labeling experiments showed that the larvae indeed took up the radioactivity. To further check for starvation one could check the activity of the insuline pathway e.g. via qRT-PCR of target genes (*InR*) or FOXO localization.

Total FAs seemed to be elevated in $schlank^{KI-NLS2}$ stage 3 larvae, but *de novo* FA synthesis was unchanged (fig. 4.12B+C). Therefore, FAs may result from elevated lipolysis. As both, total and *de novo* TAG level were reduced, thus may result from reduced synthesis, but TAG decomposition could be involved as well.

Looking at *fas* transcriptional regulation in the lines analyzed here, it may either be influenced by the homeodomain (as just mentioned) or by ceramide synthesis (as assumed by comparison of $schlank^{KO}$ with $schlank^{KI-H215D}$). Repetition of this analysis to reduce error bars may give clarity, as *fas* expression shows a tendency to be down, or up regulated in $schlank^{KI-H215D}$ larvae as compared to *white*− or $schlank^{KO}$ larvae, respectively, hinting to a regulation via the Schlank homeodomain. Including other lipogenesis genes may be worthwhile, also including stage 3 larvae as in that stage FAs seemed to be elevated in $schlank^{KI-NLS2}$ animals.

Additional phenotypes observed in the *schlank*$^{KI-NLS2}$ fly line may link the Schlank homeodomain to muscular and neuronal function

The main aspect in this theory is the impaired moving behavior of *schlank*$^{KI-NLS2}$ flies. Quantification of this was achieved using the negative geotaxis (or climbing) assay commonly used to determine behavioral and neuronal dysfunction in *Drosophila melanogaster*. It can reflect ataxia that is common in human neurodegenerative diseases. A disadvantage of this method is that loss of climbing can be due to factors other than neurodegeneration (Lessing and Bonini, 2009). In comparison to *white*$^{-}$, *schlank*$^{KI-WT}$ and also *schlank*$^{KI-NLS1}$ flies *schlank*$^{KI-NLS2}$ flies showed a strong reduction of climbing distance (fig. 4.13A). Further analysis in this direction were qRT-PCR analysis and analysis of brain and muscle structure of adult flies. Due to abnormal wing posture in *schlank*$^{KI-NLS2}$ flies that were also observed in fly models of Parkinson's disease (Greene et al., 2003; Yang et al., 2006; Fernandes and Rao, 2011) gene expression of *pink, parkin* and *usp30*, but also of autophagy genes (*atg1, atg8, atg18*) was analyzed to get a first impression (fig. 4.13B+C).

Similar wing posture phenotypes were also observed e.g. in another model of mitochondria unfolded protein response (UPR^{mt}; Pimenta de Castro et al., 2012), upon impairment of the ubiquitin pathway (Liu and Pfleger, 2013), in a *Drosophila* model for oculopharyngeal muscular dystrophy (OPMD; Chartier et al., 2006) and amyotrophic lateral sclerosis (ALS; Sanhueza et al., 2014). All those models are associated with an accumulation of proteins in different organelles, leading to dysfunction or degeneration of muscle cells and/or neurons, further suggesting an impact of Schlank^{NLS2} on muscle and neuron function. About 80 % of the few flies of the *schlank*$^{P(X)61}$ mutants that reach adulthood fail to deflate their wings after eclosion, rest 20 % show partially or fully deflated wings, which then also show the same wing posture defects (André Voelzmann, unpublished data).

Schlank knock down specifically in glial cells, but not in neurons, was shown to disrupt axonal ensheathment (Ghosh et al., 2013). Axonal ensheathment is important for motor function and survival and as it was shown to be impaired in *schlank* RNAi it may also be affected in the *schlank*$^{KI-NLS2}$ fly line. Until now, the axonal phenotype observed is discussed as a result of reduced PE-ceramide, as it also appears in *lace, spt-1* and *des1* RNAi in all of which PE-ceramide has been shown to be reduced (Ghosh et al., 2013).

Wing muscle structure in *schlank*$^{KI-NLS2}$ flies seemed normal when dissected and stained with phalloidin (Yanina Pesch, personal communication) suggesting that im-

paired moving is not due to apparent muscle damage. However, closer analysis of the muscles via microscopy e.g. with a higher resolution and specific stainings and via functional assays is necessary. This would help unravel the mechanistic background of the impaired climbing assay performance and wing posture defects of the $schlank^{KI-NLS2}$ flies.

Parkinson's disease is a neurological disorder linked to aberrant protein folding, oxidative damage and mitochondrial dysfunction with the progressive loss of dopaminergic neurons in the substantia nigra of the midbrain, but also others (Spillantini et al., 1997; Dauer and Przedborski, 2003; Braak et al., 2003; Hirth, 2010). It has also been linked to CerS (Abbott et al., 2014). Among the genes affected in familial forms of Parkinson's disease are *parkin* and the *tensin homologue (PTEN)-induced kinase I (pink1)*. *parkin* encodes a protein with E3 ubiquitin ligase activity, *pink1* a protein with a serine-threonine kinase domain and a mitochondrial targeting sequence. PINK1 and Parkin act in a linear pathway to regulate mitochondrial integrity and maintenance, probably as mediators of the mitochondrial fission machinery (Guo, 2012). The recruitment of Parkin to mitochondria depends on PINK1 and PINK1 protein level are up regulated on damaged mitochondria (Narendra et al., 2008, 2009; Vives-Bauza et al., 2010; Ziviani et al., 2010). *parkin* has been shown to be regulated also on transcript level, e.g. by ATF4, a UPR activated transcription factor, whereas PINK1 protein level seems to be regulated mainly in a posttranslational manner (Imai, 2012). USP30, a deubiquitinase localized to mitochondria, has been shown to be an antagonist of PINK1 and Parkin dependent mitophagy (Bingol et al., 2014). In $schlank^{KI-NLS2}$ flies *parkin* and *usp30* are slightly up regulated. As they are antagonists and the regulation is very weak this may not have a strong physiological effect. To check directly for UPR^{mt} activation *hsp-60* and *hsc-70-5* mRNA level could be analyzed.

Also, autophagy associated gene expression is not highly altered in $schlank^{KI-NLS1}$ and $schlank^{KI-NLS2}$ flies, the latter showing a slight tendency towards up regulation of *atg1* and *atg18*. Autophagy is a mechanism to recycle unnecessary or dysfunctional cellular components through the actions of lysosomes. It is required for normal turnover and is also observed in cancer and in response to nutritional starvation (Mortimore and Pösö, 1987; Mathew et al., 2007; Mizushima et al., 2004). Autophagy associated genes like *atg1, atg8, atg18* are transcriptionally up regulated upon autophagy induction, but as this regulation is not studied in detail and do not always need to be significant other methods should be performed as well (Klionsky et al., 2012).

Investigation of brain morphology was performed with the help of toluidine blue

staining of brain sections. This data is preliminary as it was only performed once, with the age of the control flies being unknown. Those experiments suggest a reduced size of brains of $schlank^{KI-NLS2}$ flies. Also, elongated cells have been observed that were present only in $schlank^{KI-NLS2}$ but not in control brains. Apoptosis and vacuolization could not be observed (fig. 4.14). As the elongated cells do not appear darker than surrounding cells they are probably not apoptotic. They may have evolved from brain cells or could be immune or other cells invasing the brain.

Experiments to shed light on the brain function in $schlank^{KI-NLS2}$ flies -among the repetition of the toluidine stainings- could be transmission electron microscopy (TEM) which allows better resolution of sub-cellular structures and electrophysiology which allows the direct assay of neuronal dysfunction. Also, a closer analysis of the life span could help because all neurodegenerative mutants show a shortened lifespan (Lessing and Bonini, 2009).

Lipid homeostasis and muscle/brain function

Taken together, the climbing assay performance, the abnormal wing posture and the possibly reduced brain size of $schlank^{KI-NLS2}$ flies point to an influence of the $schlank^{NLS2}$ mutation on neuronal and maybe muscular function. Expression analysis of *schlank* showed it's abundance in neurons and neuroblasts (Voelzmann and Bauer, 2011; Voelzmann, 2013). The precise phenotype and the underlying mechanisms however have to be studied in more detail.

It is possible that those phenotypes are grounded in the reduced TAG-level in stage 3 larvae and a resulting energy deficit in neurons and muscles. Measuring ATP level may help figuring out their energy status.

Yet, not much is known about how lipid and energy homeostasis influence neurodegenerative phenotypes, but some neurodegeneration *Drosophila* mutants have been linked to lipid homeostasis (Liu and Huang, 2013). For instance, mutants of two genes involved in the *de novo* Coenzyme (Co) A biosynthesis (*fumble* and *phosphopantothenoylcysteine synthetase*), and of the fatty acid CoA ligase *bubblegum* specific for very long chain FAs develop neurodegeneration phenotypes (Yang et al., 2005; Bosveld et al., 2008; Min and Benzer, 1999). Apolipoprotein D (ApoD), a lipid carrier rescues in Alzheimer's disease and Friedreich's ataxia (Muffat et al., 2008; Navarro et al., 2010). Lessing and Bonini (2009) surveyed genes causing adult onset neurodegeneration in the fly and classified them according to five key cell biological processes. They have listed e.g. the F1F0-ATP synthase subunit and the Na^+/K^+ ATPase α subunit.

Mammalian Ceramide Synthase 2 was shown to interact with vacuolar ATPase via it's homeodomain, thereby modulating V-ATPase activity (Yu et al., 2013). SREBP was shown to link lipogenesis with mitophagy in a genome wide RNAi screen (Ivatt et al., 2014; Ivatt and Whitworth, 2014). Also, there is a close connection between metabolic status and the reactivation of neuroblasts from quiescence, where Target Of Rapamycin (TOR) and Insuline-like Receptor signaling are involved (Sousa-Nunes et al., 2011).

Subramanian et al. (2013) showed in another context, that climbing assay performance was decreased in flies that were starved and therefore had reduced TAG level. The underlying mechanism by which the different mutations and conditions influence neuronal function are not yet understood.

Another factor to consider is the Ceramide Synthase activity of Schlank^{NLS2} in the nucleus. If the nuclear CerS activity is important for different processes like cell division or epigenetics (like Sphingosine Kinase; Hait et al., 2009) and is reduced in the *schlank*$^{KI-NLS2}$ line this could be responsible for some phenotypes.

Nevertheless, in this study it could be shown that point mutations within the third helix of the Schlank homeodomain influencing nuclear localization and maybe other interactions, but not overall CerS activity was responsible for a broad range of phenotypes.

Individuals of the *schlank*$^{KI-NLS2}$ line showed similar phenotypes as compared to the *schlank* mutant alleles, especially the weaker *schlank*$^{P(X)61}$ allele (lean, reduced TAG, less moving, stay outside yeast paste, wing posture). The phenotypes observed in *schlank* mutants are more severe and may result from a combination of protein functions. The mutation in the second NLS could explain some of the mutant phenotypes.

Lately, mammalian CerS6 was reported to regulate *acid ceramidase* gene expression in a CerS6 activity independent manner (Tirodkar et al., 2015) which could hint to a conserved function of CerS homeodomains.

5.2 Schlank endoproteolytic processing

Cleavage of proteins is not only a degradative event, but also involved in signaling pathways as a regulatory mechanism (Ehrmann and Clausen, 2004). To analyze the putative cleavage of the Schlank protein -which is observed as N- and C-terminal fragment bands in immunoblot analysis- several experiments have been performed to narrow down the site of cleavage and to get an insight into the regulation of this event (sec 4.4).

In *Drosophila melanogaster* there are 585 known and putative peptidases (MEROPS, Rawlings et al., 2014).

5.2.1 Schlank is split within the homeodomain

Analysis of the Schlank cleavage products revealed that the site of endoproteolytic processing would be within a 10 AA range from AA98 in both directions (fig. 4.19). Studies with HA-Schlank-GFP over expression lines with deletions and mutations within the homeodomain further showed, that deletions of AA 89-98, AA 95-100 and AA 101-109 still resulted in cleaved Schlank protein expression, whereas deletion of a larger stretch spanning this area (AA 90-110) resulted in way less cleavage product (fig. 4.20). N-terminal of this area a Schlank peptide was found in MS analysis of the smaller fragment band (AA 82-90) and in the HA-Schlank construct with all NLS mutated (78-81RPKK→QPQQ, 100-102KKK→EEE, 122-125RLRR→QLQQ) -which is also still cleaved- the mutation of AA 100-102 overlaps the deletions of AA 95-100 and AA 101-109. Unexpectedly, all deletion constructs showed the same moving behavior in SDS-PAGE, even after deglycosylation (fig. 4.20). The deletion of the 10 AA 89-98 which are most likely N-terminal of the cleavage site should result in a smaller band as observed for HA-Schlank88*.

Those results show that the Schlank protein is processed within the homeodomain. It remains unclear whether this event occurs via one site specific protease because overlapping deletion and mutation of smaller stretches of AA ranging from AA 89 to AA 109 still result in cleaved Schlank protein, with size comparisons suggesting a site within this protein region. It could be possible that the recognition site of the protease is not it's cleavage site: It may recognize an AA sequence up- (or down-) stream which is not affected by the deletions and cleave at about AA 98. HASchlankGFPΔ90-110 might not be cleaved due to misfolding and/or interfering 3D structure. Another explanation could be the existence of two sites; one at AA 110 and a second one

leading to the truncation of the N-terminal fragment.

Altogether it seems unlikely that the observed Schlank processing may be due to an experimental artifact as there are conditions observed where there is no Schlank cleavage (e.g. pupal stage, starvation) and fragment bands can be detected with different antibodies.

Now, that experiments showed that cleavage is most prominent in stage 1 larvae (fig. 4.16), one could consider repeating MS analysis of the N-terminal fragment with extracts from this stage instead of extracts from 3rd instar larvae, to investigate the site of cleavage.

5.2.2 Different conditions affect Schlank processing

The amount of Schlank fragments varied under different conditions like developmental stage, feeding condition and organ (section 4.4.1). It could be observed that with rising larval stage the smaller N-terminal fragment level decreases whereas the amount of full length protein increases. In embryo and pupal stage nearly no smaller N-terminal fragment could be detected, but a high amount of full length protein (fig. 4.16). In larvae, the deprivation of food resulted in a reduction of the smaller N-terminal fragment and an increase of full length Schlank protein; in stage 1 and stage 2 larvae this occurred quiet rapidly after 3-6 h of starvation, in stage 3 larvae a starvation period over night was necessary (fig. 4.15). To identify the organ in which this event happens, stage 3 larvae where dissected showing few N-terminal fragment in fatbody and gut, but none in brain extracts (fig. 4.17). Another indication of cleavage occurring in fatbody cells is the appearance of fragment bands of tagged Schlank protein over expressed under the control of the *cgGal4* driver line (fig. 4.20B). The analysis of different mutant larvae showed less Schlank cleavage in *Drosophila ceramide kinase (dcerk)* mutants (fig. 4.18). In *dcerk* mutants ceramide is accumulated, ceramide-1-phosphate levels seem unchanged in whole fly extracts and metabolism is reprogrammed, probably through the enhanced activation of Akt and following inhibition of FOXO (Nirala et al., 2013). As under starvation Akt phosphorylation is decreased and FOXO is activated (Calnan and Brunet, 2008), but Schlank cleavage is also reduced, a regulation via this mechanism seems unlikely.

Looking at commonalities of those conditions, Schlank cleavage may correlate with TAG level. TAG level are reduced under starvation, elevate during larval stages, are lower in males than in females, high in fatbody and low in brain. Also, in *dcerk* mutants they are decreased (Palanker et al., 2009; Carvalho et al., 2012; Guan et al.,

2013; Nirala et al., 2013). If this correlation was causative, it would still be unclear whether Schlank cleavage occurs up- or downstream of body fat regulation. Due to the hypothesized direct or indirect binding of the Schlank homeodomain to the *lipase 3* enhancer region cleavage may regulate this interaction. Therefore, the protease had to be nuclear. Aspects in the disfavor of this hypothesis are the non-nuclear localization of over expressed *schlank* in immunofluorescent stainings (but over expressed Schlank being cleaved) and no *lipase 3* regulation in *dcerk* mutants (microarray analysis, Nirala et al., 2013). For now, it is unclear, in which subcellular compartment cleavage occurs.

An impact of Schlank cleavage on Ceramide Synthase activity is also imaginable as cleavage may result in an inactive protein. Especially since the endogenous C-terminal fragment shows a low abundance using the αSchlankCT antibodies. If the Schlank full length band would correlate with CerS activity high activity would be expected in embryo, pupae, brain, in *dcerk* mutants and under starvation, but not in well fed larvae. The Ceramide Synthase activity of the Schlank protein has not yet been analyzed under the conditions mentioned above. Additionally, establishment of an *in vitro* NBD-CerS assay (Kim et al., 2012) for *Drosophila* showed an inhibition of the reaction by the addition of AcylCoAs of different chain length and could therefore not be used. The *in vivo* CerS assay could not be used to compare fed with starved larvae as uptake of radioactively labeled substrate is achieved via feeding. Looking at the ceramide level during development may be an alternative, but one has to keep in mind, that ceramide is further metabolized to other sphingolipids and that ceramide can be generated via three different pathways. Ceramide level may therefore not represent it's *de novo* synthesis. Ceramide level highly increase in embryonic stage and decrease in larval stages when normalized to total membrane lipids measured (Guan et al., 2013). If normalized to individuals they more or less increase during larval stages (Carvalho et al., 2012). Both normalization methods show a relatively constant ceramide level during pupal stage. In the brain, cermaide level are comparably high. In *dcerk* mutants ceramide level are elevated due to the loss of *ceramide kinase* (Nirala et al., 2013). One would assume that CerS activity is needed in the state of drastic growth as observed in larvae and that upon ceramide accumulation like in *dcerk* mutants CerS activity would be decreased.

Many regulative protease events result in a localization change, which could be possible here as well. However, experimentally, this is not easy to achieve, yet. Schlank localization is very broad and not all Schlank pools have been assigned, Schlank over expression does not resemble the endogenous Schlank localization and co-stainings us-

ing the αSchlankHOM and the αSchlankCT antibodies to stain the N- or C-terminus, respectively, are difficult as the αSchlankHOM antibodies do not work well in stainings.

It is also yet to find out whether the UAS lines *HA-schlank1-98* and *schlank99-400HA* functionally resemble the Schlank cleavage products or not.

Taken together, Schlank endoproteolytic processing seems to occur within he homeodomain and in a regulated manner. Further investigation could unravel new mechanisms of Schlank function.

The hypothesis of the Schlank homeodomain being cleaved off to then enter the nucleus could be disproved. The small size of the non glycosylated N-terminal Schlank fragment (fig. 4.1B) and the studies on the cleavage site (fig. 4.19+ 4.20) showed a disruption of the heomeodomain by this processing event. The alternative hypothesis of a full length nuclear Schlank protein has gained more relevance. It is also supported by the immunofluorescent stainings using antibodies directed against the Schlank C-terminus showing nuclear Schlank protein (Voelzmann, 2013; see also fig. 4.9A).

5.3 Outlook

In the future, the further experiments mentioned in the respective sections could help get better insight into Schlank nuclear and protein function, and also into the mechanisms underlying Schlank cleavage. Especially important is e.g. the lipidomic analysis of the *schlank knock out* and *schlank knock in* lines generated, because the differentiation between protein and metabolite function is crucial.

Additionally, to investigate the impact of *lipase 3* regulation on body fat, analysis of *lipase 3* repression and over expression in respect to TAG level should be performed, preferably in different *schlank* backgrounds. Not much is known about the quantitative correlation between *lipase 3* gene expression and TAG level. In cell culture experiments, *schlank dsRNA* mediated reduced TAG level could be rescued by *lipase3 RNAi* (Ute Schepers, unpublished data; André Voelzmann, personal communication).

Microarray/RNAseq and MS studies on $schlank^{KI-NLS2}$ as compared to $schlank^{KI-WT}$ and $schlank^{KI-H215D}$ as compared to $schlank^{KO}$ would help get a better overview on changes in the gene regulation and the lipidome of those lines. This is advantageous to find out e.g. the genes differentially regulated due to the (catalytically inactive) Schlank proteins presence and may help finding new Schlank target genes. Using those lines will minimize false positive regulations that might arise e.g. from over expression

artifacts (Liu and Lehmann, 2008). Also different methods that are commonly used to identify transcription factor function, like chomatin-IP and luziferase assays, may be useful. Several assays performed link the Schlank homeodomain to transcriptional regulation via direct or indirect binding to DNA, like the yeast-1-hybrid assay performed by Noyes et al. (2008), electromobility shift assays performed by Voelzmann (2013) and luciferase assays (Voelzmann et al., 2015).

New *schlank knock in* lines could be established. The $schlank^{NLS2}$ mutation is very elegant and small, but the influences on different aspects of the protein than nuclear localization are rather unclear. A deletion of a large part of the homeodomain -that does not affect CerS activity- may be beneficial in order to analyze the "complete" homeodomain function. This however can have more secondary effects on protein structure and on constraints within the TM domains. Mutations in both parts of the bipartite NLS2 could further reduce nuclear Schlank protein. Also, a *schlank knock in* line with impaired cleavage could be interesting, but therefore a smaller mutation than the deletion of AA 90-110 would be preferable. Additionally, also this mutation may lie within the homeodomain and additional unforeseeable influences could arise. Another interesting perspective could be the generation of a conditional $schlank^{KO}$ line that would allow analysis of Schlank function in a tissue dependent manner.

Until now, nuclear Schlank protein has been mainly studied in the larval fatbody. Also, Schlank cleavage has been described in this organ. Analyzing different organs like e.g. the brain may be interesting to study the interplay between those two phenomena.

5.4 Conclusions and working model

The *Drosophila melanogaster* Schlank protein is involved in ceramide biosynthesis, but also lipid homeostasis (Bauer et al., 2009; Voelzmann, 2013). This thesis dealt with the further characterization of the Schlank protein function independent of Ceramide Synthase activity. In this matter, several key points were addressed:

- A *schlank*^{KO} line generated via homologous recombination showed strong similarity to the *schlank* P-element mutants, further supporting the formerly described *schlank* deficiency phenotypes like reduced ceramide and TAG level, lethality, growth defects and *lipase 3* up regulation.
- The re-integration of target DNA into the *schlank*^{KO} locus could be established and five *schlank knock in* lines were generated. This method allowed the integration of specific mutations into the *schlank* sequence enabling the direct analysis of those mutation's impact, without over expression and background artifacts. Re-integration of target DNA carrying a mutation that results in a catalytically inactive Schlank protein proved the *lipase 3* transcriptional regulation via the Schlank protein, independent of CerS activity. Mutations affecting the putative NLSs showed different results. Mutations in the first NLS unexpectedly increased nuclear Schlank protein, suggesting that this putative NLS does not act as such *in vivo* or that the mutation introduced has no inhibiting effect. Mutations in the second putative NLS reduced nuclear Schlank protein by about 10 %, without affecting Schlank expression level and CerS activity. This points to a functionality of the second NLS *in vivo*. Interestingly, phenotypes observed in this *schlank*$^{KI-NLS2}$ line, some of which have been also observed in *schlank* P-element mutants, link this mutation to lipid homeostasis, motility and growth, and maybe brain/muscle function. The reduced TAG level strongly support the theory of the Schlank homeodomain being involved in lipid homeostasis; in this case via a mutation within this domain that influences nuclear localization but may also influence DNA and/or protein interactions as it is localized in the third helix.
- Glycosylation experiments showed a single conserved endogenous glycosylation site at AA 21. Scanning-N-glycosylation mutagenesis experimentally strongly supports the cytosolic/nucleoplasmic orientation of the homeodomain within the full length Schlank protein and revealed a TM domain structure of supposedly 7 TM domains.

– Cleavage of the Schlank protein has been proposed as Schlank fragment bands were observed in immunoblot analysis using different antibodies. This cleavage was shown to occur in larval stages under good feeding conditions, in the fatbody and other organs. It was rather absent under starvation, in embryonic and pupal stage and in the larval brain. Also, in *ceramide kinase (dcerk)* mutants less fragment band was detected. The site of cleavage was narrowed down to a 20 AA stretch within the Schlank homeodomain. As the Schlank fragment bands were detected to a different extend under different conditions a regulated reasonable cleavage of the Schlank protein was hypothesized. A former hypothesis claiming the cleavage of the homeodomain from the full length protein could be disproved, further supporting evidence of nuclear full length Schlank protein.

It has been shown, that distinct mutations within the *schlank* gene led to different phenotypes. The deficiency of the enzyme does not only affect it's metabolites but also does the lack of the protein itself influence cell function. This fact may be important when analyzing metabolite functions *in vivo* using *knock out* animals. It may be true for other enzymes as well, especially if their domain structure is complex.

A hypothetical model of Schlank function is shown in figure 5.1: Part of the expressed Schlank protein localizes to the ER and is involved in the biosynthesis of ceramides and sphingolipids in general. Sphingolipids (SL) are important for membrane function and structure, but also known to have signaling properties. Reduction of SL inhibits survival, development and growth.

Another pool of expressed Schlank protein localizes to the nucleus where it may be able to bind DNA via its homeodomain. Gene regulation via the Schlank protein has been observed e.g. for *lipase 3* which is involved in lipolysis. Less storage fat may in turn influence energy balance and growth.

Cleavage of the Schlank protein may be involved in the regulation of Schlank localization, CerS activity or gene expression.

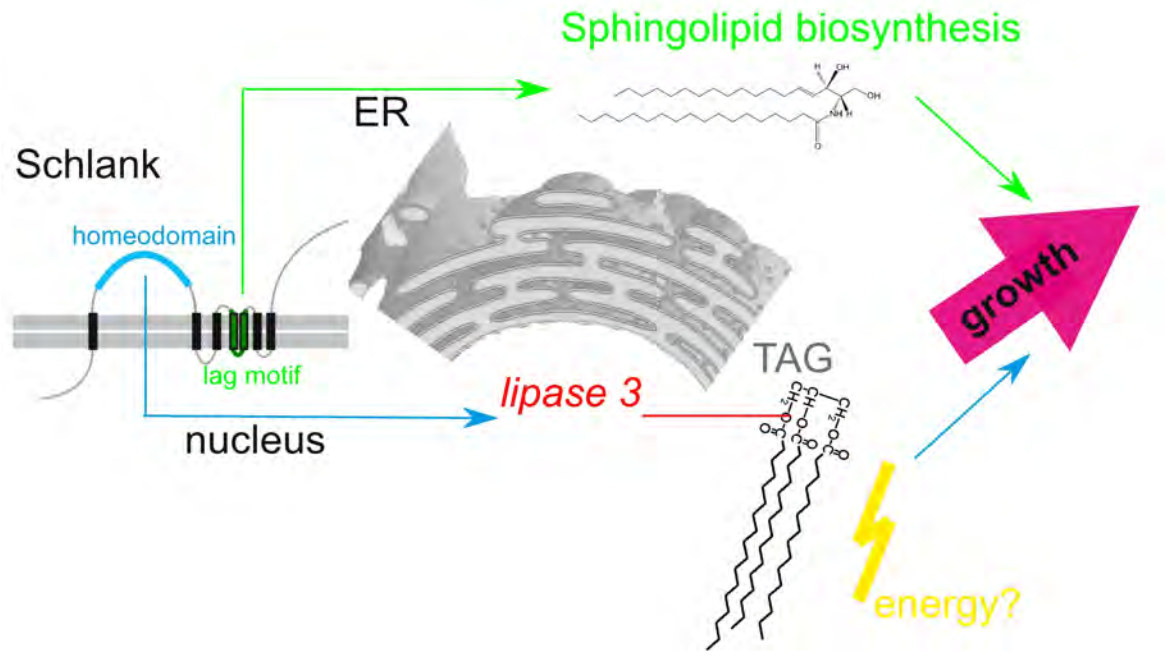

Figure 5.1: Hypothetical model of Schlank function. Nuclear and ER Schlank pool may have independent functions: Sphingolipid biosynthesis is dependent on the lag motif (green), whereas regulation of *lipase 3* gene expression and TAG level are dependent on the Schlank homeodomain (blue). Both pools therefore influence survival and growth.

List of Figures

References

Abbott, S. K., Li, H., Muñoz, S. S., Knoch, B., Batterham, M., Murphy, K. E., Halliday, G. M., and Garner, B. (2014). Altered ceramide acyl chain length and ceramide synthase gene expression in parkinson's disease. *Mov Disord*, 29(4):518–526.

Acharya, U. and Acharya, J. K. (2005). Enzymes of sphingolipid metabolism in drosophila melanogaster. *Cell Mol Life Sci*, 62(2):128–142.

Albi, E., Cataldi, S., Rossi, G., and Magni, M. V. (2003). A possible role of cholesterol-sphingomyelin/phosphatidylcholine in nuclear matrix during rat liver regeneration. *J Hepatol*, 38(5):623–628.

Albi, E. and Magni, M. V. (1999). Sphingomyelin synthase in rat liver nuclear membrane and chromatin. *FEBS Lett*, 460(2):369–372.

Arboleda, G., Morales, L. C., Benítez, B., and Arboleda, H. (2009). Regulation of ceramide-induced neuronal death: cell metabolism meets neurodegeneration. *Brain Res Rev*, 59(2):333–346.

Bauer, R., Voelzmann, A., Breiden, B., Schepers, U., Farwanah, H., Hahn, I., Eckardt, F., Sandhoff, K., and Hoch, M. (2009). Schlank, a member of the ceramide synthase family controls growth and body fat in drosophila. *EMBO J*, 28(23):3706–3716.

Baumbach, J., Xu, Y., Hehlert, P., and Kühnlein, R. P. (2014). Gαq, gγ1 and plc21c control drosophila body fat storage. *J Genet Genomics*, 41(5):283–292.

Beller, M., Bulankina, A. V., Hsiao, H.-H., Urlaub, H., Jäckle, H., and Kühnlein, R. P. (2010). Perilipin-dependent control of lipid droplet structure and fat storage in drosophila. *Cell Metab*, 12(5):521–532.

Bharucha, K. N. (2009). The epicurean fly: using drosophila melanogaster to study metabolism. *Pediatr Res*, 65(2):132–137.

Bingol, B., Tea, J. S., Phu, L., Reichelt, M., Bakalarski, C. E., Song, Q., Foreman, O., Kirkpatrick, D. S., and Sheng, M. (2014). The mitochondrial deubiquitinase usp30 opposes parkin-mediated mitophagy. *Nature*, 510(7505):370–375.

Bosveld, F., Rana, A., van der Wouden, P. E., Lemstra, W., Ritsema, M., Kampinga, H. H., and Sibon, O. C. M. (2008). De novo coa biosynthesis is required to maintain dna integrity during development of the drosophila nervous system. *Hum Mol Genet*, 17(13):2058–2069.

Braak, H., Del Tredici, K., Rüb, U., de Vos, R. A. I., Jansen Steur, E. N. H., and Braak, E. (2003). Staging of brain pathology related to sporadic parkinson's disease. *Neurobiol Aging*, 24(2):197–211.

Brand, A. H. and Perrimon, N. (1993). Targeted gene expression as a means of altering cell fates and generating dominant phenotypes. *Development*, 118(2):401–415.

Bretscher, M. S. (1973). Membrane structure: some general principles. *Science*, 181(4100):622–629.

Buszczak, M., Lu, X., Segraves, W. A., Chang, T. Y., and Cooley, L. (2002). Mutations in the midway gene disrupt a drosophila acyl coenzyme a: diacylglycerol acyltransferase. *Genetics*, 160(4):1511–1518.

Calnan, D. R. and Brunet, A. (2008). The foxo code. *Oncogene*, 27(16):2276–2288.

Carvalho, M., Sampaio, J. L., Palm, W., Brankatschk, M., Eaton, S., and Shevchenko, A. (2012). Effects of diet and development on the drosophila lipidome. *Mol Syst Biol*, 8:600.

Chartier, A., Benoit, B., and Simonelig, M. (2006). A drosophila model of oculopharyngeal muscular dystrophy reveals intrinsic toxicity of pabpn1. *EMBO J*, 25(10):2253–2262.

Cheung, J. C. and Reithmeier, R. A. F. (2007). Scanning n-glycosylation mutagenesis of membrane proteins. *Methods*, 41(4):451–459.

Colombini, M. (2010). Ceramide channels and their role in mitochondria-mediated apoptosis. *Biochim Biophys Acta*, 1797(6-7):1239–1244.

Dauer, W. and Przedborski, S. (2003). Parkinson's disease: mechanisms and models. *Neuron*, 39(6):889–909.

Dobrosotskaya, I. Y., Seegmiller, A. C., Brown, M. S., Goldstein, J. L., and Rawson, R. B. (2002). Regulation of srebp processing and membrane lipid production by phospholipids in drosophila. *Science*, 296(5569):879–883.

Ebel, P., Imgrund, S., Vom Dorp, K., Hofmann, K., Maier, H., Drake, H., Degen, J., Dörmann, P., Eckhardt, M., Franz, T., and Willecke, K. (2014). Ceramide synthase 4 deficiency in mice causes lipid alterations in sebum and results in alopecia. *Biochem J*, 461(1):147–158.

Ebel, P., Vom Dorp, K., Petrasch-Parwez, E., Zlomuzica, A., Kinugawa, K., Mariani, J., Minich, D., Ginkel, C., Welcker, J., Degen, J., Eckhardt, M., Dere, E., Dörmann, P., and Willecke, K. (2013). Inactivation of ceramide synthase 6 in mice results in an altered sphingolipid metabolism and behavioral abnormalities. *J Biol Chem*, 288(29):21433–21447.

Ehrmann, M. and Clausen, T. (2004). Proteolysis as a regulatory mechanism. *Annu Rev Genet*, 38:709–724.

Elmore, S. (2007). Apoptosis: a review of programmed cell death. *Toxicol Pathol*, 35(4):495–516.

Farooqui, A. A., Ong, W.-Y., and Farooqui, T. (2010). Lipid mediators in the nucleus: Their potential contribution to alzheimer's disease. *Biochim Biophys Acta*, 1801(8):906–916.

Fernandes, C. and Rao, Y. (2011). Genome-wide screen for modifiers of parkinson's disease genes in drosophila. *Mol Brain*, 4:17.

Gehring, W. J., Affolter, M., and Bürglin, T. (1994a). Homeodomain proteins. *Annu Rev Biochem*, 63:487–526.

Gehring, W. J. and Hiromi, Y. (1986). Homeotic genes and the homeobox. *Annu Rev Genet*, 20:147–173.

Gehring, W. J., Qian, Y. Q., Billeter, M., Furukubo-Tokunaga, K., Schier, A. F., Resendez-Perez, D., Affolter, M., Otting, G., and Wüthrich, K. (1994b). Homeodomain-dna recognition. *Cell*, 78(2):211–223.

Geier, E., Pfeifer, G., Wilm, M., Lucchiari-Hartz, M., Baumeister, W., Eichmann, K., and Niedermann, G. (1999). A giant protease with potential to substitute for some functions of the proteasome. *Science*, 283(5404):978–981.

Ghosh, A., Kling, T., Snaidero, N., Sampaio, J. L., Shevchenko, A., Gras, H., Geurten, B., Göpfert, M. C., Schulz, J. B., Voigt, A., and Simons, M. (2013). A global in vivo drosophila rnai screen identifies a key role of ceramide phosphoethanolamine for glial ensheathment of axons. *PLoS Genet*, 9(12):e1003980.

Ginkel, C., Hartmann, D., vom Dorp, K., Zlomuzica, A., Farwanah, H., Eckhardt, M., Sandhoff, R., Degen, J., Rabionet, M., Dere, E., Dörmann, P., Sandhoff, K., and Willecke, K. (2012). Ablation of neuronal ceramide synthase 1 in mice decreases ganglioside levels and expression of myelin-associated glycoprotein in oligodendrocytes. *J Biol Chem*, 287(50):41888–41902.

Gloor, G. B., Preston, C. R., Johnson-Schlitz, D. M., Nassif, N. A., Phillis, R. W., Benz, W. K., Robertson, H. M., and Engels, W. R. (1993). Type i repressors of p element mobility. *Genetics*, 135(1):81–95.

Grassmé, H., Riethmüller, J., and Gulbins, E. (2007). Biological aspects of ceramide-enriched membrane domains. *Prog Lipid Res*, 46(3-4):161–170.

Greene, J. C., Whitworth, A. J., Kuo, I., Andrews, L. A., Feany, M. B., and Pallanck, L. J. (2003). Mitochondrial pathology and apoptotic muscle degeneration in drosophila parkin mutants. *Proc Natl Acad Sci U S A*, 100(7):4078–4083.

Grönke, S., Mildner, A., Fellert, S., Tennagels, N., Petry, S., Müller, G., Jäckle, H., and Kühnlein, R. P. (2005). Brummer lipase is an evolutionary conserved fat storage regulator in drosophila. *Cell Metab*, 1(5):323–330.

Grösch, S., Schiffmann, S., and Geisslinger, G. (2012). Chain length-specific properties of ceramides. *Prog Lipid Res*, 51(1):50–62.

Guan, X. L., Cestra, G., Shui, G., Kuhrs, A., Schittenhelm, R. B., Hafen, E., van der Goot, F. G., Robinett, C. C., Gatti, M., Gonzalez-Gaitan, M., and Wenk, M. R. (2013). Biochemical membrane lipidomics during drosophila development. *Dev Cell*, 24(1):98–111.

Guan, X. L., Souza, C. M., Pichler, H., Dewhurst, G., Schaad, O., Kajiwara, K., Wakabayashi, H., Ivanova, T., Castillon, G. A., Piccolis, M., Abe, F., Loewith, R., Funato, K., Wenk, M. R., and Riezman, H. (2009). Functional interactions between sphingolipids and sterols in biological membranes regulating cell physiology. *Mol Biol Cell*, 20(7):2083–2095.

Guo, M. (2012). Drosophila as a model to study mitochondrial dysfunction in parkinson's disease. *Cold Spring Harb Perspect Med*, 2(11).

Gutierrez, E., Wiggins, D., Fielding, B., and Gould, A. P. (2007). Specialized hepatocyte-like cells regulate drosophila lipid metabolism. *Nature*, 445(7125):275–280.

Hait, N. C., Allegood, J., Maceyka, M., Strub, G. M., Harikumar, K. B., Singh, S. K., Luo, C., Marmorstein, R., Kordula, T., Milstien, S., and Spiegel, S. (2009). Regulation of histone acetylation in the nucleus by sphingosine-1-phosphate. *Science*, 325(5945):1254–1257.

Hakomori, S. (1990). Bifunctional role of glycosphingolipids. modulators for transmembrane signaling and mediators for cellular interactions. *J Biol Chem*, 265(31):18713–18716.

Hanada, K., Kumagai, K., Yasuda, S., Miura, Y., Kawano, M., Fukasawa, M., and Nishijima, M. (2003). Molecular machinery for non-vesicular trafficking of ceramide. *Nature*, 426(6968):803–809.

Hanamatsu, H., Ohnishi, S., Sakai, S., Yuyama, K., Mitsutake, S., Takeda, H., Hashino, S., and Igarashi, Y. (2014). Altered levels of serum sphingomyelin and ceramide containing distinct acyl chains in young obese adults. *Nutr Diabetes*, 4:e141.

Hannich, J. T., Umebayashi, K., and Riezman, H. (2011). Distribution and functions of sterols and sphingolipids. *Cold Spring Harb Perspect Biol*, 3(5).

Hannun, Y. A. and Obeid, L. M. (2008). Principles of bioactive lipid signalling: lessons from sphingolipids. *Nat Rev Mol Cell Biol*, 9(2):139–150.

Harder, T. and Simons, K. (1997). Caveolae, digs, and the dynamics of sphingolipid-cholesterol microdomains. *Curr Opin Cell Biol*, 9(4):534–542.

Hay, B. A. and Guo, M. (2006). Caspase-dependent cell death in drosophila. *Annu Rev Cell Dev Biol*, 22:623–650.

Hirth, F. (2010). Drosophila melanogaster in the study of human neurodegeneration. *CNS Neurol Disord Drug Targets*, 9(4):504–523.

Holland, P. W. H., Booth, H. A. F., and Bruford, E. A. (2007a). Classification and nomenclature of all human homeobox genes. *BMC Biol*, 5:47.

Holland, W. L., Brozinick, J. T., Wang, L.-P., Hawkins, E. D., Sargent, K. M., Liu, Y., Narra, K., Hoehn, K. L., Knotts, T. A., Siesky, A., Nelson, D. H., Karathanasis, S. K., Fontenot, G. K., Birnbaum, M. J., and Summers, S. A. (2007b). Inhibition of ceramide synthesis ameliorates glucocorticoid-, saturated-fat-, and obesity-induced insulin resistance. *Cell Metab*, 5(3):167–179.

Holland, W. L. and Summers, S. A. (2008). Sphingolipids, insulin resistance, and metabolic disease: new insights from in vivo manipulation of sphingolipid metabolism. *Endocr Rev*, 29(4):381–402.

Huang, J., Zhou, W., Dong, W., Watson, A. M., and Hong, Y. (2009). From the cover: Directed, efficient, and versatile modifications of the drosophila genome by genomic engineering. *Proc Natl Acad Sci U S A*, 106(20):8284–8289.

Huang, J., Zhou, W., Watson, A. M., Jan, Y.-N., and Hong, Y. (2008). Efficient ends-out gene targeting in drosophila. *Genetics*, 180(1):703–707.

Imai, Y. (2012). Mitochondrial regulation by pink1-parkin signaling. *International Scholarly Research Notices*, 2012.

Imgrund, S., Hartmann, D., Farwanah, H., Eckhardt, M., Sandhoff, R., Degen, J., Gieselmann, V., Sandhoff, K., and Willecke, K. (2009). Adult ceramide synthase 2 (cers2)-deficient mice exhibit myelin sheath defects, cerebellar degeneration, and hepatocarcinomas. *J Biol Chem*, 284(48):33549–33560.

Ivatt, R. M., Sanchez-Martinez, A., Godena, V. K., Brown, S., Ziviani, E., and Whitworth, A. J. (2014). Genome-wide rnai screen identifies the parkinson disease gwas risk locus srebf1 as a regulator of mitophagy. *Proc Natl Acad Sci U S A*, 111(23):8494–8499.

Ivatt, R. M. and Whitworth, A. J. (2014). Srebf1 links lipogenesis to mitophagy and sporadic parkinson disease. *Autophagy*, 10(8):1476–1477.

Jennemann, R., Rabionet, M., Gorgas, K., Epstein, S., Dalpke, A., Rothermel, U., Bayerle, A., van der Hoeven, F., Imgrund, S., Kirsch, J., Nickel, W., Willecke, K., Riezman, H., Gröne, H.-J., and Sandhoff, R. (2012). Loss of ceramide synthase 3 causes lethal skin barrier disruption. *Hum Mol Genet*, 21(3):586–608.

Kageyama-Yahara, N. and Riezman, H. (2006). Transmembrane topology of ceramide synthase in yeast. *Biochem J*, 398(3):585–593.

Kim, H. J., Qiao, Q., Toop, H. D., Morris, J. C., and Don, A. S. (2012). A fluorescent assay for ceramide synthase activity. *J Lipid Res*, 53(8):1701–1707.

Kirin, M., Chandra, A., Charteris, D. G., Hayward, C., Campbell, S., Celap, I., Bencic, G., Vatavuk, Z., Kirac, I., Richards, A. J., Tenesa, A., Snead, M. P., Fleck, B. W., Singh, J., Harsum, S., Maclaren, R. E., den Hollander, A. I., Dunlop, M. G., Hoyng, C. B., Wright, A. F., Campbell, H., Vitart, V., and Mitry, D. (2013). Genome-wide association study identifies genetic risk underlying primary rhegmatogenous retinal detachment. *Hum Mol Genet*, 22(15):3174–3185.

Klionsky, D. J., Abdalla, F. C., ..., Zschocke, J., and Zuckerbraun, B. (2012). Guidelines for the use and interpretation of assays for monitoring autophagy. *Autophagy*, 8(4):445–544.

Kohyama-Koganeya, A., Nabetani, T., Miura, M., and Hirabayashi, Y. (2011). Glucosylceramide synthase in the fat body controls energy metabolism in drosophila. *J Lipid Res*, 52(7):1392–1399.

Kosugi, S., Hasebe, M., Matsumura, N., Takashima, H., Miyamoto-Sato, E., Tomita, M., and Yanagawa, H. (2009). Six classes of nuclear localization signals specific to different binding grooves of importin alpha. *J Biol Chem*, 284(1):478–485.

Kosugi, S., Hasebe, M., Tomita, M., and Yanagawa, H. (2008). Nuclear export signal consensus sequences defined using a localization-based yeast selection system. *Traffic*, 9(12):2053–2062.

Kraut, R. (2011). Roles of sphingolipids in drosophila development and disease. *J Neurochem*, 116(5):764–778.

Kremser, C., Klemm, A.-L., van Uelft, M., Imgrund, S., Ginkel, C., Hartmann, D., and Willecke, K. (2013). Cell-type-specific expression pattern of ceramide synthase 2 protein in mouse tissues. *Histochem Cell Biol*, 140(5):533–547.

Künnapuu, J., Björkgren, I., and Shimmi, O. (2009). The drosophila dpp signal is produced by cleavage of its proprotein at evolutionary diversified furin-recognition sites. *Proc Natl Acad Sci U S A*, 106(21):8501–8506.

Laemmli, U. K. (1970). Cleavage of structural proteins during the assembly of the head of bacteriophage t4. *Nature*, 227(5259):680–685.

Laviad, E. L., Kelly, S., Merrill, Jr, A. H., and Futerman, A. H. (2012). Modulation of ceramide synthase activity via dimerization. *J Biol Chem*, 287(25):21025–21033.

Lessing, D. and Bonini, N. M. (2009). Maintaining the brain: insight into human neurodegeneration from drosophila melanogaster mutants. *Nat Rev Genet*, 10(6):359–370.

Levy, M. and Futerman, A. H. (2010). Mammalian ceramide synthases. *IUBMB Life*, 62(5):347–356.

Liu, H.-Y. and Pfleger, C. M. (2013). Mutation in e1, the ubiquitin activating enzyme, reduces drosophila lifespan and results in motor impairment. *PLoS One*, 8(1):e32835.

Liu, Y. and Lehmann, M. (2008). A genomic response to the yeast transcription factor gal4 in drosophila. *Fly (Austin)*, 2(2):92–98.

Liu, Z. and Huang, X. (2013). Lipid metabolism in drosophila: development and disease. *Acta Biochim Biophys Sin (Shanghai)*, 45(1):44–50.

Lucki, N. C. and Sewer, M. B. (2012). Nuclear sphingolipid metabolism. *Annu Rev Physiol*, 74:131–151.

Luo, N. (2011). Molekulare analyse des drosophila gens schlank. Master's thesis, Mathematisch-Naturwissenschaftlichen Fakultaet der Rheinischen Friedrich-Wilhelms-Universitaet Bonn.

Mathew, R., Karantza-Wadsworth, V., and White, E. (2007). Role of autophagy in cancer. *Nat Rev Cancer*, 7(12):961–967.

Menuz, V., Howell, K. S., Gentina, S., Epstein, S., Riezman, I., Fornallaz-Mulhauser, M., Hengartner, M. O., Gomez, M., Riezman, H., and Martinou, J.-C. (2009). Protection of c. elegans from anoxia by hyl-2 ceramide synthase. *Science*, 324(5925):381–384.

Mesika, A., Ben-Dor, S., Laviad, E. L., and Futerman, A. H. (2007). A new functional motif in hox domain-containing ceramide synthases: identification of a novel region flanking the hox and tlc domains essential for activity. *J Biol Chem*, 282(37):27366–27373.

Mielke, M. M. and Lyketsos, C. G. (2010). Alterations of the sphingolipid pathway in alzheimer's disease: new biomarkers and treatment targets? *Neuromolecular Med*, 12(4):331–340.

Min, K. T. and Benzer, S. (1999). Preventing neurodegeneration in the drosophila mutant bubblegum. *Science*, 284(5422):1985–1988.

Mizushima, N., Yamamoto, A., Matsui, M., Yoshimori, T., and Ohsumi, Y. (2004). In vivo analysis of autophagy in response to nutrient starvation using transgenic mice expressing a fluorescent autophagosome marker. *Mol Biol Cell*, 15(3):1101–1111.

Mizutani, Y., Kihara, A., and Igarashi, Y. (2005). Mammalian lass6 and its related family members regulate synthesis of specific ceramides. *Biochem J*, 390(Pt 1):263–271.

Mortimore, G. E. and Pösö, A. R. (1987). Intracellular protein catabolism and its control during nutrient deprivation and supply. *Annu Rev Nutr*, 7:539–564.

Muffat, J., Walker, D. W., and Benzer, S. (2008). Human apod, an apolipoprotein up-regulated in neurodegenerative diseases, extends lifespan and increases stress resistance in drosophila. *Proc Natl Acad Sci U S A*, 105(19):7088–7093.

Mullen, T. D., Hannun, Y. A., and Obeid, L. M. (2012). Ceramide synthases at the centre of sphingolipid metabolism and biology. *Biochem J*, 441(3):789–802.

Munsie, L. N., Desmond, C. R., and Truant, R. (2012). Cofilin nuclear-cytoplasmic shuttling affects cofilin-actin rod formation during stress. *J Cell Sci*, 125(Pt 17):3977–3988.

Narendra, D., Tanaka, A., Suen, D.-F., and Youle, R. J. (2008). Parkin is recruited selectively to impaired mitochondria and promotes their autophagy. *J Cell Biol*, 183(5):795–803.

Narendra, D., Tanaka, A., Suen, D.-F., and Youle, R. J. (2009). Parkin-induced mitophagy in the pathogenesis of parkinson disease. *Autophagy*, 5(5):706–708.

Navarro, J. A., Ohmann, E., Sanchez, D., Botella, J. A., Liebisch, G., Moltó, M. D., Ganfornina, M. D., Schmitz, G., and Schneuwly, S. (2010). Altered lipid metabolism in a drosophila model of friedreich's ataxia. *Hum Mol Genet*, 19(14):2828–2840.

Neumann, S. and van Meer, G. (2008). Sphingolipid management by an orchestra of lipid transfer proteins. *Biol Chem*, 389(11):1349–1360.

Nilsson, A. (1968). Metabolism of sphingomyelin in the intestinal tract of the rat. *Biochim Biophys Acta*, 164(3):575–584.

Nirala, N. K., Rahman, M., Walls, S. M., Singh, A., Zhu, L. J., Bamba, T., Fukusaki, E., Srideshikan, S. M., Harris, G. L., Ip, Y. T., Bodmer, R., and Acharya, U. R. (2013). Survival response to increased ceramide involves metabolic adaptation through novel regulators of glycolysis and lipolysis. *PLoS Genet*, 9(6):e1003556.

Noyes, M. B., Christensen, R. G., Wakabayashi, A., Stormo, G. D., Brodsky, M. H., and Wolfe, S. A. (2008). Analysis of homeodomain specificities allows the family-wide prediction of preferred recognition sites. *Cell*, 133(7):1277–1289.

Ogretmen, B. and Hannun, Y. A. (2004). Biologically active sphingolipids in cancer pathogenesis and treatment. *Nat Rev Cancer*, 4(8):604–616.

Oskouian, B. and Saba, J. D. (2010). Cancer treatment strategies targeting sphingolipid metabolism. *Adv Exp Med Biol*, 688:185–205.

Padmanabha, D. and Baker, K. D. (2014). Drosophila gains traction as a repurposed tool to investigate metabolism. *Trends Endocrinol Metab*, 25(10):518–527.

Palanker, L., Tennessen, J. M., Lam, G., and Thummel, C. S. (2009). Drosophila hnf4 regulates lipid mobilization and beta-oxidation. *Cell Metab*, 9(3):228–239.

Papadopoulos, D. K., Skouloudaki, K., Adachi, Y., Samakovlis, C., and Gehring, W. J. (2012). Dimer formation via the homeodomain is required for function and specificity of sex combs reduced in drosophila. *Dev Biol*, 367(1):78–89.

Park, J.-W., Park, W.-J., and Futerman, A. H. (2014). Ceramide synthases as potential targets for therapeutic intervention in human diseases. *Biochim Biophys Acta*, 1841(5):671–681.

Park, J.-W., Park, W.-J., Kuperman, Y., Boura-Halfon, S., Pewzner-Jung, Y., and Futerman, A. H. (2013). Ablation of very long acyl chain sphingolipids causes hepatic insulin resistance in mice due to altered detergent-resistant membranes. *Hepatology*, 57(2):525–532.

Patil, C. and Walter, P. (2001). Intracellular signaling from the endoplasmic reticulum to the nucleus: the unfolded protein response in yeast and mammals. *Curr Opin Cell Biol*, 13(3):349–355.

Pentchev, P. G. and Barranger, J. A. (1978). Sphingolipidoses: molecular manifestations and biochemical strategies. *J Lipid Res*, 19(4):401–409.

Pepperl, J., Reim, G., Lüthi, U., Kaech, A., Hausmann, G., and Basler, K. (2013). Sphingolipid depletion impairs endocytic traffic and inhibits wingless signaling. *Mech Dev*, 130(9-10):493–505.

Peters, D. (2012). Molekulare analyse der drosophila ceramid synthase schlank. Master's thesis, Mathematisch-Naturwissenschaftlichen Fakultaet der Rheinischen Friedrich-Wilhelms-Universitaet Bonn.

Peters, F., Vorhagen, S., Brodesser, S., Jakobshagen, K., Brüning, J. C., Niessen, C. M., and Krönke, M. (2015). Ceramide synthase 4 regulates stem cell homeostasis and hair follicle cycling. *J Invest Dermatol*.

Pewzner-Jung, Y., Brenner, O., Braun, S., Laviad, E. L., Ben-Dor, S., Feldmesser, E., Horn-Saban, S., Amann-Zalcenstein, D., Raanan, C., Berkutzki, T., Erez-Roman, R., Ben-David, O., Levy, M., Holzman, D., Park, H., Nyska, A., Merrill, Jr, A. H., and Futerman, A. H. (2010a). A critical role for ceramide synthase 2 in liver homeostasis: Ii. insights into molecular changes leading to hepatopathy. *J Biol Chem*, 285(14):10911–10923.

Pewzner-Jung, Y., Park, H., Laviad, E. L., Silva, L. C., Lahiri, S., Stiban, J., Erez-Roman, R., Brügger, B., Sachsenheimer, T., Wieland, F., Prieto, M., Merrill, Jr, A. H., and Futerman, A. H. (2010b). A critical role for ceramide synthase 2 in liver homeostasis: I. alterations in lipid metabolic pathways. *J Biol Chem*, 285(14):10902–10910.

Picciotto, C. (2014). Characterisation of reintroduced wildtype schlank dna into a schlank-knock-out line and of transgenic schlank-fusion-protein variants. Master's thesis, Mathematisch-Naturwissenschaftlichen Fakultaet der Rheinischen Friedrich-Wilhelms-Universitaet Bonn.

Pimenta de Castro, I., Costa, A. C., Lam, D., Tufi, R., Fedele, V., Moisoi, N., Dinsdale, D., Deas, E., Loh, S. H. Y., and Martins, L. M. (2012). Genetic analysis of mitochondrial protein misfolding in drosophila melanogaster. *Cell Death Differ*, 19(8):1308–1316.

Pistillo, D., Manzi, A., Tino, A., Boyl, P. P., Graziani, F., and Malva, C. (1998). The drosophila melanogaster lipase homologs: a gene family with tissue and developmental specific expression. *J Mol Biol*, 276(5):877–885.

Punta, M., Forrest, L. R., Bigelow, H., Kernytsky, A., Liu, J., and Rost, B. (2007). Membrane protein prediction methods. *Methods*, 41(4):460–474.

Rabionet, M., Bayerle, A., Jennemann, R., Heid, H., Fuchser, J., Marsching, C., Porubsky, S., Bolenz, C., Guillou, F., Gröne, H.-J., Gorgas, K., and Sandhoff, R. (2015). Male meiotic cytokinesis requires ceramide synthase 3-dependent sphingolipids with unique membrane anchors. *Hum Mol Genet*.

Rawlings, N. D., Waller, M., Barrett, A. J., and Bateman, A. (2014). Merops: the database of proteolytic enzymes, their substrates and inhibitors. *Nucleic Acids Res*, 42(Database issue):D503–D509.

Rawson, R. B. (2003). The srebp pathway–insights from insigs and insects. *Nat Rev Mol Cell Biol*, 4(8):631–640.

Roberts, D. B. et al. (1986). *Drosophila: a practical approach.* IRL press.

Rubin, G. M. and Spradling, A. C. (1982). Genetic transformation of drosophila with transposable element vectors. *Science*, 218(4570):348–353.

Sandhoff, K. (2012). My journey into the world of sphingolipids and sphingolipidoses. *Proc Jpn Acad Ser B Phys Biol Sci*, 88(10):554–582.

Sanhueza, M., Zechini, L., Gillespie, T., and Pennetta, G. (2014). Gain-of-function mutations in the als8 causative gene vapb have detrimental effects on neurons and muscles. *Biol Open*, 3(1):59–71.

Schmelz, E. M., Crall, K. J., Larocque, R., Dillehay, D. L., and Merrill, Jr, A. (1994). Uptake and metabolism of sphingolipids in isolated intestinal loops of mice. *J Nutr*, 124(5):702–712.

Schwarzkopf, C. (2015). Impact of mutations within the homeodomain of ceramide synthase schlank on mitochondrial and locomotor performance. Master's thesis, Mathematisch-Naturwissenschaftlichen Fakultaet der Rheinischen Friedrich-Wilhelms-Universitaet Bonn.

Scott, M. P., Tamkun, J. W., and Hartzell, 3rd, G. (1989). The structure and function of the homeodomain. *Biochim Biophys Acta*, 989(1):25–48.

Silva, L. C., Ben David, O., Pewzner-Jung, Y., Laviad, E. L., Stiban, J., Bandyopadhyay, S., Merrill, Jr, A. H., Prieto, M., and Futerman, A. H. (2012). Ablation of ceramide synthase 2 strongly affects biophysical properties of membranes. *J Lipid Res*, 53(3):430–436.

Siskind, L. J., Kolesnick, R. N., and Colombini, M. (2002). Ceramide channels increase the permeability of the mitochondrial outer membrane to small proteins. *J Biol Chem*, 277(30):26796–26803.

Sorokin, A. V., Kim, E. R., and Ovchinnikov, L. P. (2007). Nucleocytoplasmic transport of proteins. *Biochemistry (Mosc)*, 72(13):1439–1457.

Sousa-Nunes, R., Yee, L. L., and Gould, A. P. (2011). Fat cells reactivate quiescent neuroblasts via tor and glial insulin relays in drosophila. *Nature*, 471(7339):508–512.

Spassieva, S., Seo, J.-G., Jiang, J. C., Bielawski, J., Alvarez-Vasquez, F., Jazwinski, S. M., Hannun, Y. A., and Obeid, L. M. (2006). Necessary role for the lag1p motif in (dihydro)ceramide synthase activity. *J Biol Chem*, 281(45):33931–33938.

Spillantini, M. G., Schmidt, M. L., Lee, V. M., Trojanowski, J. Q., Jakes, R., and Goedert, M. (1997). Alpha-synuclein in lewy bodies. *Nature*, 388(6645):839–840.

Spradling, A. C. and Rubin, G. M. (1982). Transposition of cloned p elements into drosophila germ line chromosomes. *Science*, 218(4570):341–347.

Stiban, J., Caputo, L., and Colombini, M. (2008). Ceramide synthesis in the endoplasmic reticulum can permeabilize mitochondria to proapoptotic proteins. *J Lipid Res*, 49(3):625–634.

Stiban, J., Tidhar, R., and Futerman, A. H. (2010). Ceramide synthases: roles in cell physiology and signaling. *Adv Exp Med Biol*, 688:60–71.

Subramanian, M., Metya, S. K., Sadaf, S., Kumar, S., Schwudke, D., and Hasan, G. (2013). Altered lipid homeostasis in drosophila insp3 receptor mutants leads to obesity and hyperphagia. *Dis Model Mech*, 6(3):734–744.

Thudichum, J. L. W. (1874). *Researches on the chemical constitution of the brain.*

Tidhar, R. and Futerman, A. H. (2013). The complexity of sphingolipid biosynthesis in the endoplasmic reticulum. *Biochim Biophys Acta*, 1833(11):2511–2518.

Tirodkar, T. S., Lu, P., Bai, A., Scheffel, M. J., Gencer, S., Garrett-Mayer, E., Bielawska, A., Ogretmen, B., and Voelkel-Johnson, C. (2015). Expression of ceramide synthase 6 transcriptionally activates acid ceramidase in a c-jun n-terminal kinase (jnk)-dependent manner. *J Biol Chem*, 290(21):13157–13167.

Tsugane, K., Tamiya-Koizumi, K., Nagino, M., Nimura, Y., and Yoshida, S. (1999). A possible role of nuclear ceramide and sphingosine in hepatocyte apoptosis in rat liver. *J Hepatol*, 31(1):8–17.

Turk, B., Turk, D., and Turk, V. (2012). Protease signalling: the cutting edge. *EMBO J*, 31(7):1630–1643.

Turpin, S. M., Nicholls, H. T., Willmes, D. M., Mourier, A., Brodesser, S., Wunderlich, C. M., Mauer, J., Xu, E., Hammerschmidt, P., Brönneke, H. S., Trifunovic, A., LoSasso, G., Wunderlich, F. T., Kornfeld, J.-W., Blüher, M., Krönke, M., and Brüning, J. C. (2014). Obesity-induced cers6-dependent c16:0 ceramide production promotes weight gain and glucose intolerance. *Cell Metab*, 20(4):678–686.

Ussher, J. R., Koves, T. R., Cadete, V. J. J., Zhang, L., Jaswal, J. S., Swyrd, S. J., Lopaschuk, D. G., Proctor, S. D., Keung, W., Muoio, D. M., and Lopaschuk, G. D. (2010). Inhibition of de novo ceramide synthesis reverses diet-induced insulin resistance and enhances whole-body oxygen consumption. *Diabetes*, 59(10):2453–2464.

van Echten-Deckert, G. and Walter, J. (2012). Sphingolipids: critical players in alzheimer's disease. *Prog Lipid Res*, 51(4):378–393.

van Zanten, T. S., Gómez, J., Manzo, C., Cambi, A., Buceta, J., Reigada, R., and Garcia-Parajo, M. F. (2010). Direct mapping of nanoscale compositional connectivity on intact cell membranes. *Proc Natl Acad Sci U S A*, 107(35):15437–15442.

Venkataraman, K. and Futerman, A. H. (2002). Do longevity assurance genes containing hox domains regulate cell development via ceramide synthesis? *FEBS Lett*, 528(1-3):3–4.

Vesper, H., Schmelz, E. M., Nikolova-Karakashian, M. N., Dillehay, D. L., Lynch, D. V., and Merrill, Jr, A. (1999). Sphingolipids in food and the emerging importance of sphingolipids to nutrition. *J Nutr*, 129(7):1239–1250.

Vives-Bauza, C., Zhou, C., Huang, Y., Cui, M., de Vries, R. L. A., Kim, J., May, J., Tocilescu, M. A., Liu, W., Ko, H. S., Magrané, J., Moore, D. J., Dawson, V. L., Grailhe, R., Dawson, T. M., Li, C., Tieu, K., and Przedborski, S. (2010). Pink1-dependent recruitment of parkin to mitochondria in mitophagy. *Proc Natl Acad Sci U S A*, 107(1):378–383.

Voelzmann, A. (2013). *The homeodomain of the Drosophila Ceramide Synthase Schlank confers nuclear import information and DNA binding capabilities*. PhD thesis, Mathematisch-Naturwissenschaftlichen Fakultaet der Rheinischen Friedrich-Wilhelms-Universitaet Bonn.

Voelzmann, A. and Bauer, R. (2010). Ceramide synthases in mammalians, worms, and insects: emerging schemes. *BioMolecular Concepts*, 1(5-6):411–422.

Voelzmann, A. and Bauer, R. (2011). Embryonic expression of drosophila ceramide synthase schlank in developing gut, cns and pns. *Gene Expr Patterns*, 11(8):501–510.

Voelzmann, A., Wulf, A.-L., Eckardt, F., Thielisch, M., Brondolin, M., Pesch, Y., Bauer, R., and Hoch, M. (2015). Nuclear drosophila ceramide synthase schlank regulates lipid homeostasis. unpublished manuscript.

Walls, Jr, S. M., Attle, S. J., Brulte, G. B., Walls, M. L., Finley, K. D., Chatfield, D. A., Herr, D. R., and Harris, G. L. (2013). Identification of sphingolipid metabolites that induce obesity via misregulation of appetite, caloric intake and fat storage in drosophila. *PLoS Genet*, 9(12):e1003970.

Winter, E. and Ponting, C. P. (2002). Tram, lag1 and cln8: members of a novel family of lipid-sensing domains? *Trends Biochem Sci*, 27(8):381–383.

Wu, G., Lu, Z. H., and Ledeen, R. W. (1995). Induced and spontaneous neuritogenesis are associated with enhanced expression of ganglioside gm1 in the nuclear membrane. *J Neurosci*, 15(5 Pt 2):3739–3746.

Yang, Q., Gong, Z.-J., Zhou, Y., Yuan, J.-Q., Cheng, J., Tian, L., Li, S., Lin, X.-D., Xu, R., Zhu, Z.-R., and Mao, C. (2010). Role of drosophila alkaline ceramidase (dacer) in drosophila development and longevity. *Cell Mol Life Sci*, 67(9):1477–1490.

Yang, Y., Gehrke, S., Imai, Y., Huang, Z., Ouyang, Y., Wang, J.-W., Yang, L., Beal, M. F., Vogel, H., and Lu, B. (2006). Mitochondrial pathology and muscle and dopaminergic neuron degeneration caused by inactivation of drosophila pink1 is rescued by parkin. *Proc Natl Acad Sci U S A*, 103(28):10793–10798.

Yang, Y., Wu, Z., Kuo, Y. M., and Zhou, B. (2005). Dietary rescue of fumble–a drosophila model for pantothenate-kinase-associated neurodegeneration. *J Inherit Metab Dis*, 28(6):1055–1064.

Ye, Y. and Fortini, M. E. (2000). Proteolysis and developmental signal transduction. *Semin Cell Dev Biol*, 11(3):211–221.

Yu, W., Wang, L., Wang, Y., Xu, X., Zou, P., Gong, M., Zheng, J., You, J., Wang, H., Mei, F., and Pei, F. (2013). A novel tumor metastasis suppressor

gene lass2/tmsg1 interacts with vacuolar atpase through its homeodomain. *J Cell Biochem*, 114(3):570–583.

Zhao, L., Spassieva, S. D., Jucius, T. J., Shultz, L. D., Shick, H. E., Macklin, W. B., Hannun, Y. A., Obeid, L. M., and Ackerman, S. L. (2011). A deficiency of ceramide biosynthesis causes cerebellar purkinje cell neurodegeneration and lipofuscin accumulation. *PLoS Genet*, 7(5):e1002063.

Zigdon, H., Kogot-Levin, A., Park, J.-W., Goldschmidt, R., Kelly, S., Merrill, Jr, A. H., Scherz, A., Pewzner-Jung, Y., Saada, A., and Futerman, A. H. (2013). Ablation of ceramide synthase 2 causes chronic oxidative stress due to disruption of the mitochondrial respiratory chain. *J Biol Chem*, 288(7):4947–4956.

Zinke, I., Kirchner, C., Chao, L. C., Tetzlaff, M. T., and Pankratz, M. J. (1999). Suppression of food intake and growth by amino acids in drosophila: the role of pumpless, a fat body expressed gene with homology to vertebrate glycine cleavage system. *Development*, 126(23):5275–5284.

Ziviani, E., Tao, R. N., and Whitworth, A. J. (2010). Drosophila parkin requires pink1 for mitochondrial translocation and ubiquitinates mitofusin. *Proc Natl Acad Sci U S A*, 107(11):5018–5023.

6 Appendix

6.1 Rescue of *schlank* mutants

Over expression studies showed that *lipase 3* transcript level are dependent on Schlank protein expression, specifically the homeodomain containing Schlank N-terminus. To further analyze this, classical rescue experiments were performed. The weaker *schlank* mutant allele was "rescued" using the driver line *cgGal4* that drives expression mainly in the fatbody and haemocytes, and different UAS-lines. *lipase 3* expression was used as readout.

Figure 6.1 shows that expression of full length Schlank results in a reduced *lipase 3* expression as compared to the *schlank* mutant. Also the expression of the catalytically inactive Schlank version (SchlankH215D) and the 138 N-terminal amino acids of Schlank result in a reduced *lipase 3* transcript level. Reduction is to about 30 % in all cases.

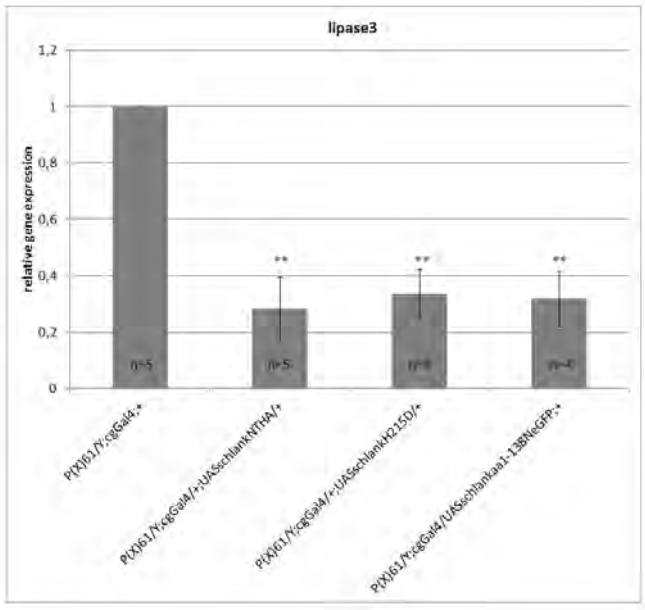

Figure 6.1: Classical *schlank* rescue. The weaker $schlank^{P(X)61}$ mutant and the*cgGal4* driver line were used. The readout was qRT-PCR on *lipase 3* transcript level. UAS-lines to rescue the mutant phenotype (=up regulation of *lipase 3*) were *UAS-HAschlank* (full length Schlank), *UAS-schlankH215D* (catalytically inactive Schlank) and *UAS-eGFPschlankAA1-138* (Schlank N-terminus until AA138). Error bars: SEM. Significance tested via Student's T-test. Level in $schlank^{P(X)61}$ was set to 1.

6.2 Subcellular localization of GFP-Schlank-AA1-138 in fatbody *in vivo*

To check whether the *schlank* construct of AA 1-138 N-terminally eGFP-taged localizes *in vivo* as it does in cell culture, immunofluorescent stainings of stage 3 larval fatbody was performed.

As seen in figure 6.2 it localizes mostly to the nuclei which are outlined by the αLamin staining. In *oregonR* fatbody no signal is detected which shows αGFP antibody specificity.

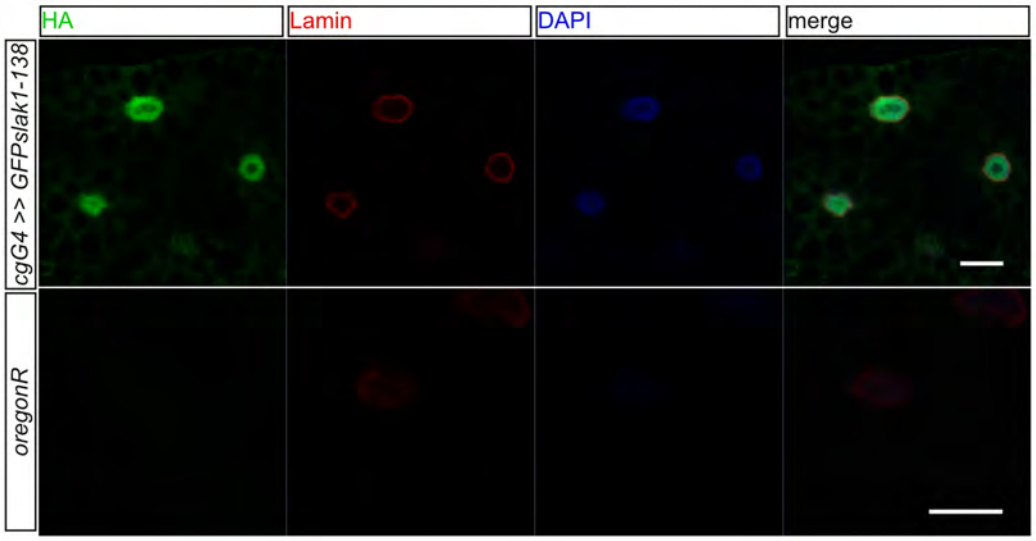

Figure 6.2: Subcellular localization of GFP-Schlank-AA1-138 *in vivo*. Males of the driver line *cgGal4* were crossed to virgins of the *UAS GFPschlank AA1-138* line. Stage 3 larval fatbody was stained with αGFP and αLamin antibodies. *oregonR* was used as a control. Scale bars: 20 μm.

6.3 Expression and subcellular localization of truncated Schlank versions *in vivo*

Immunoblot analysis showed a Schlank cleavage site at around AA 98. Resulting putative cleavage products (Schlank1-98 and Schlank99-400) were cloned into pUAST in a tagged form to establish UAS fly lines. The lines were checked for the expression of the constructs and their subcellular localization. Males of the indicated driver lines (*hsGal4, hsflp;act>CD2>Gal4, cgGal4*) were crossed to virgins of the different UAS lines. Stage 3 larval fatbody was stained with αHA and αLamin antibodies.

Like full length Schlank (upper three rows) the truncated Schlank versions localize to a cytosolic region surrounding the nuclei (fig. 6.3). Expression of AA 1-98 was rather low. Expression of Schlank in clones (*hsflp;act>CD2>Gal4 = CD2G4*) showed the αHA antibody specificity as in cells where no *schlank* is expressed no staining was detected.

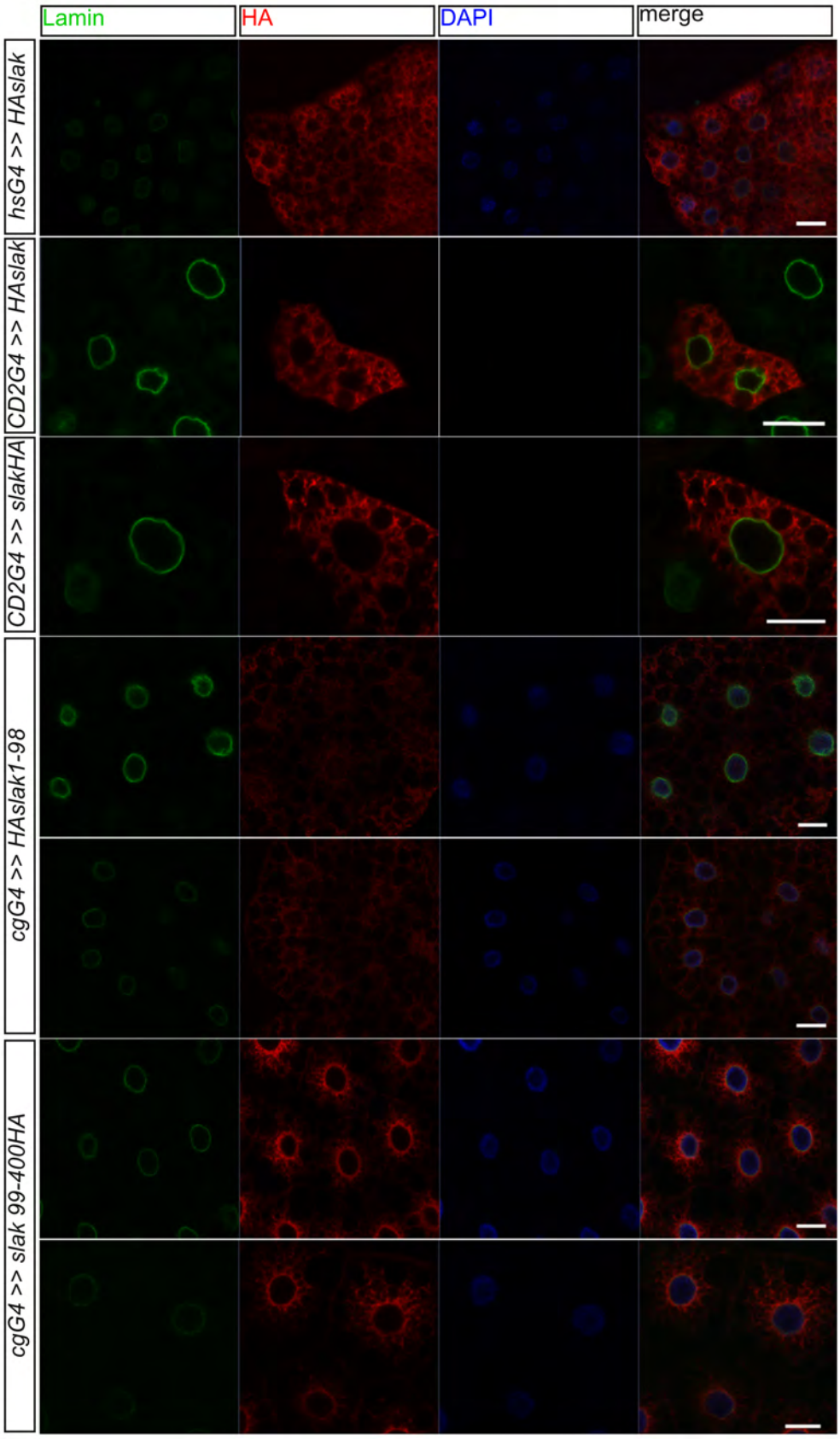

Figure 6.3: Expression and subcellular localization of Schlank over expression constructs *in vivo*. Scale bars: 20 μm.

6.4 Sub-cellular localization of Schlank in larval fatbody

Ceramide Synthases have been described as transmembrane proteins localized to the ER (Tidhar and Futerman, 2013; Stiban et al., 2008). Also, Schlank was shown to localize to the ER, and to the nucleus *in vivo* (Voelzmann, 2013). However, much of the detected Schlank protein could not be assigned to an organell. Here, co-localization studies were performed with Spectrin (a cytoskeleton component underlying the plasma membrane), mitoGFP (expressed GFP targeted to mitochondria) and lampGFP (expressed GFP targeted to lysosomes). Schlank showed partial co-staining with Spectrin and lampGFP, but no convincing co-staining with the mitochondrial marker in the fatbody of stage 3 larvae (fig. 6.4).

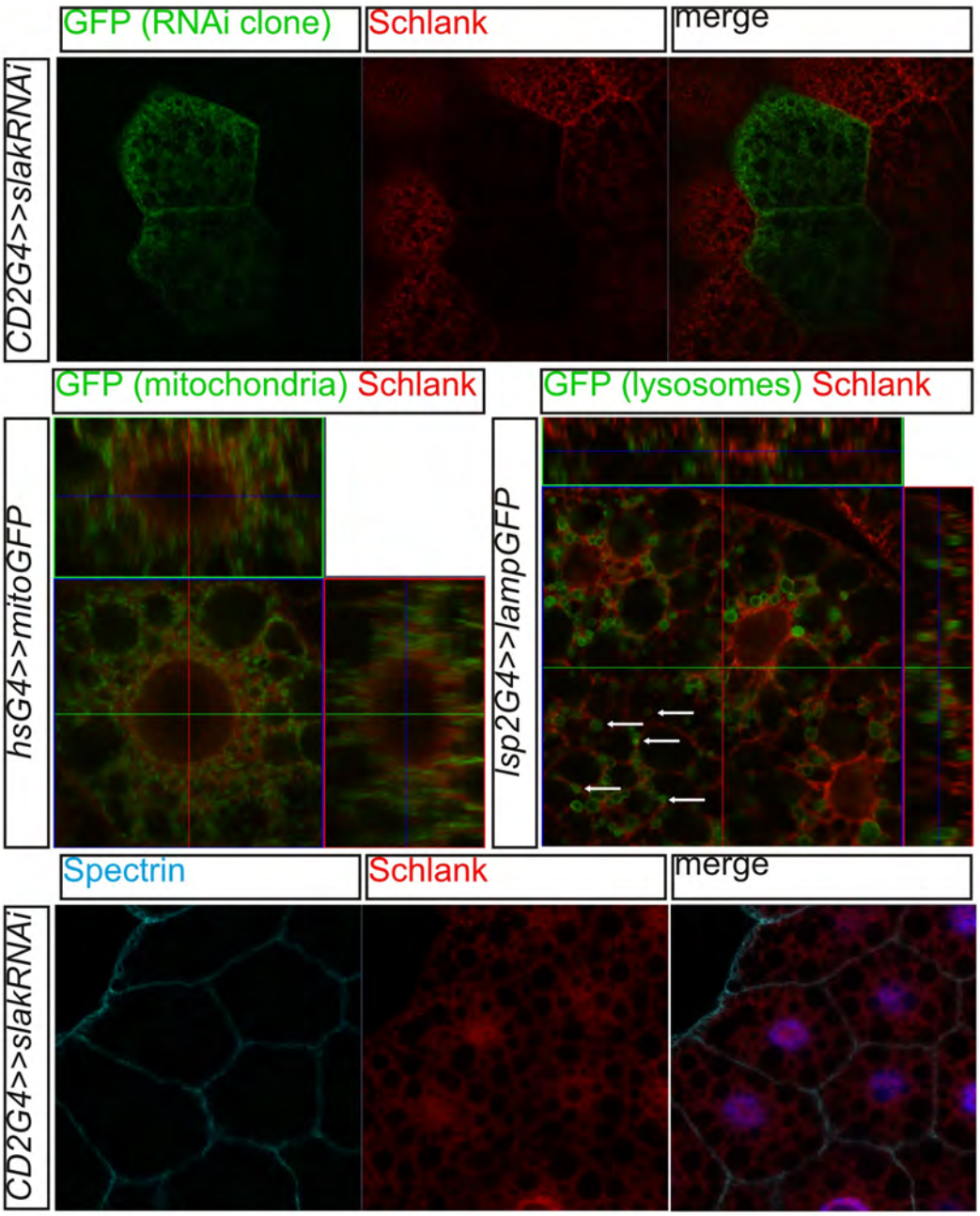

Figure 6.4: Schlank subcellular localization in L3 fatbody cells. Antibody (αSchlank-CT) specificity was tested using *schlankRNAi* clones. mitoGFP and lampGFP were over expressed using the *hsGal4* or *lsp2Gal4* driver line, respectively. Fatbody was dissected and stained in third larval stage.

6.5

Abbreviations

A. bidest	double destilled water
AA	amino acid
AEL	after egg laying
Amp	ampicillin (resistance cDNA)
ATP	adenosine triphosphate
APS	ammonium peroxide sulfate
bp	base pairs
BSA	bovine serum albumin
cDNA	complementary DNA
Cer	Ceramide
CerS	Ceranide Synthase
C-Terminus	carboxy terminus of a peptide
CyO	*Curly of Oyster* (marker)
Da	Dalton
DAPI	4',6-diamidino-2-phenylindole
DMSO	dimethyl sulfoxide
DNA	desoxy ribonucleic acid
dNTP	2'-desoxy-nucleoside- 5'-triphosphate
E. coli	*Escherichia coli*
ECL	enhanced chemo luminescence
EDTA	ethylenediaminetetraacetic acid
e.g.	for example (lat.: exempli gratia)
eGFP	enhanced green fluorescent protein
ER	endoplasmic reticulum
et al.	and others (lat.: et altera)
Fig.	figure
FM7	balancer chromosome (X)
frt	Flp-recombinase recognition target
gDNA	genomic DNA
h	hour
HR	homologous region
HRP	Horseradish Peroxidase
hs	heat shock
INM	inner nuclear membrane
kb	kilo base pairs
kDa	kilo dalton
KI	knock-in
KO	knock-out
l	liter
L	larval stage (1,2,3)
loxP	locus of crossing over P1

m	milli
MCS	Multiple Cloning Site
min	Minute
mRNA	messenger-RNA
n	nano
n	independent biological replicates
NLS	nuclear localization sequence
N-terminus	amino terminus of a peptide
ORF	open reading frame
p	pico
PAGE	polyacrylamide gel electrophoresis
PBS	phosphate buffered saline
PCR	polymerase chain reaction
PFA	paraform aldehyde
polyA	polyadenylation site
RNA	ribonucleic acid
RNAi	RNA interference
RT	room temperature
S1P	sphingosine-1-phosphate
SEM	standard error of the means
SDS	sodium dodecyl sulfate
TAG	triacylglycerol
TBS	tris buffered saline
TEMED	N,N,N',N'-Tetramethyl-ethylendiamin
TLC	thin layer chromatography
TM	trans membrane (domain)
TM3	balancer chromosome (3rd)
Tris	tris-(hydroxymethyl)- aminomethane
U	unit
UAS	Upstream Activating Sequence
UTR	untranslated region
v	volume
V	Volt
WT	wildtype
YFP	yellow fluorescent protein
+	WT chromosome

Danksagung

Herrn PD. Dr. Reinhard Bauer -meinem Doktorvater- danke ich für die Überlassung des Themas und für die Betreuung und Begutachtung dieser Arbeit. Außerdem möchte ich mich für die Hilfsbereitschaft und die eingeräumten Freiheiten zur Gestaltung dieser Arbeit bedanken.

Herrn Prof. Dr. Klaus Willecke danke ich für die Übernahme des Koreferats.

Frau Prof. Dr. Gerhild van Echten-Deckert und Herrn Prof. Dr. Peter Vöhringer danke ich für die Bereitschaft als fachnahe und fachfremde Gutacher zur Verfügung zu stehen.

Dr. Bernadette Breiden danke ich herzlich für die freundliche Kooperation bei den radioaktiven *in vivo* Assays.

Hier erwähnen möchte ich auch all die Praktikanten, Bachelor, Master und Diplomanden, die während meiner Zeit im LIMES das kleine Labor mit mir geteilt haben (vor allem jene, die von mir betreut wurden), ein ganz besonderer Dank geht hier u.a. an Ningning Luo, Georg Petkau, Laura Jussen, Raija Ebert, Anne Ohm, Hannes Maib, Cara Picciotto, Anna Höfges, Christoph Schwarzkopf und Nadine Weinstock!

...